TECHNISCHE UNIVERSITEIT DELFT

MASTER THESIS

Validation of the 4 component model through experiments done in a 300mm diameter pipeline

---

Author:
C. J. LUTEIJN

Supervisor:
Dr. Ir. A. M. TALMON

A thesis submitted in fulfillment of the requirements
for the degree of Master of Science

in the

Section Dredging Engineering
Department of Maritime and Transport Technology

September 12, 2018

TU Delft

Abstract

Faculty of Mechenical, Maritime, and Materials Engineering
Department of Maritime and Transport Technology

Master of Science

Validation of the 4 component model through experiments done in a 300mm diameter pipeline

by C. J. LUTEIJN

In the field of hydrotransport a model that is designed to predicting pressure losses in complex slurries has been developed in the form of the 4 component model over the last decade. Complex slurries are characterized by a very wide sieve curve or multiple distinct sieve curves within a single particle size distribution.

The goal of this thesis is to gain insight into the accuracy of the current version of the 4 component model. This was accomplished by gathering data of a wide variety of slurry mixtures over multiple flow regimes in a 300mm diameter pipeline. Sediments ranging in diameter from about 10μm to roughly 10mm were used in the experiments at concentrations ranging from about 5% to about 25%. The experimental results were then compared to a calculated hydraulic gradient using the 4 component model.

It can be concluded from the results that the hydraulic gradient is generally predicted to within 20% relative error for velocities above stationary bed regime by the 4 component model. Exceptions are when particles with a diameter larger than 1.5% of the pipe diameter are present in the mixture. Low concentrations of these large particles are universally detrimental to the accuracy of the 4 component model. It was shown that low concentrations of these large particles are best calculated using the heterogeneous transport model from the 4 component model instead of the stratified transport model.

The experiments also provided a good opportunity to test stationary deposition velocity prediction models on accuracy when transporting widely graded slurries. The Wilson model (1979) and two versions of the Durand model (1952 and 1953) were considered. The Wilson model was found to be the most accurate overall while also showing the most scatter in the results. The 1952 version of the Durand model is shown to be more accurate in predicting the stationary deposition velocity than the 1953 version, but the 1953 version provides some merit in being more conservative in its predictions.

In addition to the stationary deposition research, three methods of incorporating a widely graded slurry into the models were tested. It was concluded that simply using the d_{50} of the broad or multi-component sieve curve was the best course of action.

Acknowledgements

Contents

List of Figures

List of Tables

List of Symbols

A' modifying constant for effects of intergranular support in X_p fraction [-]

$B"$ modifying coefficient for effects of intergranular support from previous fractions in X_h fraction [-]

C' early version of the modifying coefficient currently known as C" [-]

C''' modifying coefficient for effects of intergranular support from previous fractions in X_s fraction [-]

C_v volumetric concentration of solids [-]

C_{vd} delivered volumetric concentration of solids [-]

d particle diameter [L]

d_h d_{50} of the X_h fraction [L]

d_{50} mass median diameter [L]

d_{85} diameter at which 85% of particles by mass are smaller [L]

D diameter of the pipe [L]

f_f Darcy friction factor [-]

g gravitational acceleration [LT^{-2}]

i hydraulic gradient [height of water/length of pipe]

i_f value of i for fluid flow [height of water/length of pipe]

i_m value of i for flow of mixture [height of water/length of pipe]

i_w value of i for flow of water [height of water/length of pipe]

j fraction gradient [height of mixture/length of pipe]

j_m measured fraction gradient [height of mixture/length of pipe]

j_s simulated fraction gradient [height of mixture/length of pipe]

M coefficient related to the width of the particle size distribution [-]

n_B correlation coefficient [-]

n_C correlation coefficient [-]

S_f relative density of fluid [-]

S_{fp} relative density of carrier fluid and pseudo-homogeneous fractions [-]

S_{fph} relative density of carrier fluid, pseudo-homogeneous, and heterogeneous fractions [-]

S_l relative density of liquid [-]

S_m relative density of mixture [-]

S_s relative density of solids [-]

X_f fraction of fine solids [-]

X_h fraction of heterogeneous solids [-]

X_{hl} fraction of the lower part of the heterogeneous solids [-]

X_{hu} fraction of the upper part of the heterogeneous solids [-]

X_p fraction of pseudo-homogeneous solids [-]

X_s fraction of stratified particles [-]

u_* shear velocity [LT^{-1}]

v_t terminal settling velocity of a particle [LT^{-1}]

V_{dl} velocity at limit of stationary deposition [LT^{-1}]

$V_{Hl,s}$ velocity of the 0.015D sized particle in the liquid [LT^{-1}]

V_m average slurry velocity [LT^{-1}]
V_r relative velocity, see Eq 2.12 [LT^{-1}]
V_{sm} maximum velocity at limit of stationary deposition [LT^{-1}]
V_{50} velocity at which 50% of particles are in suspension [LT^{-1}]

μ_s sliding friction coefficient [-]
μ_f dynamic viscosity of fluid (liquid + solids) [ML^{-1}T^{-1}]
μ_l dynamic viscosity of the liquid (no solids) [ML^{-1}T^{-1}]
μ_w dynamic viscosity of water at $20°C$ [ML^{-1}T^{-1}]
ρ_f density of the fluid [ML^{-3}]
ρ_m density of the mixture [ML^{-3}]
ρ_s density of the solids [ML^{-3}]
τ surface shear stress [ML^{-1}T^{-2}]

Chapter 1

Introduction

This introductory chapter provides a brief introduction towards the topic of physical modeling of slurry flow and specifically the 4 component model. Besides introducing the reader towards these topics, the structure of the thesis and the research are treated in this chapter as well.

1.1 Introduction towards physical modeling

Many models to calculate head loss in pipeline systems exist within the field of hydraulic engineering. Depending on the intended use of the model they can give wildly varying answers to the same question. Early models, like the Führböter model (1961), and Juffin & Lopatin model (1966), were mostly intended to be used in the mining industry and were concerned with the transportation of coal. They have the advantage of being highly versatile and modifiable and some of them are still being used today. A disadvantage of these models is that they model heterogeneous flow and as such are inaccurate when a sliding or stationary bed is formed in the pipeline. These older models are based almost solely on empirical data and as such, they offer the highest accuracy when the circumstances under which the experiments were performed are matched.

Since the 1980's there has been a large effort to construct a single model which captures all the physics for every imaginable solid-liquid flow. All physical phenomena, up to microscopic level, must be covered within this model to truly capture all the physics required to make accurate predictions. To this day no one has succeeded in achieving this, although not for lack of effort.

A promising model was developed by Wilson in 1979, a two layer model which predicted accurately the critical velocity of the mixture. The experiments conducted for this model resulted in the famous Wilson demi-McDonald nomograph. This model was later expanded by Wilson and Sellgren into the 4 component model. This model splits the mixture into multiple components each governed by its own set of rules for interactions with the liquid and particles. The smallest particles are rheologically inactive and contribute only towards the density of the carrier fluid. Larger particles are distributed according to increasing particle size into a pseudo-homogeneous, heterogeneous, and fully stratified regime respectively. An advantage of this model is that it can be applied to any distribution of particles due to its fractional nature. The fact that the effect of stratification is also considered offers great potential, but also a great challenge. The model has been extensively tested in laboratory settings but a certain degree of empiricism remains. Another problem is that unverified hypotheses are still present in certain coefficients within the model.

1.1.1   Introduction to the 4 component model

The main concern when pumping slurry over long distances is the head loss between two booster stations. Energy requirements for pumping slurry are directly related to the loss of pressure over the distance making this also an economic issue. The particle size and grading of the solids that make up the slurry have a major influence on the energy requirement of the slurry transport. It is these simple findings that already elude to the fact that differing particles behave differently towards the carrier fluid but also towards other particles. Early papers such as Wilson & Sellgren (2001), Wilson et al. (2006), and Sellgren & Wilson (2006) provided an increasing understanding on the effect of particle size distributions on friction losses.

Particles in the 4 component model are classified according to their behavior, which is directly related to the size of the particle. Up until recently the boundary values of each component were still being researched but definitive boundaries have since been established (Wilson et al. 2006). The behavior of the smallest particles is dominated by the viscosity of the fluid. A variable upper boundary of the pseudo-homogeneous component is directly related to the relative viscosity of the carrier fluid. The larger particles are being suspended by turbulent diffusion and as such, inertial effects of the turbulence are dominant here. Because the size of largest eddies is related to the pipe diameter, the boundary between the heterogeneous component and the stratified component is defined as a fraction of the pipe diameter. Energy transfer due to turbulent diffusion is not sufficient to sustain permanent suspension of the largest particles, these form a bed at the bottom of the pipe.

The smallest particles, the fines, typically smaller than 40μm, combine with the liquid and form a carrier fluid which resembles Newtonian behavior. Head loss is reasonably modeled by an equivalent liquid model.

The second smallest particles are classified as the pseudo-homogeneous fraction. These particles are typically between 40μm and 200μm, although the upper boundary may increase if the viscosity of the carrier fluid differs significantly from that of water.

Particles between 200μm and 0.015D are classified as the heterogeneous fraction. Here it is no longer the microscopic phenomena that dictate the interactions of particles. An upper boundary that is related to the pipe diameter and therefore eddy size is set. Inertial effects of the turbulence are dominant in this range.

Particles larger than 0.015D make up the grits of the slurry. When pumping conventional slurry densities, these particles are too heavy to be permanently suspended due to turbulence. Because of this they will occupy the bottom of the pipe where a bed is formed.

1.2 Problem statement

Under real world circumstances the sand production at the start of the pipeline system often consists of very wide particle gradings. The 4 component model attempts to describe how these widely varying particles interact with the fluid and with each other to predict pressure losses over distance. Current problems of the model are the lack of experimental data for larger pipeline sizes and the presence of empirical coefficients which are attributed to unverified physical phenomena.
Another expected issue with the model is the definition of the heterogeneous fraction. This fraction is related at the lower bound by the dynamic viscosity of the fluid and at the upper bound by the pipe diameter. It is hypothesized that head loss in this fraction will no longer be accurately predicted in large pipe diameters.
A secondary problem related to widely graded slurries has to do with the determination of a stationary deposit velocity. There is no agreed upon method of calculating the critical velocity when multiple particle size gradings are present in a slurry.

1.3 Research objectives

This study attempts to validate for the use of the 4 component model in large diameter pipelines. Tweaking of empirical coefficients and development of scaling parameters are secondary objectives. For purposes of clarity a single research question is stated like follows:

> *"To what degree is the current state of the 4 component model accurate in predicting pressure losses in a 300mm diameter pipeline?"*

Because such an expansive research provides a good opportunity to contribute towards other outstanding research topics as well, a secondary objective is formulated. The effect of slurry composition on the formation of a stationary deposition is examined. Data will be gathered on the V_{dl}, the velocity at which a stationary bed of sediments developed at the bottom of the pipe. Current models often make use of a d_{50}, the mass mean particle size. When applying these models on slurry compositions with multiple particle size gradings, determining the d_{50} is quite awkward. A multitude of methods exist to adjust V_{dl} determination models so predictions on the critical velocity can still be made. These will be tested against each other on accuracy. A secondary research question is formulated as follows:

> *"How to most accurately include the effects of multiple particle size gradings within a single slurry in a deposit limit velocity prediction model?"*

1.4 Thesis structure

Chapter 1 contains a very brief introduction towards the topic of physical modeling of slurry flow, and specifically the four component model. In addition the challenges and goals of the research are mentioned.
In chapter 2 the theoretical background of the individual models that makeup the 4 component model are explained in detail. Background on the parameters that are used in the equations is also provided to give an in-depth view of the way the model works. Some papers that have been important in the development of the model over the years are also touched upon to give additional background information. Finally

the topic of the deposit limit velocity is briefly treated, to provide theoretical background on the secondary objective of the effects of a wide particle grading on the accuracy of current prediction models.

The third chapter is about the laboratory equipment and the sediments used in the experiments. Some background information on the state of the lab or other conditions when carrying out the experiments is given as well.

Chapter 4 provides some insight into the experimental protocol. The test matrix is explained and a motivation for the experiments is provided. Additionally, it is explained how the obstacles that were ran into during the experiments were handled. There is also some information about the computer model that was used to extract the information from the raw data. The validity of the results is also briefly touched upon.

Many of the results from the experiments can be found in chapter 5. Such a vast amount of data results in a large amount of graphs and figures, many of these can be found in the appropriate appendices. In chapter 5 an interpretation of the results is also given. This is done by comparing the results of different experiments.

In the final chapter the conclusions of the entire research are drawn. Recommendation for further research are also made.

Chapter 2

Theoretical background

2.1 The 4 component model

Particle behavior can differ widely depending on the diameter. These different behaviors results in a hydraulic gradient that is dependent on the particle diameter. To make accurate predictions on pressure loss of a certain slurry, it can be useful to apply different models for different fractions within the slurry. The fractions are are defined based on particle behavior which is directly related to the particle diameter. Four different flow regimes are recognized in the four component model: (pseudo-)homogeneous flow, heterogeneous flow, and stratified flow. In this section The underlying physics which make up the base equations used in the four component model are explained.

2.1.1 Principles of solid-water interaction

Understanding how solid particles interact with the fluid is paramount in making sense of any physical model in existence. Water makes up the carrier fluid in all dredging practices, and will thus be the only fluid considered in this work. Firstly, visualization of the results is usually done in a graph that plots the pressure gradient as a function of delivered concentration and average velocity. This would have been sufficient to model any slurry, if it was not for the fact that both velocity and delivered concentration vary significantly in vertical direction resulting in complex structures within the flow. This stratification is due to the settling nature of the particulate matter within the slurry. A characteristic vertical concentration profile, dependent on mean velocity and mean concentration, appears after some distance from the pump. In this segregated flow a few distinct flow patterns can be deciphered. It should be noted that these flow patterns are highly dependent on particle size distribution, velocity and concentration. It can be observed during experiments that within a single cross-section, multiple flow regimes are present. This complicates the modeling as each regime is governed by its own set of equations, and interaction between regimes leads to difficult behavior. Flow regimes are treated separately before moving on to the more difficult subjects of interaction between the various particles fractions. The principles described in this section are based mainly on the third edition of the book "Slurry transport using centrifugal pumps" by Wilson et al (2006).

Homogeneous flow

A homogeneous flow is characterized by an evenly distributed concentration profile. The particles are evenly distributed throughout the cross-section of the pipe by turbulent diffusion. The smallest fraction of particles ($<40\mu$m) will combine with

the liquid to form the carrier fluid which typically resembles Newtonian behavior. Due to the rheological inactivity of these small particles, this combination of liquid and particles is perfectly modeled by an equivalent liquid model where the pressure gradient of the flow is only affected by the particles due to an increase in density of the fluid:

$$j = \frac{1}{\rho_m g}\left(-\frac{\Delta p}{\Delta x}\right) \tag{2.1}$$

Where j is the hydraulic gradient expressed in m of slurry per m of pipe. In calculations, the Darcy-Weisbach equation is almost universally applied for calculating pressure losses in homogeneous liquids. The same is done in the 4 component model where the hydraulic gradient of the carrier fluid is calculated like follows:

$$i_f = S_f f_f \frac{v^2}{2gD} \tag{2.2}$$

In which f_f is the Darcy friction factor and coefficient S_f is the relative density of the carrier fluid to that of water at 20°C, it can be calculated as follows:

$$S_f = S_l + \frac{C_v(S_s - S_l)}{1 - C_v} \tag{2.3}$$

Where S_l is the density of the liquid and C_v is the concentration of solids as a fraction of the whole. Equation 2.1 is used to calculate the hydraulic gradient of the carrier fluid. Particles larger than 40μm may no longer resemble Newtonian behavior. When this is the case the effect of these particles on the hydraulic gradient is typically given as a 'solids effect' or 'excess hydraulic gradient'. The solids effect is the increase in pressure loss on top of the hydraulic gradient of the fluid. It is defined as full mixture hydraulic gradient minus the hydraulic gradient of the carrier fluid ($i_m - i_f$). The solids effect can also be written down as Δi signifying the difference between the fluid hydraulic gradient and the mixture hydraulic gradient.
Particles slightly larger than 40μm will behave similar to the true homogeneous behavior described previously. Particles with a diameter between 40μm and 200μm will be similarly distributed throughout the pipe cross-section as the homogeneous fraction although a slight decrease in concentration with increasing distance from the bottom of the pipe can be measured. Because of this minor difference particles in this range will be referred to as 'pseudo-homogeneous' and in contrast to true homogeneous slurries it can no longer be considered as a Newtonian fluid. The reason they are still linked to the finest particles is that this fraction too can be modeled with reasonable accuracy by an equivalent liquid model. Using the hydraulic gradient of the carrier fluid and multiplying it by the term $C_v(S_s - S_f)$ to only capture the effect of the particles results in the excess hydraulic gradient for pseudo-homogeneous slurries. The expression for the excess hydraulic gradient of pseudo-homogeneous slurry flow is written like follows:

$$i_m - i_f = C_v(S_s - S_l)i_f \tag{2.4}$$

It can be seen that the excess hydraulic gradient in pseudo-homogeneous slurries really only takes into account an increase in density due to the particles. It is calculated identical to true homogeneous slurries.

Heterogeneous flow

There are various definitions used to describe heterogeneous flow. Universally these definitions agree that some percentage of the particles travel as contact loads and a major concentration profile gradient is present in the flow. When increasing particle size past roughly 200μm to a particle diameter of about 0.015 times the pipe diameter, the effect of particle settling becomes of major importance in the modeling of flow behavior. When entering the heterogeneous regime, the mean velocity of the slurry has drastic impact on the distribution of particles over the pipe cross-section. Especially near the limit deposit velocity a strong degree of non-uniformity can be observed. Due to this non-uniformity the expected pressure loss is far greater than that of homogeneous mixtures. The degree of heterogeneity or partial stratification, can be described by taking the ratio of the mean velocity and the settling velocity (v_m/v_t). Partial stratification is accompanied by a major increase in friction losses. The degree to which viscous and mechanic friction losses are proportioned in a partially stratified flow can be described by the stratification ratio:

$$\frac{i_m - i_f}{S_m - S_f} = 0.5\mu_s C_{vd}\left(\frac{V_m}{V_{50}}\right)^{-M} \tag{2.5}$$

In this equation μ_s is the mechanical friction coefficient which is usually defined as 0.44 and in the literature 0.5μ is often found as simply 0.22. Angularity of the particles composing the heterogeneous fraction should play a big part when defining this constant. Round particles may tend to roll instead of slide, decreasing the mechanical friction significantly. Some further remarks on the determination of this coefficient are presented in section 2.3.1. The coefficient V_{50} represents the velocity at which 50 percent of the particles in the pipe cross section are in suspension and M is a coefficient related to the width of the particle size distribution. These coefficients are calculated as follows:

$$M \approx [ln(d_{85}/d_{50})]^{-1} \tag{2.6}$$

$$V_{50} \approx 44.1d_{50}^{0.35}[(S_s - 1)/(1.65)]^{0.45}\nu_r^{-0.25} \tag{2.7}$$

In the 2017 publication on the 4 component model by Visintainer et al. it is mentioned that the value of M is always 1.0 when using the 4 component model. The constant 44.1 seen in the V_{50} calculation is sometimes seen as 3.93. This has to do with the dimension of the d_{50}, when the particle diameter is defined in meters a value of 44.1 should be used, and when the particle diameter is defined in millimeters a value of 3.93 should be used. The coefficient ν_r is the relative viscosity which represents the ratio of the actual viscosity of the carrier fluid to that of water at 20 °C, it can be calculated as follows:

$$\nu_r = \frac{\mu_f}{\mu_w}\frac{1}{S_f} \tag{2.8}$$

With all coefficients defined, the excess hydraulic gradient for heterogeneous flow can now be written as follows:

$$i_m - i_f = 0.5\mu_s C_{vd}(S_m - S_l)\left(\frac{V_m}{V_{50}}\right)^{-M} \tag{2.9}$$

This method of calculating pressure losses in heterogeneous flow regimes was developed by Wilson in 1992 and is known as the Wilson V_{50}-model.

Stratified flow

All, or almost all, particles in the stratified fraction travel as contact loads. Solids effect of stratified flow is therefore expected to be much larger than for any of the previous flow regimes. Identification of particles which will travel in a stratified manner is dependent on the ratio of particle diameter to pipe diameter. Large particles require large eddies to maintain turbulent suspension. If the pipe diameter is not large enough to produce eddies of sufficient size to carry certain particles in a suspended manner, they will settle at the bottom and form a bed. Typically particles with a diameter larger than 0.015D will travel in a stratified manner. Modeling the stratified fraction of the 4 component model is on the basis of relative velocity. The relative velocity is the ratio of the mean velocity over the limit deposit velocity of the 0.015D sized particle:

$$V_r = \frac{V_m}{V_{sm}} \tag{2.10}$$

The relative velocity gives a relation between the slurry velocity and the stationary bed. Wilson & Addie (1995) found that the relative excess pressure gradient can be approximated within reason by the following expression:

$$i_m - i_f = C_{vd}(S_m - S_l)\left(\frac{0.55V_{sm,s}}{V_m}\right)^{0.25} \tag{2.11}$$

It can be seen that the friction loss in stratified flow regimes is a function of the concentration and relative velocity.

2.1.2   Widely graded slurries

The different flow regimes as described in section 2.1.1 were related to the particle diameter. The contribution of a particle to the excess hydraulic gradient can be calculated by which flow regime it falls into. When a particles size distribution encompasses several of the flow regimes it becomes necessary to split the particle size distribution into multiple parts and calculate each portion according to the model that best predicts the excess hydraulic gradient due to that fraction. The flow regime dominant for particle size ranges were previously defined as:

X_f	$<40\mu$m	Homogeneous flow regime
X_p	40μm $<$ d $< 200\mu$m	Pseudo-homogeneous flow regime
X_h	200μm $<$ d < 0.015D	Heterogeneous flow regime
X_s	>0.015D	Stratified flow regime

The left hand side of the list above displays the fractions which are used in the four component model. Each fraction signifies a portion of the solids in the slurry which fall in the particle diameter range displayed in the middle column. The contribution of these particles to the hydraulic gradient are then calculated according to the model which best suites the flow regime which the particles fall under. To combine the models described in section 2.1.1, some additions must be made to the equations. The first equation calculating the hydraulic gradient of the carrier fluid contains a parameter denoting the density of the carrier fluid. This parameter

must be modified when multiple fractions are present in the mixture. A term X_f is included in the calculation of the fluid density to only include the fines (particles falling under the true homogeneous flow regime) in the calculation of S_f:

$$S_f = S_l + \frac{X_f C_v (S_s - S_l)}{1 - C_v (1 - X_f)} \tag{2.12}$$

The same is necessary in the calculation of the excess hydraulic gradient due to the pseudo-homogeneous fraction. When fines are present in the mixture the coefficient S_l is replaced with S_f (like shown in equation 2.12) to include the increase in density of the carrier fluid due to the fines. Also a parameter X_p is added to only capture the pseudo-homogeneous particles in the flow. And finally, a coefficient (A') to account for the effects of hydrodynamic lift is added in the equation resulting in the following expression for the excess hydraulic gradient of the pseudo-homogeneous fraction:

$$\Delta i_p = A' X_p C_v (S_s - S_f) i_f \tag{2.13}$$

A similar approach is taken when modifying the heterogeneous fraction equation. To specifically define the solids effect of the heterogeneous fraction, the right hand side of equation 2.9 must be multiplied with the fraction of heterogeneous particles X_h, and $(S_m - S_f)$ must be replaced with $C_v (S_s - S_{fp})$ where S_{fp} represents the relative density of the carrier fluid and pseudo-homogeneous fraction. S_{fp} is calculated as follows:

$$S_{fp} = S_l + \frac{(X_f + X_p) C_v (S_s - S_l)}{1 - C_v (1 - X_f - X_p)} \tag{2.14}$$

Finally the coefficient $C"$, taking into account the effect of intergranular support, must be added to the equation. When all these changes are made the final equation expressing the excess hydraulic gradient of the heterogeneous fraction is formulated:

$$\Delta i_h = C" \frac{\mu_s}{2} C_v X_h (S_s - S_{fp}) \left(\frac{V_m}{V_{50}} \right)^{-M} \tag{2.15}$$

Lastly the equation for the stratified fraction is modified in the same manner. By rewriting $(S_m - S_f)$ to $C_v (S_s - S_{fph})$ and multiplying it by the fraction of stratified particles X_s the solids effect of the stratified particles can be expressed. The coefficient S_{fph} is the relative density of the X_f, X_p, and X_h-fractions and is expressed as follows:

$$S_{fph} = S_l + \frac{(X_f + X_p + X_h) C_v (S_s - S_l)}{1 - C_v (1 - X_f - X_p - X_h)} \tag{2.16}$$

Like in the calculation of the previous fractions, adding a term that takes into account the effects of intergranular support is done in the form of $B"$ and then finally adding a friction factor, the following expression for the solids effect of the stratified component is formulated:

$$\Delta i_s = B" \frac{\mu_s}{0.44} C_v X_s (S_s - S_{fph}) \left(\frac{0.55 V_{sm,s}}{V_m} \right)^{0.25} \tag{2.17}$$

With the equations to calculate excess hydraulic gradients for each fraction now defined we can combine them into a single formula:

$$i_m = i_f + \Delta i_p + \Delta i_h + \Delta i_s \tag{2.18}$$

Together, equation 2.2, 2.13, 2.15, and 2.17 makeup the four component model like shown above in equation 2.18. With these four equations the hydraulic gradient of slurries consisting of multiple or very wide particle size gradings can be calculated. Some unexplained coefficients remain in the model. The intergranular support coefficients are treated in the next section.

2.1.3   Intergranular support

Equations for estimating head loss in different flow regimes were treated earlier. In theory these equation should be sufficient to determine the head loss for any pipeline imaginable. Sadly, in practice this is not the case. This is why empirical coefficients have been developed in recent years. These coefficients are added to the 3 larger components, as the equivalent liquid model used to model the behavior of the fines accurately predicts headloss in this fraction making it unnecessary to add a coefficient to this fraction. The equations for the pseudo-homogeneous, heterogeneous, and stratified components respectively, were previously determined as follows:

$$\Delta i_p = A' X_p C_v (S_s - S_f) i_f \tag{2.19}$$

$$\Delta i_h = C'' \frac{\mu_s}{2} X_h C_v (S_s - S_{fp}) \left(\frac{V_m}{V_{50}}\right)^{-M} \tag{2.20}$$

$$\Delta i_s = B'' \frac{\mu_s}{0.44} X_s C_v (S_s - S_{fph}) \left(\frac{0.55 V_{sm,s}}{V_m}\right)^{0.25} \tag{2.21}$$

With A, B, and C the modifying coefficients for the effects of intergranular support from previous fractions for the pseudo-homogeneous, stratified, and heterogeneous components respectively. Sophisticated formulae have been developed for the determination of coefficients A, B, and C.

$$A' = 1 - 0.25 X_p \tag{2.22}$$

$$B'' = 1 - (B''_f X_f + B''_p X_p + B''_h X_h) \left(\frac{V_{Hl,s} - V_m}{V_{Hl,s} - V_{sm,s}}\right)^{n_B} \tag{2.23}$$

$$C'' = 1 - (C''_f X_f + C''_p X_p) \left(\frac{V_{Hl,s} - V_m}{V_{Hl,s} - V_{sm,h}}\right)^{n_C} \tag{2.24}$$

The parameter $V_{sm,h}$ and $V_{sm,s}$ used in equation 2.24 and 2.23 respectively are the maximum velocity at the limit of stationary deposition for the d_h and the 0.015D sized particles. These are read from Wilson's famous demi McDonald nomograph (Wilson 1979).
The parameter $V_{Hl,s}$ used in the equations above is the velocity of the 0.015D sized particle. It is calculated according to the Newitt method (Newitt et al. 1955):

$$V_{Hl,s} = \sqrt[3]{1800 g D v_t} \tag{2.25}$$

An average hydraulic gradient prediction error of slightly over 5% was achieved using the above formula in a study by Visintainer et al. (2017). In the GIW experiments dating from 2016, some good results for B″ and C″ were obtained with four of the correlation coefficients set as 0.5 and the rest set as unity. Using these values for the correlation coefficients, equation 2.23 and 2.24 reduce to the following form:

$$B" = 1 - (X_f + X_p + 0.5X_h)\left(\frac{V_{Hl,s} - V_m}{V_{Hl,s} - V_{sm,s}}\right)^{0.5} \tag{2.26}$$

$$C" = 1 - (X_f + 0.5X_p)\left(\frac{V_{Hl,s} - V_m}{V_{Hl,s} - V_{sm,h}}\right)^{0.5} \tag{2.27}$$

Using these equations to calculate the coefficients A′, B″, and C″ resulted in an average error of 5.4% in the 100mm loop and 5.3% in the 200mm loop in the 2017 GIW experiments.
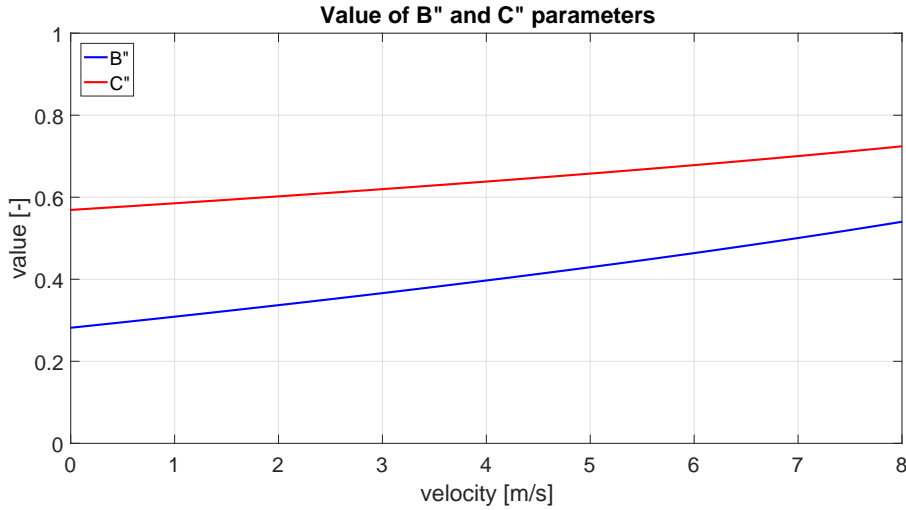
FIGURE 2.1: Values of the coefficients B″ and C″ for a slurry with characteristics: C_v=30%, X_f=0.25, X_p=0.25, X_h=0.25, and X_s=0.25. B″ and C″ are defined as equation 2.26 and 2.27 respectively.

The effects of intergranular support have been attributed to the effects of hydrodynamic lift. This effect describes how particles are repelled from a surface in the presence of a boundary layer. Particles within the turbulent portion of horizontal pipeline flow are kept in suspension by turbulent diffusion. In a steady state, a characteristic concentration profile is formed and for any particles that settle downward an equal amount of particles must move upward to maintain this concentration profile. This condition of the upward and downward flux of particles being equal is met within the fully turbulent part of the suspension, but it leads to complications near the bottom wall of the pipe. Within the viscous boundary-layer, turbulence is no longer effective. So any particles that fall from the turbulent part of the flow into the laminar boundary layer near the wall will no longer be suspended through merit of turbulent diffusion. The steady state concentration profile condition must remain to be met though, so for any particles that fall into the boundary layer an equal amount of particles must be repelled from it. The repelling force has been dubbed hydrodynamic lift and it has been theorized that it contributes to a high-lift zone near the wall.

This effect is not yet what is called intergranular support. Wilson & Sellgren (2002)

argued that the turbulent energy spectrum within a turbulent fluid is affected by solid particles. It is known that stationary objects within a flow may create spectral peaks in the turbulent energy spectrum by shedding vortices. It is expected that movable particles will have an opposite effect, damping eddies of roughly their own size, causing a small gap of reduced energy density at this frequency. For highly concentrated broadly graded slurries this gap may widen to a large trough. Sellgren & Wilson (2006) hypothesized that a benefit may be obtained when a slurry contains particles that are directly affected by the hydrodynamic lift force, and slightly larger particles. The smaller particles, subject to significant hydrodynamic lift forces, will rise from the boundary layer until they bump into larger particle contributing to its support within the fully turbulent part of the flow. The smaller particle is reflected back into the boundary layer where it again experiences a large repelling force.

It seems intuitive to assume that a thicker boundary layer would contribute more to the hydrodynamic lift effects than a thin boundary layer. This feeling is supported by the current definition of the coefficients B" and C" which reduce the resistance with decreasing velocity. A visualization of the effects of hydrodynamic lift can be seen in figure 2.1 where coefficients B" and C" are displayed for a slurry containing 30% solids of equal parts C_f, C_p, C_h, and C_s at various velocities. It can readily be seen that the modeled intergranular support is much larger for the stratified part of the particles than it is for the heterogeneous part of the particles.

Although coefficient A′ is named similarly, it should be seen independently from the intergranular support coefficients B″ and C″. the coefficient A′ reduces the friction due to the effects of hydrodynamic lift and turbulence effects. Although the literature does not offer much explanation into how exactly these phenomena achieve this reduction.

Having mentioned all of this, it is important to note that while applying the modifying coefficients in this way leads to good results, the physical explanation of near wall hydrodynamic lift and intergranular support have not been proven.

Remarks on intergranular support coefficients

In the current definition of the intergranular support for the heterogeneous and stratified fraction (equation 2.18 and 2.19) there is a weighted contribution of the previous fractions. For the heterogeneous fraction the fines contribute fully, and the larger pseudo-homogeneous particles contribute only half. The intergranular support coefficient of the stratified fraction is reduced fully by the fines and pseudo-homogeneous fractions while being only reduced half by the heterogeneous fraction. This seems very counterintuitive given the explanation of intergranular support: The smaller particles bump into the larger particles keeping them in suspension. It seems strange that the small fines fraction ($d < 40\mu m$) has a larger impact in keeping the stratified particles in suspension than the much larger heterogeneous particles would.

It appears to be quite likely that due to the complexity of these functions they no longer represent the actual physics happening in the flow, but rather serve to align the analytical values to the experimental data.

2.1.4   Remarks on various parameters used in 4 component model

The 4 component model is very complicated and uses many parameters. All of these parameters will have to be determined before a calculation can be ran. In this subsection some important parameters will be treated. This will make it easier to compare

results with any future experiments.

Sliding friction factor

The sliding friction coefficient, μ_s, is used in the calculation of the heterogeneous and the stratified fraction. This factor has a major influence on the calculation of the excess hydraulic gradient of the heterogeneous (eq. 2.11) and of the stratified fraction (eq. 2.15). A fixed ratio appears to be present in the current version of the 4CM where μ_s is divided by 2 in the heterogeneous fraction and μ_s is divided by 0.44 in the stratified fraction. It would seem more logical to determine sliding friction coefficient independently for each fraction.

If it was possible to determine a universal constant for the sliding friction coefficient, there appears to be no consensus on the value. In a paper by Sellgren et al. 2016, a value of μ_s=0.44 is used. While in visintainer et al. 2017 a value

FIGURE 2.2: Photos of X_s-fraction used in the experiments for this thesis (top) and those used in the 2017 GIW experiments ,Visintainer et al. 2017, (bottom).

of μ_s=0.50 is used. An earlier paper by Sellgren and Wilson published in 2007 makes no use of a sliding friction coefficient yet. This makes it seem like the addition of this coefficient is a recent addition to the 4 component model and additional data might be much needed to fine tune the contribution this coefficient makes.

Something to consider is that the very round particles that make up the stratified fraction in this research (see figure 2.2) may tend to roll instead of slide. This will dramatically reduce hydraulic gradient which is reflected in the results of this research. When pumping solely X_s-fraction a sliding friction factor of 0.25 results in much more accurate predictions of the model. When working with compositions made up of multiple fractions however, a sliding friction factor of 0.50 gives more accurate predictions. This leads to the suspicion that sliding friction factor is affected by the interaction between the different fractions.

Particle terminal settling velocity of X_s-fraction

The terminal settling velocity plays a minor role in the calculation of $V_{Hl,s}$, as seen in equation 2.25. To get a full picture of the entire model it should be made clear how this parameter is determined. The calculation of the terminal settling velocity is done according to the calculation of a sphere. This is deemed reasonable for the particles used in the experiments for this thesis. See figure 2.2 for a picture of the X_s-fraction.

For large Reynold's numbers the drag coefficient of a sphere is effectively constant at 0.445 (Wilson et al. 2003). The terminal settling velocity for the d_{50} of the X_s-fraction can now be determined according to the following relation:

$$0.455 = \frac{8}{(v_t/u_*)^2} \tag{2.28}$$

The shear velocity is the square root of the surface shear stress over the fluid density. A mean surface shear stress is calculated by taking the downward force (submerged weight) over the surface area of the d_{50}-sized sphere:

$$u_* = \sqrt{\overline{\tau}/\rho_f} \qquad (2.29)$$

$$\overline{\tau} = (\rho_s - \rho_f)gd/6 \qquad (2.30)$$

The terminal settling velocity of a 0.015D sized particle can now be determined according to the combined equation:

$$v_t = 4.24u_* \qquad (2.31)$$

Keep in mind that when working with very angular particles this approximation may no longer be accurate. A shape factor should be applied in this case.

Velocity at limit of stationary deposition

The parameter V_{sm} is used in the determination of the coefficients B" and C" (see eq. 2.26 and 2.27), and plays a role in the calculation of the excess hydraulic gradient due to the X_s-fraction (see eq. 2.17). Multiple methods for determining the mean flow velocity at the limit of stationary deposition exist, most famously Wilson's nomograph (Wilson 1979). As an extension on Wilson's nomograph, a publication by Sanders at al. (2004) presented an approximation that is more suitable for larger diameter particles:

$$V_{sm} = \left(\frac{0.018}{f_f}\right)^{0.13} \sqrt{2gD(S_s - S_f)} \qquad (2.32)$$

Application of this method for the 0.015D sized particle in a 300mm size pipe and a friction factor of 0.012 yields a value of 3.29 m/s. This is significantly higher than the 2.2 m/s which Wilson's nomograph indicates. The sanders cutoff for large diameter particles is relevant when considering the 0.015D sized particle, but there are some additional extensions on the Wilson model for determining V_{sm}, these are treated in more detail in section 2.3.

A concern with using the V_{sm} (which is independent on particle concentrations in the mixture) in opposition to V_{dl} is that, especially for large diameter particles, concentration plays a huge factor in the establishment of a stationary bed. Using V_{sm} is easier because it only needs to be calculated once for a single particle diameter. But when concentrations are known, using V_{dl} may prove to yield more accurate results.

2.2   Analysis of previous publications

With the theoretical foundation laid a look should be taken to the available data on the model. The 4 component model finds it origin in the Wilson V_{50} model which was introduced in 1992. In more recent years research on the effect of particle size grading on friction losses have increase our understanding of the subject. A multi-component model proposed in the early 2000's by Wilson and Sellgren laid the foundation for a composite model which used different calculations for particles of varying sizes. More recent publications have helped establishing the four component model in the way we are currently familiar with.

2.2.1 Wilson & Sellgren 2007

Early work was done by Wilson and Sellgren in 2007 which combines work from publications made in the early 2000's (Wilson & Sellgren (2006), Wilson et al. (2001) and Sellgren & Wilson (2006)) in an attempt to create a single model which is applicable for broad graded slurries. They compared a wide range of sediments, concentrations, and pipe diameters. The data they used were collected from various publications. A limitation of the collected data in this publication is that it states the pressure gradient only for one velocity. And besides the limited velocity interval, the intergranular support coefficients weren't yet defined as they are in current publications. The concepts of hydrodynamic lift were only proposed in the decade prior to this publication. Hydrodynamic lift and turbulence effect were assumed to affect 25% of X_p particles resulting in the previously discussed equation: $A' = 1 - 0.25X_p$. There was no coefficient taking into account the effects of intergranular support on the heterogeneous fraction. A coefficient '0.22' in the calculation of the hydraulic gradient of the heterogeneous fraction is related to the portion of particles that contribute to the mechanical friction at the wall pipe. The coefficient B' in the stratified hydraulic gradient calculation was defined individually for each experiment to provide the best fit, values between 0.20 and 0.25 seemed to be conventional.

Taking these things into account, comparison of the data of this early publication with results from more recent publications should be done with caution. The data of this publication is displayed in table 2.1, where j_m is the measured friction loss in meter slurry per meter pipe and j_s is the simulated result.

#	D(m)	V(m/s)	$C_v(\%)$	S_s	d_{50}	d_h	d_{max}	X_f	X_p	X_h	X_s	j_m	j_s
1	0.305	4.5	15	2.65	0.70	0.90	12	2	23	60	15	0.060	0.063
2	0.305	4.5	27	3	0.85	0.85	65	20	15	30	35	0.075	0.075
3	0.1	2	13	2.65	0.085	0.23	0.25	-	98	2	-	0.034	0.034
4	0.438	4	38	2.65	0.20	0.40	0.9	18	32	50	-	0.029	0.028
5	0.263	3.1	26	2.65	0.17	0.27	1.5	28	30	42	-	0.026	0.027
6	0.206	2	30	2.71	0.085	0.33	0.6	25	65	10	-	0.016	0.015
7	0.206	3	32	2.65	0.2	0.32	0.5	4	46	50	-	0.030	0.033

TABLE 2.1: Data from rows 1 through 3 are repectively from Sundqvist et al. (1996a), Sundqvist and Sellgren (2004), Whitlock et al. (2004). Row 4 contains oil-sand tailings data. Data in row 5 was obtained by Shook & Roco (1991), and the data presented in row 6 and 7 are gold-tailings results from Sauermann (1982). This data was published by Wilson and Sellgren in 2007.

The materials used in the experiments do contain some sediments which are not often encountered in conventional offshore dredging operations. The 2007 version of the 4 component model does seem to model the experimental results to within 10%.

Experimental results of a study, Whitlock & Sellgren (2004), on the effect of fine particles on the hydraulic gradient were also compared to simulated results in this paper. Two sets of experimental results were given, the first with mostly X_h-particles and the in the second a good portion of the X_h particles replaced with rock flour particles with median size 0.04mm.

The large reduction in friction loss which can be observed in table 2.4 was contributed mainly to the hydrodynamic lift gradient contribution of the X_f particles. A final table with data from a phosphate matrix containing clay first presented by

#	D(m)	V(m/s)	C_v(%)	S_s	d_{50}	d_h	d_{max}	X_f	X_p	X_h	X_s	j_m	j_s
1	0.495	4.5	24	2.65	0.35	0.3	0.9	-	5	95	-	0.038	0.037
2	0.495	4.5	24	2.65	0.35	0.3	0.9	10	15	75	-	0.028	0.027

TABLE 2.2: Comparison of modeled friction losses with the reported experimental data for sand with added rock flour (#2) and without rock flour (#1). This data was presented in this way by Wilson and Sellgren in 2007.

Addie et al. (2005) was given in this paper. It was mentioned in a later paper (Sellgren et al. 2016) that the upper boundary of the X_p-fraction increases for rheologically active particles according to the viscosity ratio. The clay particles will definitely have an effect on the viscosity of the carrier fluid, resulting in X_p-fraction which may have been defined as too small when comparing it to the newer version of the 4 component model. The data of the phosphate matrix products is presented in table 2.6 below.

#	D(m)	V(m/s)	C_v(%)	S_s	d_{50}	d_h	d_{max}	X_f	X_p	X_h	X_s	j_m	j_s
1	0.495	5	27	2.65	0.25	0.35	1.5	10	30	70	-	0.035	0.034
2	0.495	4.4	27	2.65	0.25	0.80	6.0	17	28	55	-	0.047	0.044
3	0.495	4.4	27	2.65	0.50	0.45	20	14	21	51	8	0.045	0.042

TABLE 2.3: Comparison of modeled friction losses with the reported experimental data from phosphate-matrix products with added clay from the research by Addie et al. (2005). This data was presented in this way by Wilson and Sellgren in 2007.

The modeled values of the simulated hydraulic gradient of the data presented in table 2.6 is the same as that of water. It can be seen that even with this simplification the model is very accurate, with all results falling within 10% accuracy.

All in all, the performance of the model seem to be extraordinarily optimistic. An explanation for the accuracy of the model as presented in this paper may be that the majority of the data was gathered well into the heterogeneous regime at 4 m/s and up. When data at lower velocity was presented it was often with large parts X_p and X_f which show very little settling behavior. Also the B' coefficient present in the calculation of the X_s-fraction hydraulic gradient is defined at will according to what suits the experimental data.

2.2.2   Sellgren et al. 2016

A second study from 2016, conducted by Sellgren, Visintainer, Furlan, and Matousek, introduced a coefficient in the heterogeneous part of the model. Like the coefficient B', this coefficient quantifies the reduced friction loads as a result of hydrodynamic lift. The coefficient C' is not yet defined in the form we are currently familiar with, it was defined in this paper as:

$$C' = \frac{d_h - 0.0002}{0.0005 - 0.0002} \quad \text{for} \quad 0.0002 < d_h < 0.0005 \quad \text{and} \quad \nu_r = 1 \qquad (2.33)$$

$$\text{otherwise} \quad C' = 1 \qquad (2.34)$$

The problem with coefficient B' remains that it is not well defined and basically chosen to the liking of the user of the model to best suit the experimental data. A

number of sands have been tested in the experiments. But like the 2007 tests conducted by Wilson and Sellgren, data has been published at only one velocity per run. The table also only shows X_f and X_s-fractions which composed the mixture. The accompanying graph, figure 2.2, shows the particle size gradings as they were published in the original paper, the remaining X_p and X_h can be read from this graph. Table 2.2 shows the values that were obtained by the publishers.

#	D(m)	V(m/s)	$C_v(\%)$	S_s	d_{50}	d_{85}	d_{max}	X_f	X_s	j_m	j_s
1	0.098	2.5	20	2.65	0.47	0.6	1.2	-	-	0.098	0.098
2	0.098	2.5	20	2.65	1.56	2.3	7	-	55	0.100	0.100
3	0.203	4	27	2.85	0.3	3.4	20	30	18	0.100	0.079
4	0.305	4.5	27	3	0.85	20	65	20	35	0.075	0.077
5	0.305	4.5	15	2.65	0.7	4.5	12	2	15	0.060	0.064
6	0.205	4	13.5	2.65	4.1	12	15	-	57	0.11	0.081

TABLE 2.4: Comparison of modelled losses versus measured losses for various sands, pipeline diameters, and velocities. Displayed data was published by Sellgren et al. in 2016. The full particle size distribution is as displayed in figure 2.2
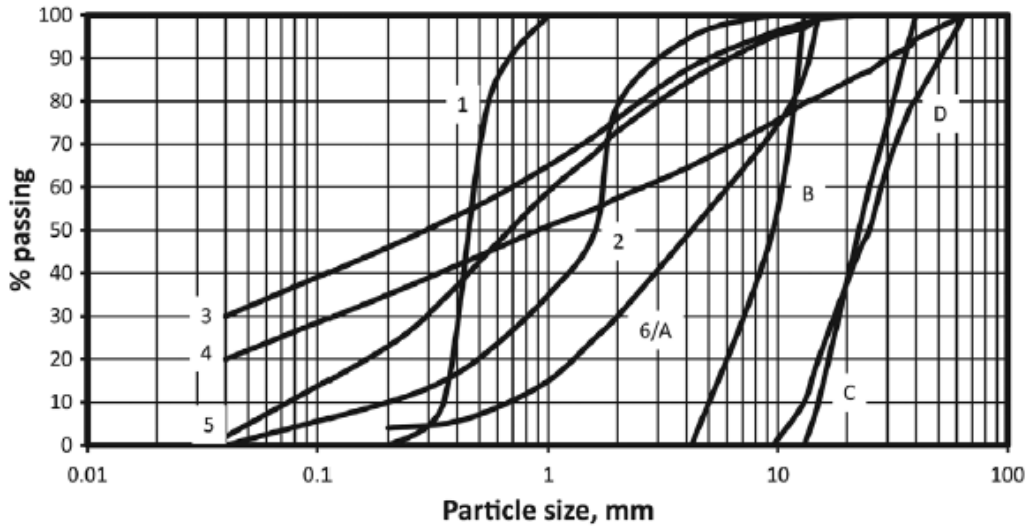
FIGURE 2.3: Particle size distribution of slurries used in the 2016 experiments by Sellgren et al. The source of this image is that same paper.

It can be seen that rather large errors in the calculated losses were made in experiment 3 and 6. These characteristics of these experiments do not seem to have much in common and an explanation for these underestimates cannot be given. The original authors attempted to link the underestimation of the model to a misrepresentation of coefficient B'. This coefficient was described a value of ~0.35 which led to the massive underestimation of test #3 in table 2.7. The coefficient B' should not have been represented by a single constant for all possible scenarios. According to this explanation it would seem that experiment 2, which also has a sizable stratified fraction, would also be falsely predicted by the model which is not the case. The findings in this paper led to the definition of a dynamic coefficient B' and C' as they were defined in equation 2.20 and 2.21.

Another addition that was made in this version of the 4 component model is in the upper boundary of the X_p-fraction. Previously this boundary was set at a hard value of 200μm, in this version the boundary is defined as $0.0002\nu_r$.

2.2.3   Miedema 2016

Miedema, associated with the Technical University of Delft, studied the 4 component model extensively and has made a comprehensive report on it. The result of his study has been published in 2016. It is a good idea to take a look at Miedema's findings and opinions.

The first criticism is that the four fractions defined in the four component model are defined too rigidly and do not depend on the velocity and only partly (only the stratified fraction) on the pipe diameter. The four component model bases these fraction boundaries on experiments done mainly around the working point of a conventional dredging pump. At velocities lower or higher than the working point, the boundaries of the components will differ from the fixed definition.

A second point raised in Miedema's work is on the Wilson V_{50} model used for determining the hydraulic gradient of the heterogeneous fraction. The velocity $'V'_{50}$ symbolizes the speed at which 50% of the particles are in suspension, and 50% travel as contact loads. The sliding friction factor which is usually taken as $'\mu_s = 0.44'$ is taken as only half. This makes the awkward assumption that the 50% of particles that are in suspension make no contribution to the hydraulic gradient at all. An adjusted equation is given in Miedema's work which includes the contribution to the hydraulic gradient of the particles that are in suspension.

Another remark is that the μ_s coefficient used to symbolize the sliding friction is used as 0.44 in the model used to calculate the heterogeneous fraction contribution and this same coefficient is used as 0.40 (Miedema studied the 2006 Wilson et al. publication, 0.50 is used for μ_s in the most recent 2017 publication by Visintainer et al.). The four component model should be internally consistent and use a single value for the sliding friction factor.

2.2.4   Visintainer et al. 2017

The conclusions of the 2016 paper by Sellgren et al. described before were incorporated into the most resent publication on the 4 component model which was presented at the 2017 Hydrotransport conference in Melbourne. The theory described in this paper is described in detail in chapter 2.1 and 2.2. In this paper a massive amount of experiments were executed in a 4 inch and an 8 inch pipeline. The great thing about these experiments is that the data was recorded for the first time over a velocity interval. This gives greater insight into the performance of the 4 component model when approaching stationary deposition velocity and when pumping near commercial velocities. Sadly, because of the vast amount of data, not all of the data has been published in this one paper and no tables with exact values of the experiments have been included. The data can be read with reasonable accuracy from the graphs, but it should be noted that there are no exact values available. Especially since the data has been plotted on a double logarithmic scale, reading the graph can be a little bit difficult.

The slurries that were used in the 2017 GIW experiments were composed of four different sands. These sands were then blended to form widely varying slurries easily spanning all four fractions of the model. The four base sediments were described in the paper as follows:

X_f A silica based 'rock flour' with approximately 88% passing 40μm.

X_p A silica sand product with roughly 90% falling between 40 μ m and 0.2mm.

X_h Waste rock from a granite quarry, screened in the lab to remove fines, resulting in a product with approximately 80% falling between 0.2mm and 3mm.

X_s A commercially screened granite product with approximately 90% lareger than 3mm and a topside of approximately 12.5mm.

With these 4 sands a wide range of experiments have been performed in both a 100mm pipe and a 200mm pipe. This vast amount of data allowed for a massive study on the coefficients B" and C". The theoretical definitions of these coefficients are found in equation 2.20 and 2.21. A study on the optimization of the correlation coefficients concluded that by setting setting 4 of the correlation coefficients (B_h", C_p", n_B and n_C) to 0.5 the relative error can be reduced to slightly over 5%. The resultant of this study on the correlation coefficients resulted in the current form of C" and B". In chapter 2.2 a more detailed analysis of the intergranular support coefficients is found.

2.2.5 Remarks on publications on four component model

The density of the used sediments is not mentioned in the paper, so we have no choice but to assume it is somewhere around 2650 kg/m3. This seems like a safe assumption since it is specifically stated that silica and granite products were used. Another property of the two largest sands that should not be overlooked is the angularity. The X_h and the X_s fractions appear to be extraordinarily angular. This may point to very high friction in sliding bed regimes. Since there is still some debate about the correct value of the Coulomb friction coefficient within slurry transport models, it appears to be a good idea to inventorize commonly used values. Within the 4 component model though, the Coulomb friction coefficient cannot be seen separately from the intergranular support coefficients B" and C" which have been treated in section 2.2. The coefficients B" and C" take into account the volumetric concentration and the velocity of the concerning fractions, while the Coulomb frictions factor takes into account the mechanical friction of the concerning fraction. Since only one constant value for the Coulomb friction has been defined, it is assumed in the model that the friction coefficient is the same for the heterogeneous part and the stratified part. This would make no sense when an angular crushed sand, and a smooth natural gravel occupy respectively the heterogeneous fraction and the stratified fraction. It seems that a Coulomb friction factor would have to be defined per fraction for a multi-component slurry.

A remark about the method of achieving optimal correlation in the intergranular support coefficients is that the correlation coefficients seem to have been defined as either 0.5 or 1.0 seemingly at random without any explanation. The coefficients B" and C" appear to have no basis left in actual physics and just serve to fit the analytical results to the experimental data.

A final remark about an unclarity is regarding the definition of the friction factor, f_f, used in the Darcy-Weisbach equation. No mention has been made in any of the publications about the definition of this coefficient. Since a large number of equations are available on how to calculate the friction factor, only a guess can be made about which one has been used by the authors. It also appears to be constant which would result in inaccuracies when approaching sliding bed and stationary bed regimes.

2.3   Velocity at limit of stationary deposition

Wide gradings or multiple gradings within a single slurry affect many properties of
the flow. Besides the pressure gradient also the deposit limit velocity of the slurry
is influenced. To make a calculated guess of the deposit limit velocity, again a four
component approach can be applied. In the publication of Matousek et al. (2017),
a large amount of data has been processed. Wide graded slurries have been tested
using different calculation methods and averaging methods. For sake of clarity it is
mentioned that there are many different terms for the deposit limit velocity. Critical
velocity, velocity at limit of stationary deposition and deposit limit velocity can all
be encountered in this section. All these terms mean the same thing: the highest
velocity at which a stable stationary bed of sediment, however small, is formed on
the bottom of the pipe.

The definition for the V_{dl} that was used in the 2017 publication by Matousek is the
average velocity at which grains first stop moving and start to form a deposit at the
bottom of the pipe. This definition can be somewhat difficult to apply under real
world circumstances, as especially for coarse grained slurries a bed is not really well
defined. In coarse grained slurries the sediment tends to form temporary clusters at
the bottom of the pipe when approaching V_{dl}. A stationary bed may appear stable
but will be washed away occasionally by a density wave before instantly reestab-
lishing itself. This semi stationary state leaves pinpointing the establishment of a
stationary bed to the interpretation of the observer. For finer grained sediments the
development of a deposit is a much more stable process where usually clusters or a
sliding bed are not formed. Instead, a stationary deposit is formed with no transi-
tional phases.

Determining when the deposit limit velocity is reached by visual observation of a
clear section of the pipe is subject to a great degree of uncertainty. Especially when
considering that the development of a deposit may be an unstable process. The
judgment of the viewer influences the visual data to a large degree. A considerable
scatter in the data is to be expected. Because of the errors made when visually de-
termining the deposit limit velocity a relative error is to be determined. This is done
by evaluating the agreement between the (visually) measured deposit limit velocity
and the calculated velocity in the following manner:

$$E_r = \sum \left[ABS \left(\frac{V_{dl,calc} - V_{dl,meas}}{V_{dl,meas}} \right) \right] / N \tag{2.35}$$

In this equation N is the number of experimental data points and E_r is the rela-
tive error.

The calculation of the deposit limit velocity can be done by a multitude of equations.
In this thesis two of the most conventional methods will be treated. The method
used by Durand (Durand & Condolios 1952), and the famous nomograph method
developed by Wilson (Wilson 1979).

2.3.1 V_{dl} calculation methods for widely graded slurries

When multiple sediments are present in a single slurry the calculation of a deposi-
tion limit velocity becomes quite difficult. The only current way to do this revolves
around taking a weighted average. The question remains where and how to apply a
weighted average. Recent work (Matousek et al. 2017) has attempted to offer some

insight into this problem. This work compares the results of the Shanghai experiments with the findings of Matousek et al. (2017). Three methods calculating the V_{dl} have been proposed in the paper by Matousek:

I. The mass-median d_{50} is determined from the PSD curve and used in a V_{dl} model.

II. The weighted mean size of transported solids is determined and used instead of the d_{50} in a V_{dl} model.

III. V_{dl} is calculated separately for each fraction and the weighted mean V_{dl} is determined.

The mean diameter for the first method is easily read from a particle size distribution just like a conventionally distributed sediment. For the second and third method a minor calculation must be done. The calculation of the mean diameter for the second method is like follows:

$$d_m = \sum (X_i d_i) \tag{2.36}$$

In which index i denotes the individual fraction in the same way it does in the four component model (i = f,p,h,s) and the X is the proportion of the fraction in relation to the whole, i.e. $\sum X_i = X_f + X_p + X_h + X_s = 1$. The third method does not depend on a single d_{50} for which a deposit limit velocity is calculated. For the third method the V_{dl} is calculated for each fraction for which a weighted average is then calculated like so:

$$V_{dl} = \sum (X_i V_{dl,i}) \tag{2.37}$$

In this equation $V_{dl,i}$ is the deposition velocity for the fraction i.

2.3.2 Durand model for stationary deposition

The Durand model makes use of a graph from which a coefficient, related to the volumetric concentration of solids and the particle size diameter, is read. This parameter is a modified Froude number. In Durand's experiments it was found that the Froude number remained constant once a stationary bed was formed. This lead to the development of an empirical coefficient $F_L(C_{vd}, d)$ which is used in the following equation to predict the stationary deposition velocity:

$$V_{dl} = F_L \sqrt{2g(S_s - 1)D} \tag{2.38}$$

The coefficient F_L can be read from the graph shown in figure 2.5. This is the original graph published by Durand in 1952. In figure 2.4 the more conventionally known graph attributed to Durand and Condolios is shown. It can readily be seen that values of F_L in the 'conventional-Durand'-graph fall about 50% higher than in the original graph. Also, the convergence of the lines at larger particle diameters does not take place in the original graph. It is unclear when the 'conventional-Durand'-graph replaced the original graph in popular use.

There are ways to numerically calculate the coefficient F_L. Many of these curve fits have been inventorised by Miedema (2016). These models based on the Durand graph are often able to calculate F_L for high concentrations. Durand & Condolios only published a graph able to determine F_L up to a solids concentration of 15%. The problem with the curve fit models is that oftentimes multiple parameters are included which are unclear in their definition. This makes using of these models quite difficult and more or less arbitrary since no two people will use exactly the same values for the multitude of parameters. Using of the original graphs published by Durand in 1952, and Durand & Condolios in 1953 is deemed the safest method of determining Durand's

FIGURE 2.4: Graph published by Durand and Condolios in 1953. Used for the determination of the semi-empirical Froude number, F_L, that is used in equation 2.38.

Froude number. Using of the graph by eye will result in slight inaccuracies so it is advised to document the values which are read and used in calculations so the calculations can be reproduced.
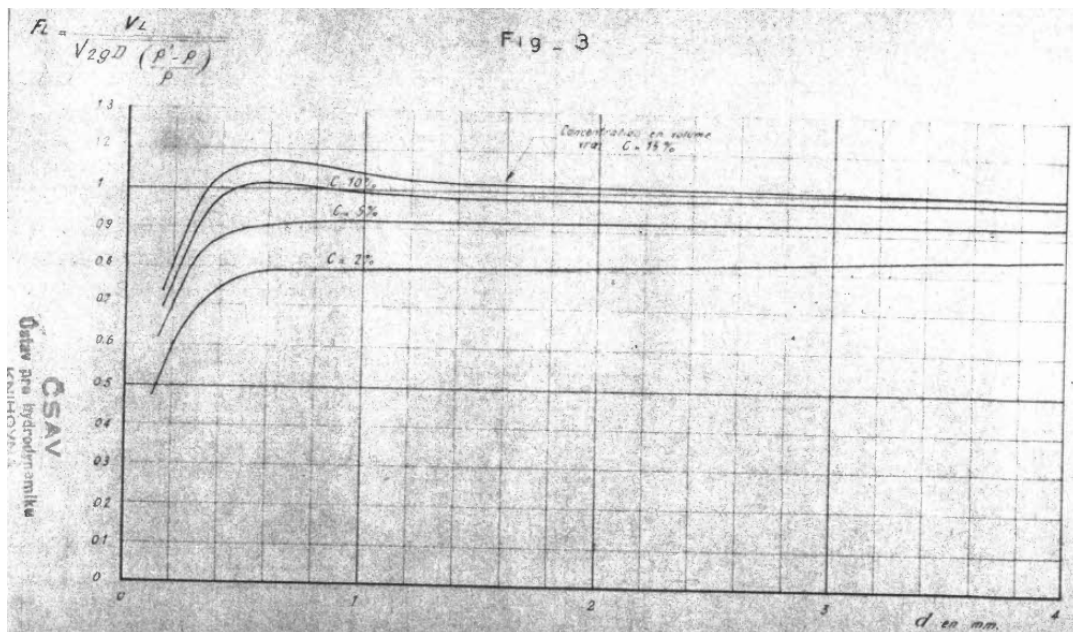
FIGURE 2.5: Original graph used for the determination of F_L, published by Durand in 1952.

2.3.3   Wilson model for stationary deposition

The second model used for the determination of the limit deposit velocity was created by Wilson in 1979. It is based on a two layer model that was used to calculate friction head loss in a fully stratified situation. A nomograph was created to remove the need for iteration in determining. From this nomograph the head loss can

be read when the relative concentration and the relative velocity in the pipe were known. Wilson then proceeded to note V_{dl} values for input differing in particle size, pipe diameter and solids density. The results of this research was a nomograph in which the V_{sm} could be read. The V_{sm} is different from the V_{dl} in that the former is dependent only on particle size and pipe diameter while V_{dl} also takes solid concentration into account. The V_{sm} is the maximum value of the deposit limit velocity and could be interpreted as a conservative estimate of the V_{dl}.

The nomograph of Wilson can be recreated as an equation quite accurately. An equation makes processing of data easier and results more accurate when recreating the calculations. Visual determinations from the nomograph will have more scatter. The following curve fit is applied to recreate Wilson's nomograph:

$$V_{sm} = \frac{8.8\left[\frac{\mu_s(S_s - S_f)}{0.66}\right]^{0.55} D^{0.7} d_{50}^{1.75}}{d_{50}^2 + 0.11 D^{0.7}} \tag{2.39}$$

It is important to note that d_{50} is in millimeters and D in meters. the coefficient μ_s will be taken as 0.44 but the determination of this parameter is heavily debated. The original nomograph does not extend below particle sized of 150μm. For particles of this size the following equation by Wilson & Judge (1976) is recommended:

$$V_{sm} = 2.0 + 0.3 \cdot log\left(\frac{d_{50}}{C_D D}\right) \sqrt{2gD(S_s - S_f)} \tag{2.40}$$

In this equation C_D is the drag coefficient of particles d_{50} is in millimeters and D is the pipe diameter in meters.

Another extension on Wilson's nomograph is on the larger particle sizes. A publication by Sanders (2004) found that Wilson's method overpredicts V_{sm} for large particles. Again for these larger particle sizes the establishment of a stationary bed was shown to be independent of particle diameter. A curve fit of the data by Sanders gives:

$$V_{sm} = \left(\frac{0.018}{f_f}\right)^{0.13} \sqrt{2gD(S_s - S_f)} \tag{2.41}$$

The value of f_f used in equation 2.40 depends only on the fluid friction factor for the portion of the pipe above the deposit.

When the Wilson nomograph approximation is used along with the extensions on the model the results will be like shown in figure 2.6. The Wilson & Judge extension in figure 2.6 uses a C_D of 0.47 corresponding to a sphere. The Sanders extension uses a f_f of 0.012. Variations on these parameters could be found depending on the pipe and sediments used.

2.4 Thoughts upon completion of literature study

Conducting a new set of experiments offers an opportunity to check whether some of the previous assumptions hold up under different circumstances. There are quite a few constants included in the model, making it exceptionally difficult to prove that a certain value that has been attributed to a constant is indeed correct when there are three other deterministic constants in the equation. The intergranular support coefficients are an obvious case of this. But they have been treated extensively in this chapter already. Two constants that should be mentioned as being questionably
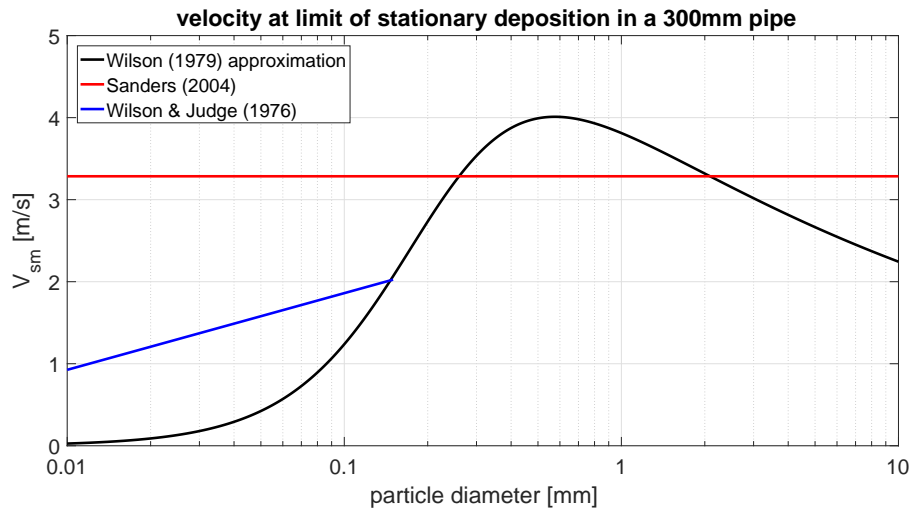
FIGURE 2.6: Approximation of Wilson's nomograph according to
equation 2.39 with extensions by Wilson & Judge and Sanders.

assumed constant are the Coulomb friction factor and the Darcy-Weisbach friction factor when dealing with velocities below the stationary deposition velocity.

The Coulomb friction factor is assumed to be 0.5 in the publications by Wilson and Sellgren. This value for the Coulomb friction is used in both the heterogeneous and the stratified equations. The friction factor is divided by two in the V50 model to compensate for the 50% of particles that are in suspension. The value of 0.44 used in the stratified equation was explained as adjusting for the effects of sliding of sand and gravel on a steel pipe by Sellgren et al. (2016), although no thorough explanation has been given. It would appear that the single value for the Coulomb friction factor is used on the assumption that a very wide particle size distribution from a single sand is used. When transporting multiple sands and gravels though, a single value for the Coulomb friction factor may no longer apply. When for example a very angular crushed gravel makes up the stratified part and a very round sand makes up the heterogeneous part, it would seem wrong to use the same Coulomb friction factor for both.

Other than the Coulomb friction factor, the Darcy-Weisbach friction factor would also need adjusting. It would make more sense if this factor was dynamic because the shape of the pipe is also dynamic for the relevant fractions. The Darcy-Weisbach friction factor is used in the fines-, and pseudo-homogeneous fractions. When stratification occurs, an increase in the friction factor would make sense. An argument can be made that the 4 component model is not particularly useful at velocities below the stationary deposition velocity anyway, so it doesn't matter.

Chapter 3

Experimental setup

The setup of the lab, and the conduction of the experiments are described in this section. The used materials and equipment are also treated here. The results of the experiments are not touched upon in this chapter. These are discussed in detail in Chapter 4.

3.1   The lab

The facilities where the test were conducted are located in the outskirts of Pudong in Shanghai. A large hall containing a 220m long, 300mm diameter open loop pipeline system is where the experiments took place. A schematic drawing of the pipeline system with most components can be seen in figure 3.1 below.
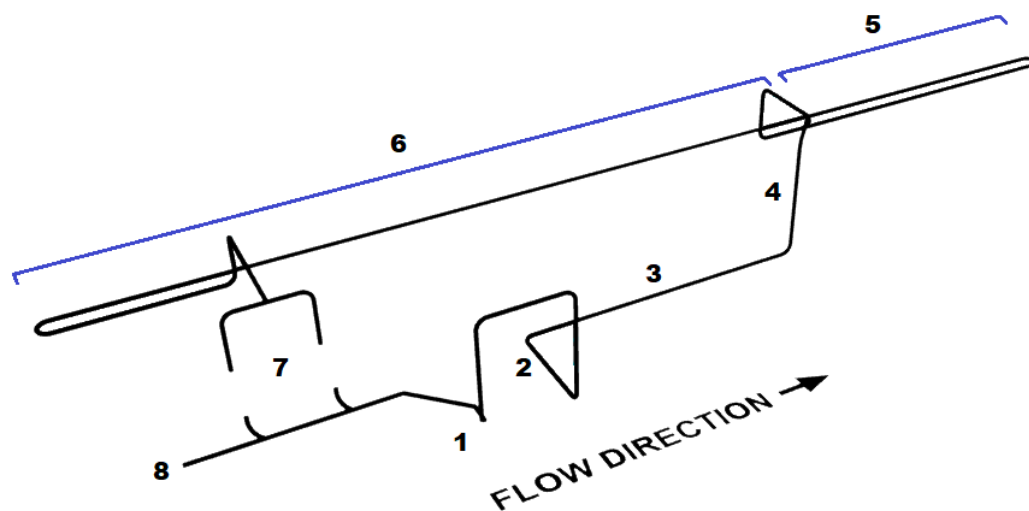
FIGURE 3.1: Schematic figure of the laboratory. (1) pump, (2) uloop, (3) cooling section, (4) vehicle crossing, (5) incline adjustable section, (6) loss section, (7) storage and loading tanks, (8) towards dump tank.

The experiments start by loading the sediments into one of the hoppers at the highest flow velocity. The sediments are loaded into the hopper by using a 0.5m³ clamshell mounted on a beam on rails just below the roof of the test hall. The sediments were laid out in large piles on plastic sheets on the floor of the hall. The sediment would then pass the pump at location (1) and enter the U-loop (2). An ultrasonic density meter is also mounted on the riser of the U-loop. In an attempt to

keep the temperature of the slurry somewhat constant over the course of the experiments, the slurry then passes a cooling section at location (3). The cooling section is basically a large concrete tank which can be filled with water. Past the cooling section the sediments enter the vehicle crossing (4). On the upper most part of the vehicle crossing there is a vent to release air bubbles that may have entered the pipeline. In the riser of the vehicle crossing an electromagnetic flow meter is located. Past this, the sediments enter the section of the pipeline system where the pressure meters are located. Section (5) can be set to incline. For the duration of the experiments in this report this section has remained horizontal. The long straight section (6) is where most of the data of this report comes from. A pressure meter is mounted at a 45 degree angle from the top of the pipe every 3 meters over a length of 48 meters. A perspex section, about 1 meter long, is present about halfway this section for visual monitoring of the slurry behavior. Past this part the slurry enters a T-split at location (7). This is also where a valve is located. The valve can be used to increase the pressure in the pipeline by partially closing it. Increasing the pressure was often necessary to prevent gas from forming in the pipeline. During experiments the slurry will then flow past the T-split into a hopper where it will reenter the flow. When the experiments are finished the slurry can be redirected to a different hopper where it is then dumped into a storage tank at location (8).

3.1.1   Dredge pump

The pump that has been used in the experiments is a 'Sanlian Pump' brand centrifugal dredge pump of type ASP1050-300-7000030W. In depth information including the pump curve and a performance report can be found in appendix A. This information is written in Chinese however, so a summation of some important parameters of the design point of the pump are displayed in table 3.1.

Sanlian ASP1050-300-7000030W		
Power	156	kW
Revolutions	740	rpm
Head	25.35	m
Discharge	1600	m^3/h
Efficiency	72.5	%

TABLE 3.1: Parameters of dredge pump in the design point.

During a typical slurry run the experiments were usually started at a throughput of 1500 m^3/h at 375 rpm, and stopped at around 800 m^3/h and 230 rpm. Very rarely were tests conducted outside this range when pumping slurry.

3.1.2   U-loop

The U-loop in the laboratory is located near the beginning of the pipeline system. The riser of the U-loop is mounted directly on the outlet of the pump. On the riser two pressure sensors measure the absolute pressure at a distance of 2 meters from each other. Another two pressure sensors measure the pressure differential in the downcomer. These two pressure sensors are also situated 2 meters from each other at an appropriate distance from the bend downward.
A large amount of work was done to calibrate the U-loop to display a correct density

of the slurry. It was concluded that a systematic error related to the flow velocity was made in the determination of the differential pressure in both up- and downward leg of the U-loop. The pressure sensors that were used to determine the pressure differential in the ascending and descending leg of the U-loop are Rosemount 3051SAL differential pressure transmitters with diaphragm seals. The sensors make use of a closed system with oil in the impulse tubes. This makes it impossible for sediments to get into the pressure tubes.

3.1.3 Ultrasonic density meter

The density meter is a 'Tengine' brand ultrasonic density meter of type 'TPD' with serial number 'S2DN300P10C20'. This piece of equipment uses two transducers mounted on opposing sides of the pipeline. The transducers send and receive sound waves and calculate the volume percentage of solids in the slurry. An ultrasonic density meter used a non-intrusive method of determining mixture density so it should not interfere with the pressure sensors of the U-loop. The maximum measurable concentration of solids of the density meter is 40% by volume with an accuracy of $\pm2.5\%$. A calibration error caused the meter to indicate a concentration 1.8 times higher than actual did have an effect on the experiments. All experiments were conducted at a lower concentration than intended due to simultaneous trouble with the U-loop and the ultrasonic density meter.

FIGURE 3.2: Upward leg of the U-loop showing pressure sensors (1), and ultrasonic density meter (2).

3.1.4 Cooling basin and thermometers

To help keep the temperatures in the pipeline somewhat constant during experiments, a large cooling basin is present in the experimental setup. Right after the U-loop there is a basin which can be filled with water to submerge the pipe and help cool the contents. During long experiments the temperature of the slurry will usually increase. Significant increases in temperature may influence the measurements. In the experiments conducted for this report the cooling basin was never filled as temperatures did not increase significantly. A thermometer with an insertion depth of 100mm into the pipe is located between pressure meter 18 and 19 (see figure 3.4), and another thermometer is located right before the T-split at the end of the pipeline at location 7 (see figure 3.1). A typical run increases the temperature of the slurry by about 5 degrees Celsius over the course of the day. A larger influence is the ambient temperature. Table 3.2 gives some information on the temperature deviation of the slurry.

Test	Date	t_1	t_2	T_1	T_2	$T_{ambient}$
1	16 okt 2017	10:34	16:23	$21.4°C$	$25.8°C$	$20°C$
8	11 dec 2017	10:12	15:17	$15.3°C$	$17.8°C$	$6°C$

TABLE 3.2: Displayed temperatures are measured by thermometer 1. Ambient temperatures are from timeanddata.com and are a daily mean. Start and finish times are from the moment the equipment was turned on to when it was switched off.

3.1.5 Electromagnetic flow meter

To measure flow velocities a Guanghua LDG-300S electromagnetic flow meter is installed on the riser of the vehicle crossing. A detailed list of specifications can be found in appendix B. But since all the information is in Chinese some important parameters are displayed in table 3.3 below.

Guanghua LDG-300S		
Velocity range	$0.5 \sim 10.0$	m/s
Pressure range	$0.6 \sim 4.0$	MPa
Temperature range	$-25 \sim +150$	$°C$
Accuracy	0.5	%

TABLE 3.3: Parameters of electromagnetic flow meter.

One thing that may affect the electromagnetic flow meter is the fact that it is installed on a riser. The flow meter determines the velocity in the pipe through the conductivity of the liquid. The liquid conducts electricity through the particles that are present in it. The particles travel at a slower velocity than the liquid due to settling. This will influence the results of the electromagnetic flow meter slightly. Real velocities in the pipeline are likely to be slightly higher than indicated by the flow meter.

3.1.6 Pressure measuring section

A large part of the pipeline is fitted with pressure sensors to measure the development of the pressure over the distance. After passing the vehicle crossing the slurry enters the pressure measuring section. This part of the pipeline is 123 meters long and has 34 pressure sensors installed. In figure 3.4 the layout of this pressure measuring section can bee seen.

The first part around the 180° bend is incline adjustable. The pipe here is fitted with a flexible part which allows the pipe to be set at different inclinations. No use of this feat was made in the experiments described in this thesis. The second long straight part (sensor 19-34) is the where the measurements for this

FIGURE 3.3: Pressure tap with: absolute pressure sensor (a), venting tube (b), differential pressure sensor (c). Photo courtesy of M. de Vreede.

research were done. Sensor 19 is located 31.23m (104D) after the bend. Sensor 34 is located 76.23m (254D) after the bend. This distance allows for the flow to assume a somewhat steady state which is necessary to test the model.

3.1.7 Pressure sensors

Each sensor location indicated in subsection 3.1.6 is outfitted with two types of pressure sensors to ensure redundancy. A MicroSensor MPM4730 Intelligent Pressure Transmitter is used to measure the total pressure at the location. This pressure sensor has a range of -0.1MPa∼10.0MPa and a typical accuracy of ±0.15%.

Rosemount 3051 DP-meters are used to determine pressure differentials between locations. These DP measurements are used to verify the validity and accuracy of the absolute pressure measurements. The differential pressure sensors have a range of 0∼10kPa and a typical accuracy of ±1.65%. A graph showing the performance of the DP-meters versus the absolute pressure sensors is shown in figure 3.5.

The Pressure sensors are mounted on a pressure tap as can be seen in figure 3.3. The pressure taps are installed at a 45° angle from the top of the pipe. A tertiary tube can be seen on the photo. This venting tube is used to remove air bubbles from the system. It is inevitable that some air will get into the pipeline in an open loop system. Especially when loading the sediments at the start of the experiments a not insignificant amount of air will get into the system. Before the tests start, the air can be removed from the pressure taps by flushing out the venting tubes.
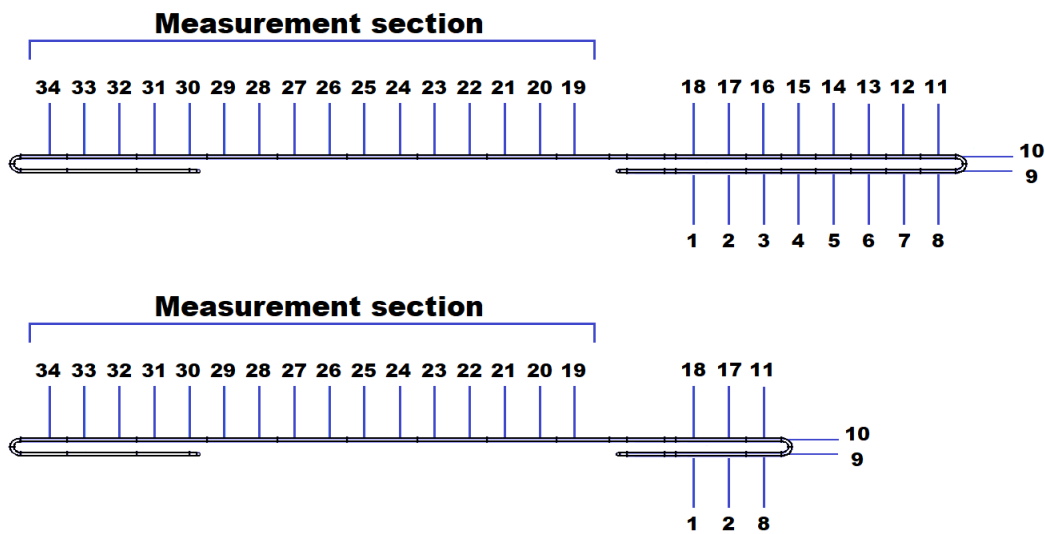
FIGURE 3.4: Top views of the pipeline section where the pressure monitoring was done. The top schematic corresponds to the maximum extend of the pipeline setup, the bottom schematic corresponds to the pipeline setup that was used in the experiments for this research. These top views corresponds to location 5 and 6 in figure 3.1. The pressure taps under the indication 'measurement section' are the loss section used for the 4 component model data.
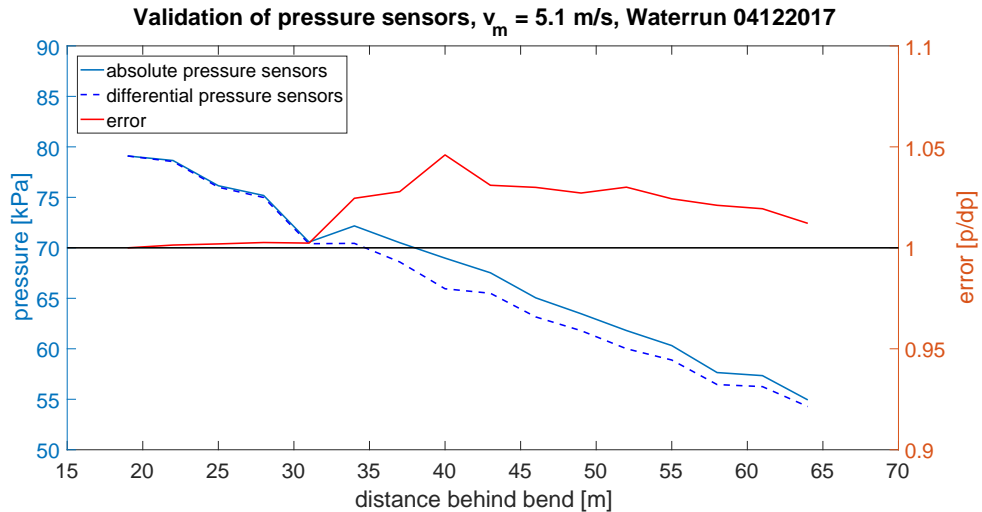
FIGURE 3.5: Validation of the pressure sensors 19-34 as seen in figure
3.4.

3.1.8   perspex section

A perspex section of 1.5m is installed between pressure sensor 25 and 26 at a distance of 51m after the 180° bend. It is used to visually monitor behavior of the flow. It is an excellent tool to determine which flow regime is dominant in the pipe and it has often been used to determine when a stationary deposition was formed.

3.1.9   Valves

To control the flow of the slurry a number of valves are located around location 7 (see figure 3.1). Valves are used to close off the hopper from the pipeline and to determine which hoppers are connected to te pipeline. This is done through remotely controlled valves which are operated from the control room. A manually controlled valve is located right before the T-split just before location 7. This valve was often used to increase the pressure in the pipeline by partially closing it. When pumping high concentrations at low velocities the pressure in the pipeline may fall below the vapor pressure. Chocking the flow at the very end of the pipeline has proven to be good method of increasing the pressure in the system.

3.1.10   Storage and loading tanks

A total of four reservoirs are available in the lab. Each reservoir has a maximum capacity of 100m^3. During these experiments only two of the four reservoirs have been used. One of the reservoirs was used as a mixing tank where the sediments were loaded into the system. The fluid level in this tank is always kept at a level that is high enough to keep the end of the pipe submerged to prevent air bubbles. Since it is an open flow loop the hopper remains part of the system at all times. At the end of the experiment the slurry is directed towards the second tank from where it is moved further to a dump tank where used slurry is stored.

3.1.11 Data acquisition station

All of the signals sent by the equipment in the lab is received by a Chengtec CTDAQS-5000 data collection system. A total of 76 channels were received during the experiments. For the sake of future readability of the data; table 3.4 displays the identity of all channels as they are named in the raw data excel files.

The data was acquired at a rate of 20Hz. When working with the data it can be seen that the channels corresponding to pressure sensor 1-8 and 11-18 show a flat signal. These pressure taps were disconnected from the system after the previous research on the inclined section of the pipeline was concluded.

Channel description	Column
Absolute pressure	A-AH
Flow meter	AI
Ultrasonic density meter	AJ
Temperature	AK,AL
dp riser U-loop	AM
dp downcomer U-loop	AN
Pressure before pump	AO
Pressure after pump	AP
Pump power	AQ
Pump rpm	AR
Differential pressure	AS-BX

TABLE 3.4: Channel description of the raw data in the Excel files. Please note that the absolute pressure channels A-AH correspond to absolute pressure sensors 34-1 (as seen in figure 3.3) in that order. The pressure differential measured in column AS corresponds to the pressure differential between pressure tap 34 and 33. Column AT is the pressure differential between 33 and 32, and so forth.

3.2 The materials

A large quantity of sediments have been collected for the experiments. The fractions, as defined by the 4 component model, have all been collected with the exception of the X_f-fraction. There are two reasons that the X_f-fraction is not included in the experiments. The first reason is that the Darcy-Weisbach equation accurately predicts the losses in homogeneous mixtures. Only when X_f-concentrations are so high that they start to influence the viscosity of the carrier fluid do experimental results diverge from the model results. The fact that the Darcy-Weisbach equation with a large amount of experimental backing accurately predicts pressure loss contributions of this fraction, makes it quite uninteresting to include in this research. The second reason the fines fraction is not included in the research, is that the rock flour which would make up these fine sediments pose a health risk to the lungs. Precautions would have to be taken which would make it such a hassle for no interesting results at all.

According to the 4 component model there is no restriction to the upper bound of the X_s-fraction. Out of practical consideration the upper bound of the stratified fraction has been set at 10 mm, this is to prevent damage to the equipment in the laboratory. It has also been mentioned in the previous chapter that it is strongly suspected that in large pipe diameters the heterogeneous fraction gets stretched so wide that the

Wilson v50 model no longer accurately predicts the losses in this fraction. Because of this suspicion there are some tests that split the heterogeneous part into an upper and a lower fraction, X_{hu} and X_{hl} respectively.

Taking all of the above into account the boundaries of the sediments are defined as follows:

X_p $0.04mm < d < 0.20mm$

X_h $0.20mm < d < 4.50mm$

X_{hl} $0.20mm < d < 1.00mm$

X_{hu} $1.00mm < d < 4.50mm$

X_s $4.50mm < d < 10.0mm$
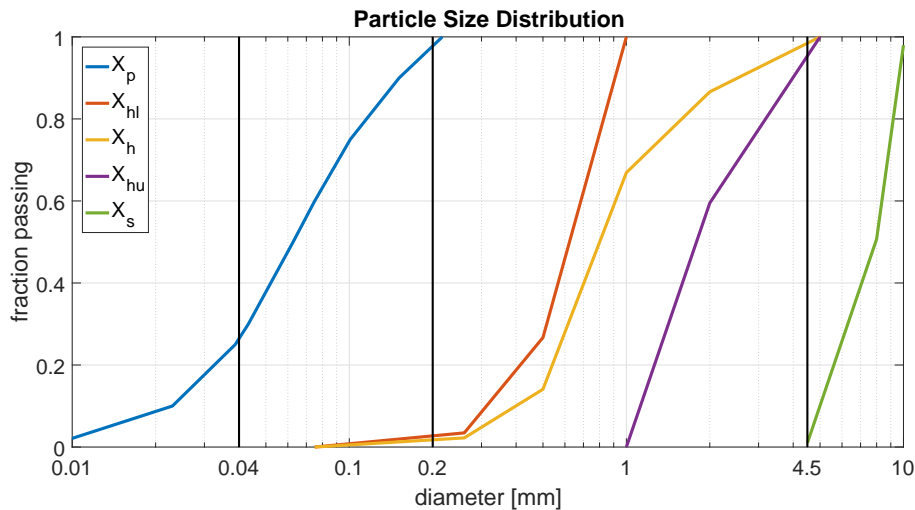
FIGURE 3.6: Particle size distribution of the sediments used in the experiments.

Of course it would be very difficult to keep each fraction perfectly within its own bounds. Care has been taken to make sure that a sufficient amount of the sediment falls within the intended fraction. And lastly, the upper- and lower heterogeneous fraction have been made by sieving the heterogeneous sediments. This means that both of these fractions miss one part of the tail of the particle size distribution. This shouldn't matter for the model, but you would not encounter a PSD like this under natural circumstances. It is something to take into account when evaluating the data. The smaller grain size sediments have been analyzed using a Malvern Instruments laser diffraction particle analyzer. The grains of the stratified component were too large to analyze in this manner. Sieving by hand and weighing of the sediments was done to construct the sieve curve of this component. This explains the low resolution of the PSD of the stratified component.

In figure 3.7 the photographs of the sediments can be viewed. Discoloration between the three different heterogeneous fractions is only due to the lighting, they are all composed of the same source sand. Something to note is that the gravel that was used in the experiments is very round. This is in stark contrast with the gravel that was used in the GIW experiments where they used a very angular crushed granite for their stratified component. This must be kept in mind when comparing the

results with the data from the GIW experiments. This will prove a opportunity to analyze the sliding friction factor that is part of the stratified component hydraulic gradient calculation. The sediments making up the pseudo-homogeneous fraction appear to be stuck together in the photograph. When submerged into water these clumps dissolve and this will have no further influence on the results.

FIGURE 3.7: Photographs of the sediments used in the experiments. Starting from the top left: $X_p, X_{hl}, X_h, X_{hu}, X_s$.

Chapter 4

Experiments

The execution of the experiments is vital for the acquisition of trustworthy data. In this chapter the experimental protocol and the extraction of information from the raw data is discussed. The motivation for doing the specific experiments and some words of caution when drawing conclusions from the data are also contained in this chapter.

4.1 Experimental protocol

The performed tests were mostly based on the 2017 GIW experiments (Visintainer et al.). This was done so a good comparison could be made to analyze the effect of upscaling. Due to restricted time and economic considerations it has been attempted to perform the most amount of tests in a single day. A difficult paradox plays out when performing the tests; To get a good resolution on a velocity interval a large amount of tests must be performed. But to reduce the amount of particle degradation that takes place the experiments must be carried out as quick as possible. No systematic approach has been applied to deal with this problem but experiments are adjusted on site according to the judgment of the writer of this thesis. Often a second run (a repeat of the experiment over the entire velocity interval using the exact same sediments) of a test has been performed to check for the effect of particle degradation. A test matrix of the performed experiments can be viewed in table 3.1 and a motivation for each experiment can be found in appendix C. In table 3.1, the experiment ID's are named by a number first and then a letter. Experiments with the same number indicate that they were done in the same day. The letter than indicates the different experiments that were done on that day. Every morning before the experiments, new sediments were loaded into the pipeline. And every afternoon the sediments that were used during the day are discarded.

It can be seen that no experiments using solely the heterogeneous fraction are present in the test matrix. No experiments using this sediment have been performed by the author. Instead a colleague (J. de Ridder 2018) has executed these tests some months prior in the same pipeline system, these experiments are described in some more detail in section 4.3. Sadly, the u-loop pressure sensors were not yet operational at that time. This makes comparing the results a little more difficult than what would have been preferred, but conclusions can still be drawn by comparing results. Data from the three X_h-fraction experiments with target delivered concentrations of 10%, 20%, and 25% were provided by J. de Ridder.

The experiments are started at the highest velocity on the interval. The velocity in the pipeline was then gradually lowered until a stationary bed was observed. In the GIW experiments the flow stabilized more quickly when starting high and then lowering the velocity so this practice was continued in the Shanghai experiments.

	1a	1b	2a	2b	3a	3b	4a	4b	5	6a	6b	6c	7	8a	8b	8c	9
X_p	1	.33	.33	.25					1								
X_{hl}										1	1	.67	.50			.33	
X_h		.67	.67	.50		.67		.67								.67	
X_{hu}												.33	.50	1	1	.67	
X_s			.25	1	.33	1	.33										1
C_{vd}	10	30	15	20	5	15	10	30	20	10	20	30	20	10	20	30	20

TABLE 4.1: Test matrix showing the target delivered concentrations. A motivation for doing each experiment can be found in appendix C.

Occasionally, when deemed safe, the velocity was lowered even below stationary deposition. A time average of the collected data was usually taken over a 30 to 60 second interval once the flow had stabilized. Stabilization of the bed can often take quite a long time, in the range of three to sometimes ten minutes. This means that to acquire a single data point at a low velocity, sometimes 15 minutes of pumping at a constant rpm is required. When pumping large diameter sediments the flow never truly seems to stabilize and a larger time interval is used to collect the average data. Because especially the large diameter particles suffer from particle degradation and collecting a single data point on the velocity interval takes a long time due to the unstable nature of the flow when containing these large particles. The decision was made to reduce the amount of data points on the velocity interval when doing experiment containing the largest particles. Trading in resolution for data quality.

4.1.1   Observations with regards to stationary deposition

The determination of a stationary deposition velocity has been a primary task during the experimentation process. Like discussed in the theory (chapter 2.7), the determination of a deposit limit velocity is not an exact science and two different observers will have two different opinions on exactly when a stationary bad has formed. Often, a transitional phase where sediments are transported in a sort of dune like fashion is observed from the perspex section. This makes determination of when a stationary deposit has formed quite difficult. To mitigate personal bias the behavior of the flow was described in detail during the experiments. These notes can be found in appendix C.

The experiments are started at the highest velocity that is possible in the pipeline. By gradually lowering the pump-rpm the mean velocity in the pipe is lowered until a stationary bed is formed or until the velocity cannot be lowered further. Sometimes the velocity is lowered slightly beyond the critical velocity to see of behavior changes. Often, a second run is performed at different pump-rpm points to see if the critical velocity can be pinpointed further. During the process of lowering the velocity towards the limit deposit velocity, any and all strange or divergent behavior of the flow is noted carefully for future reference.

4.2   Volumetric concentrations of sediments used in the experiments

After performing the experiments it was noted that the pressure losses appeared to be suspiciously low when compared to the calculated losses. For some time the cause of this was investigated, it was eventually figured out that the equipment was calibrated wrongly. When loading the sediments, the concentrations indicated by

test 4b run 1, 0.67 X$_h$ + 0.33 X$_s$, [20171027]

measured delivered concentration
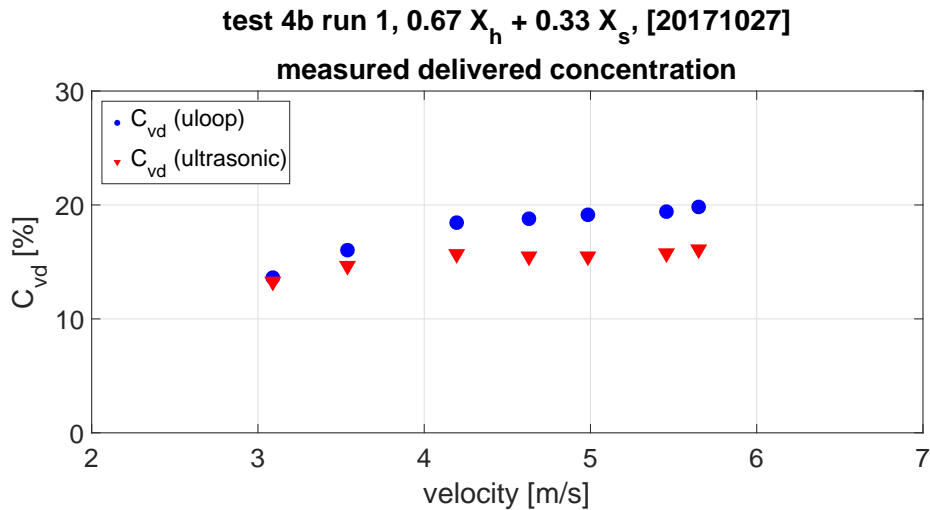
FIGURE 4.1: Graph showing the decreasing delivered concentration when lowering the mean velocity in the pipeline.

the U-loop and the ultrasonic density meter were monitored until a somewhat stable value around the target concentration was established. Unfortunately both the U-loop and the ultrasonic seemed to have been calibrated to show a value near half of what was intended. This was only figured out by M. de Vreede, who used the lab prior to the experiments done for this research, after all of the experiments were executed so the entire test matrix is affected by this error. The real concentrations could be retrieved by recalibrating the U-loop using data from clear water runs. These clear water runs were executed periodically over the course of the slurry experimentation. The recalibration process of the U-loop can be viewed in appendix E. The ultrasonic concentration meter indicated a concentration of dry sand including the pore volume reducing the indicated percentage to about 55% of the initial value. A new matrix with the concentrations measured in the experiments is displayed below. The indicated C_{vd} is in most cases the value as given by the U-loop over the entire velocity interval. The concentration indicated by the U-loop is deemed more reliant than the that of the ultrasonic. The ultrasonic values are checked to see whether a broad conformity can be observed. In a few instances the U-loop (test ID 3a and 4a, see table 3.6) and in one instance the ultrasonic (test ID 1a, only one of the two runs is affected by this anomaly. The indicated ultrasonic concentration in table 3.6 is from run 2) show broadly divergent values. When this is the case a note is made in the table with an explanation of the chosen solution. Table 3.6 shows the adjusted concentrations of the experiments.

	1a	1b	2a	2b	3a	3b	4a	4b	5	6a	6b	6c	7	8a	8b	8c	9
X_p	1	.33	.33	.25					1								
X_{hl}										1	1	.67	.50			.33	
X_h		.67	.67	.50		.67		.67									
X_{hu}												.33	.50	1	1	.67	
X_s				.25	1	.33	1	.33									1
$C_{vd,u}$	6.4*	19.9	8.3	8.1	4.0	8.9	6.4	15.2	8.5	10.3	13.5	18.6	14.9	12.4	16.6	21.0	10.8
$C_{vd,l}$	3.2	14.2	4.8	6.4	-0.5**	4.5	0**	18.2	10.0	5.7	12.9	20.6	13.9	8.0	14.2	24.5	11.1
C_{vd}	10	30	15	20	5	15	10	30	20	10	20	30	20	10	20	30	20

TABLE 4.2: Test matrix showing slurry composition function and delivered concentrations in percentage according to the ultrasonic $C_{vd,u}$, and the U-loop $C_{vd,l}$. The target delivered concentration is shown in the bottom row.

Extra explanation on asterisks in table 3.6:

* Ultrasonic density meter was not turned on for run 2, shown concentration is mean of run 1 only.

** U-loop does not seem to work properly when only pumping X_s-particles in low concentrations.

The C_{vd} as indication in the bottom three rows in table 4.2 shows from top to bottom: the average concentration over the entire velocity range of the ultrasonic and the U-loop, and the target concentrations is displayed in the bottom row. When multiple runs have been performed for a single slurry composition the average concentration of the two runs is noted in the table. The delivered concentration usually decreases slightly when lowering the velocity in the pipe so concentrations might be somewhat higher at high velocities and lower at low velocities, for an example of this phenomenon see figure 4.1. Occasionally either the U-loop or the ultrasonic gives a strange value. These anomalies are denoted by an asterisk in table 4.2.

4.3 Experiments by J. de Ridder

For a portion of this study results from experiments performed by J. de Ridder will be used. These experiments make use of only the X_h-fraction. The experiments carried out by de Ridder were done in the same laboratory some moths prior to the experiments carried out for this study. The laboratory setup was mostly the same except for two things. The incline adjustable section, section 5 in figure 3.1, was slightly longer in the experiments by de Ridder. This is because between the two studies the incline section was in use for research done my M. de Vreede. The incline section was shortened to accommodate a 45deg incline angle. The entire length of te incline adjustable section would not fit under the roof, thus the shortening of section 5. A second difference between the laboratory setup of this study and the study by de Ridder is the U-loop. The U-loop was not yet in use during the research by de Ridder so only the concentration measurements of the ultrasonic concentration meter are available.
Because the purely X_h-fraction experiments were already done before in an almost identical test setup, a choice has been made to not do these experiments again. Instead the experiments with the split X_h-fraction have been done. This will give some extra information on the behavior and accuracy of the Wilson V-50 model when the X_h-fraction is spread very wide in large diameter pipelines.
The sediments used in the experiments by de Ridder are the exact same as the ones

used in this research. The experiments of which the results will be used in this study are displayed in table 4.3.

	JdR1	JdR2	JdR3
X_p X_{hl} X_h X_{hu} X_s	1	1	1
$C_{vd,u}$	4.5	12.7	15.1
$C_{vd,l}$	n/a	n/a	n/a
C_{vd}	10	20	25

TABLE 4.3: Test matrix of experiments done by J. de Ridder show-ing slurry composition and delivered concentrations in percentage according to the ultrasonic $C_{vd,u}$, and the U-loop $C_{vd,l}$. The target delivered concentration is shown in the bottom row.

4.4 Motivation for experiments

A short motivation for choosing to do each of the experiments shown in figure 4.1 are written down in this section. The concentrations as indicated in this section are the average measured concentrations.

Test 1a; 1.00 X_p , C_{vd} = 4.8%: Check the individual characteristics of the pseudo-homogeneous fraction, can be compared to test 5 to observe the effects of concentration increase.

test 1b; 0.33 X_p + 0.67 X_h , C_{vd} = 17.1%: Check the effects of a pseudo-homogeneous fraction added to the heterogeneous fraction. The heterogeneous fraction has an intergranular support coefficient. We would like to check whether the current defi-nition of this coefficient leads to accurate results in the model. The effects of concen-tration can be observed when comparing the results with test 2a, which is the same slurry composition at lower concentration.

test 2a; 0.33 X_p + 0.67 X_h , C_{vd} = 6.6%: Check the effects of a pseudo-homogeneous fraction added to the heterogeneous fraction. The heterogeneous fraction has an intergranular support coefficient. We would like to check whether the current defi-nition of this coefficient leads to accurate results in the model. The effects of concen-tration can be observed when comparing the results with test 1b, which is the same slurry composition at higher concentration.

test 2b; 0.25 X_p + 0.50 X_h + 0.25 X_s , C_{vd} = 7.3%: Check whether the 4cm can ac-curately predict pressure loss on a general very wide particle size distribution. This often leads to complication in other models.

test 3a; 1.00 X_s , C_{vd} = 4.0%: Check the individual characteristics of the stratified fraction, can be compared to test 4a and 9 to get high resolution behavior of this fraction.

test 3b; 0.67 X_h + 0.33 X_s , C_{vd} = 6.7%: Check the effects of a stratified fraction added to the heterogeneous fraction. The stratified fraction and the heterogeneous

fraction both have an intergranular support coefficient in the 4cm model. We would like to check whether the current definition of these coefficients leads to accurate calculations when compared to the experimental results. We can also check on the effects of concentration when comparing the results with test 4b.

test 4a; 1.00 X_s , C_{vd} = 6.4%: Check the individual characteristics of the stratified fraction, can be compared to test 3a and 9 to get high resolution behavior of this fraction.

test 4b; 0.67 X_h + 0.33 X_s , C_{vd} = 16.7%: Check the effects of a stratified fraction added to the heterogeneous fraction. The stratified fraction and the heterogeneous fraction both have an intergranular support coefficient in the 4cm model. We would like to check whether the current definition of these coefficients leads to accurate calculations when compared to the experimental results. We can also check on the effects of concentration when comparing the results with test 3b.

test 5; 1.00 X_p , C_{vd} = 9.3%: Check the individual characteristics of the pseudo-homogeneous fraction, can be compared to test 1a to observe the effects of concentration increase.

test 6a; 1.00 X_{hl} , C_{vd} = 8.0%: We noticed the heterogeneous part of the 4 component model get stretched really wide when used on large diameter pipelines. We would like to check if a distinction in particle behavior on pressure loss can be observed when separating the heterogeneous part into an upper and a lower fraction. This test serves to get data of only the lower part of this new fraction. We would then like to compare the results with test 8a and 8b which measure only the upper fraction of the heterogeneous part. We would also like to compare it with test 6b to get an idea into the effect of concentration on this fraction.

test 6b; 1.00 X_{hl} , C_{vd} = 13.2%: We noticed the heterogeneous part of the 4 component model get stretched really wide when used on large diameter pipelines. We would like to check if a distinction in particle behavior on pressure loss can be observed when separating the heterogeneous part into an upper and a lower fraction. This test serves to get data of only the lower part of this new fraction. We would then like to compare the results with test 8a and 8b which measure only the upper fraction of the heterogeneous part. We would also like to compare it with test 6a to get an idea into the effect of concentration on this fraction.

test 6c; 0.67 X_{hl} + 0.33 X_{hu} , C_{vd} = 19,6%: We would like to have some results of different blends of the X_{hu} and X_{hl}-fractions.

test 7; 0.50 X_{hl} + 0.50 X_{hu} , C_{vd} = 14.4%: The Xiamen sand, which is used as the heterogeneous fraction, is split at 1mm to form the upper and lower part of the heterogeneous fraction. When combining X_{hu} and X_{hl} in equal parts the newly constructed mixture does not return the Xiamen sand, as the d_{50} of the composite X_h-fraction is exactly at 1mm where the Xiamen sand was split. A visualization of the pure X_h-fraction (the Xiamen sand) and the composite X_h-fraction can be seen in figure 4.2.

test 8a; 1.00 X_{hu} , C_{vd} = 10.2%: We noticed the heterogeneous part of the 4 component model get stretched really wide when used on large diameter pipelines. We

would like to check if a distinction in particle behavior on pressure loss can be observed when separating the heterogeneous part into an upper and a lower fraction. This test serves to get data of only the upper part of this new fraction. We would then like to compare the results with test 6a and 6b which measure only the lower fraction of the heterogeneous part. We would also like to compare it with test 8b to get an idea into the effect of concentration on this fraction.

test 8b; 1.00 X_{hu} , C_{vd} = 15.4%: We noticed the heterogeneous part of the 4 component model get stretched really wide when used on large diameter pipelines. We would like to check if a distinction in particle behavior on pressure loss can be observed when separating the heterogeneous part into an upper and a lower fraction. This test serves to get data of only the upper part of this new fraction. We would then like to compare the results with test 6a and 6b which measure only the lower fraction of the heterogeneous part. We would also like to compare it with test 8a to get an idea into the effect of concentration on this fraction.

test 8c; 0.33 X_{hl} + 0.67 X_{hu} , C_{vd} = 22.8%: We would like to have some results of different blends of the X_{hu} and X_{hl}-fractions.

test 9; 1.00 X_s , C_{vd} = 11.0%: Check the individual characteristics of the stratified fraction, can be compared to test 3a and 4a to get high resolution behavior of this fraction.
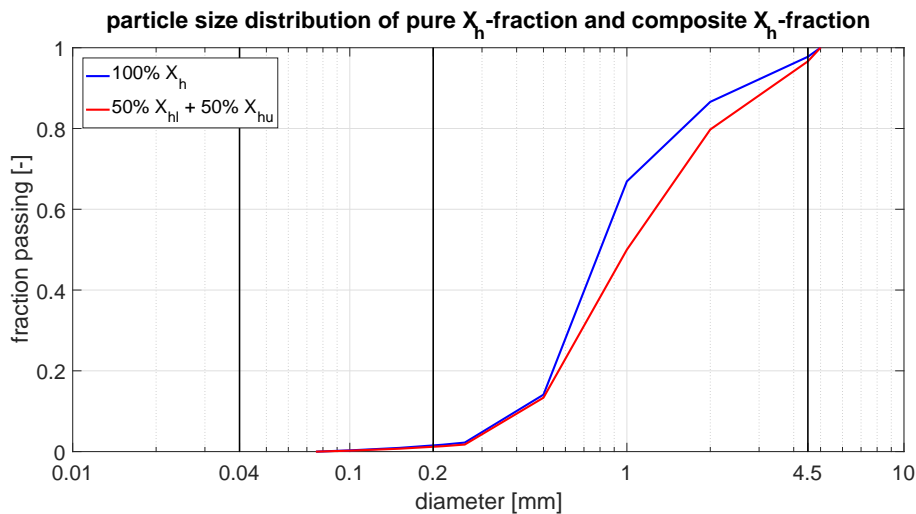
FIGURE 4.2: Comparison of the Xiamen sand and the composite X_h-fraction.

4.5 Validity of the results

Several factors are of importance when it comes to the accuracy of the results. The equipment's accuracy is what comes to mind first. Usually the equipment comes with a booklet in which the equipment characteristics are written down. In chapter 3.1 most of the equipment's accuracy along with other characteristics is discussed. For many of the sensors the appendix can be consulted for more in detail information. Accuracy of the equipment according to the manufacturers is never more than 2.5%.

Apart from the equipment's inaccuracy there are also environmental causes that can result in errors in the results. Environmental causes can be the results of equipment placement or behavior of the flow or sediments in relation to the equipment. The pressure taps to which the absolute and differential pressure sensors are connected can deviate from each other when they are imperfectly aligned or when the holes of the pressure taps deviate in diameter. A typical result of the validation process of the pressure taps is shown in figure 3.5. It can be seen in this figure that the results of the dp-pressure sensors and the absolute pressure sensors coincide to within a few percent relative error. Results are quite accurate but a few percent error is uncircumventable.

Another issue that can occur with the pressure sensors is air bubbles getting into the impulse tubes. This was specifically an issue with experiments containing large portions of X_p sediments. When air gets into the impulse tubes the system must be vented. The tubes are checked for air bubbles very frequently during the experiments but it is possible that air bubbles have had some effect on the results presented in this chapter.

Another point of concern is the riser that is installed directly on the pump. The pressure meters of the upward leg of the U-loop and the ultrasonic density meter are installed on this piece of pipe (see figure 3.2 for a photograph of the situation in the riser). When the pump is turned on it causes a lot of vibration in the pipe. The vibration caused by the pump, especially at high rpm, may cause misreadings by the equipment. The upward leg of the U-loop shows different behavior than the downward leg. It is not certain what causes this strange behavior but the vibrations in the pipe could play a part. For more information on the U-loop and the recalibration process please see appendix D.

Something that may also result in misreadings in the in-situ concentration of solids in the pipe has to do with the ultrasonic density meter. The ultrasonic density meter is ideally calibrated for every single sediment. Due to the wide variety of different slurry compositions that were created for the experiments, it was obviously not feasible to calibrate it for every different slurry. The ultrasonic density meter has been calibrated using the X_h-particles (see figure 3.6). Minor errors may be the result of these unideal circumstances under which the ultrasonic density meter was used.

Typical behavior of the pipeline is based on water tests. Important parameters like the friction factor used in the Darcy-Weisbach equation are determined based on data from the water tests. Ideally these tests are done using clean water. It is unrealistic to expect the water in a dredging pipeline to be entirely free of solids. When performing water tests the pipeline was flushed clean as well as deemed feasible but it could be observed in the perpex section that a small fraction of solids was still present in the pipeline during these experiments. This may have had a very minor effect on the water data and all the theory that was derived from the water data.

A final point has to do with the calculation of slurries containing more than one kind of sediment. The calculation is done according to the desired slurry composition. So when 5 buckets of X_p particles and 5 buckets of X_h particles are loaded into the system the calculation assumes that the makeup of the delivered particles is exactly 50% X_p and 50% X_h particles. Especially at low velocities and big portions of large particles this assumption may be inaccurate.

4.6 Calculation and visualization of the results

4.6.1 Model input

Often there is no agreement on the determination or the exact value of a parameter or constant. For sake of absolute clarity and reproducibility, all constant input parameters and their values are presented here:

D	0.30	[m]	Pipeline diameter.
f_f	0.012	[-]	Darcy-Weisbach friction factor.
g	9.81	[m/s^2]	Gravitational acceleration.
M	1.0	[-]	Coefficient related to the PSD width.
S_l	1.00	[-]	Relative density of liquid.
S_s	2.65	[-]	Relative density of solids.
v_{sms}	3.29	[m/s]	Maximum stationary deposition velocity for the 0.015D sized particle. Calculated according to Sanders (2004).
v_t	0.47	[m/s]	Terminal settling velocity of the 0.015D sized particle.
μ_l	0.001	[Pa/s]	Dynamic viscosity of the liquid.
μ_s	0.44	[-]	Mechanical friction factor.
μ_w	0.001	[Pa/s]	Dynamic viscosity of water at $20°C$.

Using the equations given in Chapter 2, it should be possible to reproduce the entire process and calculate the exact same values as this study.

4.6.2 Data collection process

It requires a huge effort to extract useful data from the vast amount of data gathered during the Shanghai experiments. This section aims to give some insight into the data extraction process for the 4 component model plots. The first thing that was done after each experiment was to convert the TDMS files in Excel files. The Excel files could then be read into MATLAB. In MATLAB the entire Excel file was converted into a single matrix containing every single data point gathered during the day. A simple plot with slightly smoothened signals showing some important measurements like pressure, mean velocity, pump rpm, and delivered concentration was then created. From this plot, data intervals over which mean values should be created can easily be spotted. The pump rpm is the most constant parameter so this is used as a guide to spot data intervals. With data gathered at 20Hz a three minute data interval contains 3600 data points. From each data interval a mean is created to extract a workable data point. When all data intervals are compressed into data points the data points are loaded into a matrix and saved as a plain text file. The text file can then be called upon to use the data contained within to create the final plots like shown in figure 4.3. The example in figure 4.3 contains seven data intervals which are represented by the seven data points.

4.6.3 Layout of plotted results

The results of the 4 component calculation are presented in a plot containing four subplots. At the top of the plot the title is presented in the format: 'test ID','slurry composition','date of experiment'. The top left plot contains the hydraulic gradients that were collected during the experiment and the ones calculated using the four component model. A hydraulic gradient of clear water is also plotted to make interpretation of the results easier for the user.

The top right displays the error made in the calculation. The relative error is calculated by dividing the calculated value by the collected data at each velocity for which a data point is available.

The solids concentration is plotted in the bottom right. Two methods of determining the concentration are available and both are plotted in this graph. For some slurry compositions very strange behavior was observed in the U-loop. Since the concentration is one of the most important parameters when making a calculation with the 4 component model it is very important that it is indicated clearly how the concentration was determined. An average of the two concentration determination methods can be used in the calculation or either the U-loop or ultrasonic data can be used. The concentration determination method is always indicated in the top right below the mean concentration. A '1' indicates the ultrasonic concentration data is used, a '2' means the U-loop concentration data is used, and a '3' means the average of the two is used. Above the number indicated the concentration determination method the mean concentration is written down. This mean concentration is the average of all the points on the plot. This mean concentration can be quite deceptive. Especially when a stationary bed forms the delivered concentration goes down drastically. So take this mean concentration with a grain of salt. It can be used to get a general idea of just what sort of concentration was used in these experiments.

Lastly in the bottom right the particle size distribution of the slurry can be found. The thick black vertical stripes indicate the boundaries of different fractions so an idea of the composition of the slurry can be easily read from this graph. One thing that is noticed when viewing the example plot in figure 4.3 is that in the title it seems to imply that one hundred percent of the sediments fall within the X_p-fraction, while the particle size distribution clearly shows this is not the case. The title simply means that all of the sediments come from the particles which was meant to represent the X_p-fraction. Not all of the particles within this fraction fall neatly within the bounds of the X_p-fraction. The calculation is done according to the boundaries determined in section 3.2 which are indicated by the black vertical lines. In the case of figure 4.3, a good 25% of particles are calculated according to the X_f-fraction calculation.
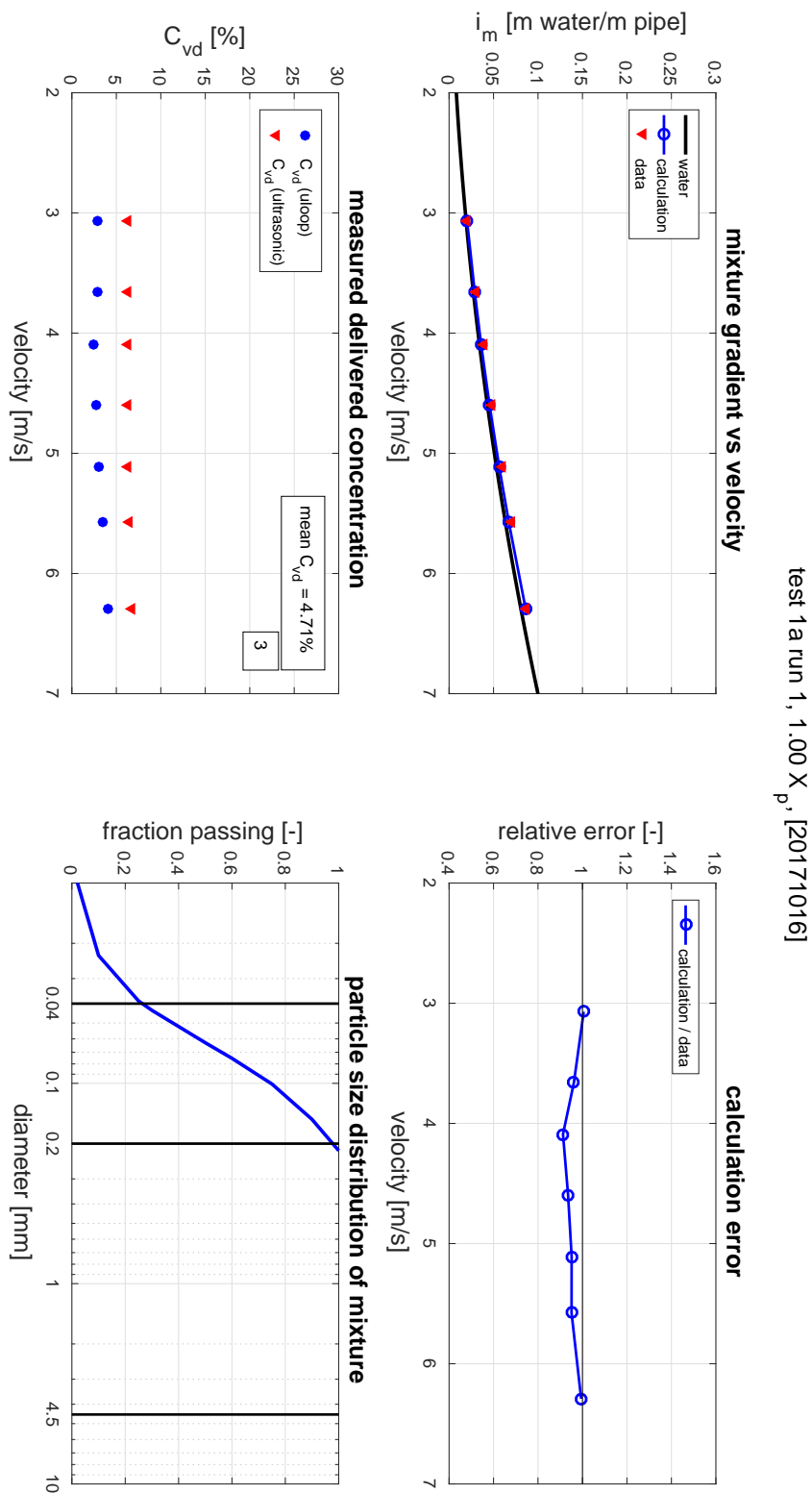
FIGURE 4.3: Example graph of results of typical Slurry data compared to the calculated results.

Chapter 5

Analysis of results

In this chapter the results of the experiments will be shown. A large amount of data has been collected during ten days of experimentation. Displaying the data in such a way that conclusions can be drawn from them is quite challenging. Because reference will often be made to only the experiment ID and not the corresponding slurry composition, the experiment matrix is reiterated here once more:

	1a	1b	2a	2b	3a	3b	4a	4b	5	6a	6b	6c	7	8a	8b	8c	9
X_p	1	.33	.33	.25					1								
X_{hl}										1	1	.67	.50			.33	
X_h		.67	.67	.50		.67		.67									
X_{hu}												.33	.50	1	1	.67	
X_s				.25	1	.33	1	.33									1
$C_{vd,u}$	6.4*	19.9	8.3	8.1	4.0	8.9	6.4	15.2	8.5	10.3	13.5	18.6	14.9	12.4	16.6	21.0	10.8
$C_{vd,l}$	3.2	14.2	4.8	6.4	-0.5	4.5	0	18.2	10.0	5.7	12.9	20.6	13.9	8.0	14.2	24.5	11.1

TABLE 5.1: Test matrix showing slurry composition function and delivered concentrations in percentage according to the ultrasonic $C_{vd,u}$, and the U-loop $C_{vd,l}$.

5.1 Validation of basic logical trends in the data

First and foremost it should be verified that the data that was gathered during the experiments conforms to logical rules. Large particles should result in more pressure loss compared to smaller particles when transported in equal concentrations. Similarly, higher concentrations of the same sediment should results in more pressure loss than lower concentrations. Confirmation of these simple conditions give a good indication that the gathered data is at least accurate in these general trends. Figure 5.1 gives confirmation that larger particles do indeed result in higher measured pressure losses. The trend that higher concentrations of the same sediment result in higher pressure

FIGURE 5.1: Validation that larger particles result in higher pressure losses when transported in similar concentrations.

losses is also true in all experiments. This can be observed in figure 5.2 through 5.5. The data shown in these figures will be discussed in detail in section 5.3.

With these simple conditions validated, the results can be studied with the certainty that at least these basic logical conditions are met.

5.2   Analysis of stationary deposition results

The large amount of tests that have been done in the Shanghai laboratory in the second half of 2017 provide much needed data on the deposit limit velocity. A wide variety of slurries, shown in table 5.1, have been tested in a 300mm pipeline. Observations by the author have been documented as the tests were performed, these notes can be found in appendix C. The observations were possible through a roughly 1 meter perspex section of the pipeline at about 40 meters from the nearest upstream bend. The theoretical background applied in this section can be found in section 2.3.

5.2.1   Stationary deposition observation

The experiments started with the loading of the sediments at the highest pump rpm. Gradually the rpm was lowered until a stationary bed was formed. Often the rpm was lowered slightly into the stationary bed regime. This gives some extra information on the behavior of the bed at velocities below the limit deposit velocity.
The observed stationary deposition velocities are presented in figure 5.2. In the case of multiple runs having been done on a single slurry composition, the denoted mean velocity is the highest velocity at which a stationary deposition has been observed. When drawing conclusions from this graph it is advised to also consult the notes that were made during the experiments in appendix C. The formation of a stationary bed is not a clear process and often two different observers will not agree on exactly when a bed can be considered stationary. The notes will give extra insight in the slurry behavior above and during a stationary bed regime. The data displayed in figure 5.2 can also be used to explain the characteristic increase in the hydraulic gradient when approaching the V_{dl}.
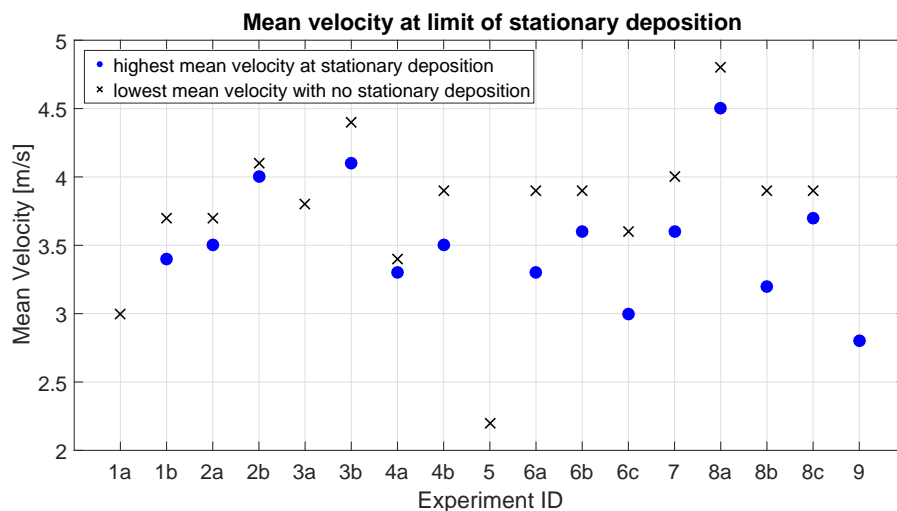
FIGURE 5.2: observed V_{dl} for each of the experiments. When no dot is present, no stationary deposit was observed. Please read the observations section carefully when drawing conclusions from this graph. Especially test 9 is deceiving because no velocity above 2.8 m/s was possible with the installed pump.

5.2.2 Durand model

The original Durand model uses the modified Froude number (F_L) as read from figure 2.5. Reading the modified Froude number from the graph is subject to some degree of inaccuracy as two people are unlikely to read exactly the same numbers from the graph. To ensure absolute reproducibility, all F_L values are documented in table 5.2. The values F_L I, F_L II, and F_L III are calculated according to the processes for method I, II, and III as described in section 2.3.1.

The conventional Durand model uses the modified Froude number as read from figure 2.4. The values for F_L are written down in table 5.3 to ensure reproducibility. The process of calculating the V_{dl} with these numbers is the same as for the original Durand model. A detailed explanation of calculating the V_{dl} according to the Durand model can be found in section 2.3.

The deposit limit velocity is calculated by applying the appropriate F_L value into equation 2.38. The calculated values according to both Durand models can be found in table 5.4 and 5.5.

original	1a	1b	2a	2b	3a	3b	4a	4b	5	6a	6b	6c	7	8a	8b	8c	9
C_v	5	15	7.5	7.5	5	7.5	5	15	10	10	12.5	15	15	10	15	20	10
F_L I.	0.50	1.08	0.95	0.95	0.96	0.95	0.96	1.01	0.50	1.01	1.04	1.06	1.03	0.98	1.01	1.04	0.98
F_L II.	0.50	1.08	0.95	0.95	0.96	1.00	0.96	1.00	0.50	1.01	1.04	1.03	1.02	0.98	1.01	1.04	0.98
$F_L(X_p)$ III.	0.50	0.55	0.50	0.50	0	0	0	0	0.50	0	0	0	0	0	0	0	0
$F_L(X_{hl})$ III.	0	0	0	0	0	0	0	0	0	1.01	1.04	1.07	1.07	0	0	1.11	0
$F_L(X_h)$ III.	0	1.06	0.96	0.96	0	0.96	0	0	0	0	0	0	0	0	0	0	0
$F_L(X_{hu})$ III.	0	0	0	0	0	0	0	0	0	0	0	1.01	1.01	0.98	1.01	1.03	0
$F_L(X_s)$ III.	0	0	0	0.97	0.96	0.97	0.96	1.01	0	0	0	0	0	0	0	0	0.98
F_L III.	0.50	0.89	0.81	0.85	0.96	0.96	0.96	1.01	0.50	1.01	1.04	1.05	1.04	0.98	1.01	1.06	0.98

TABLE 5.2: Rounded off C_v and F_L values. The values for F_L are read from the original Durand (1952) graph (figure 2.5). These numbers are used in the Durand calculation (equation 2.38).

conventional	1a	1b	2a	2b	3a	3b	4a	4b	5	6a	6b	6c	7	8a	8b	8c	9
C_v	5	15	7.5	7.5	5	7.5	5	15	10	10	12.5	15	15	10	15	20	10
F_L I.	0.70	1.50	1.40	1.40	1.35	1.38	1.35	1.38	0.70	1.45	1.50	1.50	1.45	1.38	1.38	1.40	1.35
F_L II.	0.70	1.50	1.40	1.35	1.35	1.35	1.35	1.35	0.70	1.45	1.50	1.45	1.40	1.38	1.38	1.40	1.35
$F_L(X_p)$ III.	0.70	0.70	0.70	0.70	0	0	0	0	0.70	0	0	0	0	0	0	0	0
$F_L(X_{hl})$ III.	0	0	0	0	0	0	0	0	0	1.45	1.50	1.55	1.55	0	0	1.55	0
$F_L(X_h)$ III.	0	1.50	1.40	0	1.40	0	1.40	0	0	0	0	0	0	0	0	0	0
$F_L(X_{hu})$ III.	0	0	0	0	0	0	0	0	0	0	0	1.38	1.35	0	0	1.38	0
$F_L(X_s)$ III.	0	0	0	1.35	1.35	1.35	1.35	1.35	0	0	0	0	0	0	0	0	1.35
F_L III.	0.61	2.82	2.82	2.70	2.37	3.40	2.37	3.40	0.61	4.00	4.00	3.79	3.69	3.38	3.38	3.58	2.37

TABLE 5.3: Rounded off C_v and F_L values. The values for F_L are read from the conventional Durand and Condolios (1953) graph (figure 2.4). These numbers are used in the Durand calculation (equation 2.38).

original	1a	1b	2a	2b	3a	3b	4a	4b	5	6a	6b	6c	7	8a	8b	8c	9
I.	1.56	3.37	2.96	2.96	2.99	2.96	2.99	3.15	1.56	3.15	3.27	3.30	3.21	3.05	3.15	3.24	3.05
II.	1.56	3.37	2.96	2.96	2.99	3.12	2.99	3.12	1.56	3.15	3.27	3.21	3.18	3.05	3.15	3.24	3.05
III.	1.56	2.77	2.52	2.65	2.99	2.99	2.99	3.15	1.56	3.15	3.27	3.27	3.24	3.05	3.15	3.30	3.05
obs	-	3.4	3.5	4.0	-	4.1	3.3	3.5	-	3.3	3.6	3.0	3.6	4.5	3.2	3.7	2.8

TABLE 5.4: Durand results of the V_{dl}-calculation using the F_L values read from the original Durand graph (figure 2.5). The indicators I, II and III represent the different methods of calculation V_{dl} for wide slurries. The indicator obs represents the velocity at which a stationary bed was observed. All values displayed in this graph are in meters per second.

conventional	1a	1b	2a	2b	3a	3b	4a	4b	5	6a	6b	6c	7	8a	8b	8c	9
I.	2.18	4.67	4.36	4.36	4.21	4.30	4.21	4.30	2.18	4.52	4.67	4.67	4.52	4.30	4.30	4.36	4.21
II.	2.18	4.67	4.36	4.21	4.21	4.21	4.21	4.21	2.18	4.52	4.67	4.52	4.36	4.30	4.30	4.36	4.21
III.	2.18	3.85	3.64	3.78	4.21	4.31	4.21	4.52	2.18	4.52	4.67	4.66	4.52	4.30	4.30	4.48	4.21
obs	-	3.4	3.5	4.0	-	4.1	3.3	3.5	-	3.3	3.6	3.0	3.6	4.5	3.2	3.7	2.8

TABLE 5.5: Durand results of the V_{dl}-calculation using the F_L values read from the conventional Durand graph (figure 2.4). The indicators I, II and III represent the different methods of calculation V_{dl} for wide slurries. The indicator obs represents the velocity at which a stationary bed was observed. All values displayed in this graph are in meters per second.

5.2.3 Wilson model

The Wilson model was described in section 2.3 with an extension by Wilson & Judge (1976) and an extension by Sanders (2004). With the results of the experiments available a comparison of the experimentally observed limit deposit velocities and the model can be made. Table 5.6 displays the V_{sm} values as calculated by the Wilson nomograph approximation without making use of the extensions by Wilson & Judge, and Sanders. Figure 5.3 shows the Wilson nomograph approximation according to equation 2.39 and the two extensions, equation 2.40 and 2.41, with the observed limit deposit velocities. When a mixture consists of more than one component a d_{50} is not easily determined. Two methods for doing this have been proposed as described in section 2.3.1. When the indicators for method I and II coincide in figure 5.3 it indicates that the slurry consists of a single component and the two methods give the same d_{50}.

When looking at figure 5.3 it can be concluded that the Wilson model may not prove to be as conservative as it is intended to be. Many data points fall above the curve and while the Sanders cutoff does appear to make the determination of the critical velocity more accurate, it is at the expense of the promised conservatism of the model. The determination of the d_{50} does have a large effect on the accuracy of the model. Method I seems to universally calculate a higher mean particle diameter which proves detrimental to the accuracy of the model, at least on the right side of the peak of the curve.

Wilson	1a	1b	2a	2b	3a	3b	4a	4b	5	6a	6b	6c	7	8a	8b	8c	9
I.	0.61	4.01	4.01	3.91	2.37	3.59	2.37	3.59	0.61	4.00	4.00	3.91	3.81	3.38	3.38	3.57	2.37
II.	0.61	4.01	4.01	3.17	2.37	2.97	2.37	2.97	0.61	4.00	4.00	3.78	3.66	3.38	3.38	3.56	2.37
III.	0.61	2.82	2.82	2.70	2.37	3.40	2.37	3.40	0.61	4.00	4.00	3.79	3.69	3.38	3.38	3.58	2.37
obs	-	3.4	3.5	4.0	-	4.1	3.3	3.5	-	3.3	3.6	3.0	3.6	4.5	3.2	3.7	2.8

TABLE 5.6: Wilson method results of the V_{dl}. The indicators I, II and III represent the different methods of calculation V_{dl} for wide slurries. The indicator obs represents the velocity at which a stationary bed was observed. All values displayed in this graph are in meters per second.

5.2.4 Comparison of Wilson and Durand models

Comparing all of the results displayed in the tables 5.4, 5.5, and 5.6, the graphs as shown in figure 5.4 are obtained. The graphs shows the comparison of the observed limit deposit velocities and the calculated limit deposit velocities. The left column shows results for all experiments and the right column shows only the results of

the multi-component experiments. Comparing the different versions of the Durand model, it can be seen that the original version is slightly more accurate in predicting the limit deposit velocity. Applying the conventional Durand model, the results may be a little more scattered and inaccurate, but a merit of using this model is that the calculated V_{dl} is more conservative. The conservatism of this model may be appreciated in risk averse operations.

The Wilson model is the most accurate overall. However, it does also have the most scatter in the results. The calculated values of the V_{sm} lean slightly on the optimistic side where the calculated velocities are lower than the observed velocities.
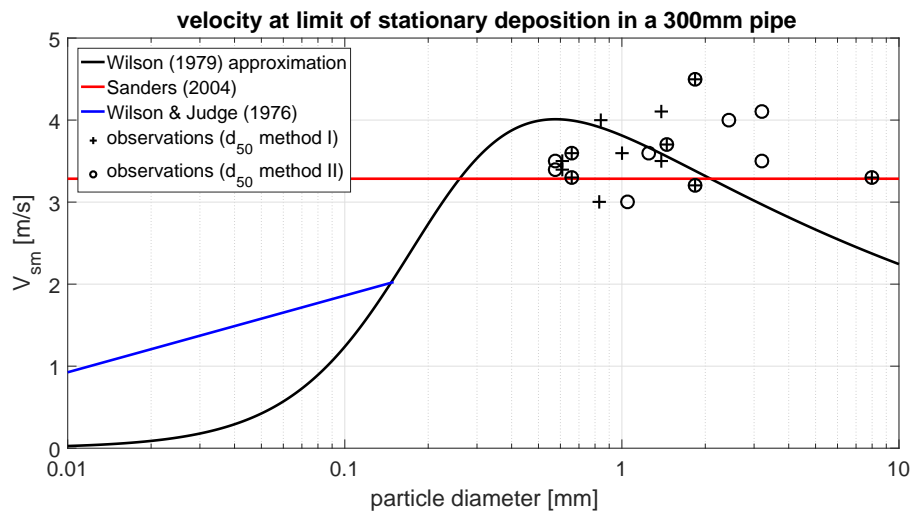
FIGURE 5.3: Approximation of Wilson's nomograph according to equation 2.39 with extensions by Wilson & Judge and Sanders. The observations are linked to d_{50} values determined by method I and II as described in section 2.3.1.

5.2.5 Comparison of the methods of incorporating broad sieve curves into the V_{dl}/V_{sm} calculation

Three methods of incorporating a broad or multicomponent sieve curve into the V_{dl}/V_{sm} calculation were proposed. Method I and II use a modified single d_{50} and calculate the critical velocity in this manner. Method III uses the d_{50} of every component present in the slurry and calculates the critical velocity for each component individually before combining them.

In figure 5.4 it is seen that method III generally results in the lowest calculated critical velocity. Method I and II usually do not differ too much from each other. But when they do method I is universally results in a higher V_{dl} than method II.

When dicing which method is best, the criteria are accuracy and conservatism as dredging practices are generally risk averse operations. With these criteria established the most useful method will have to be method I. Maybe surprisingly the method most suited for determining the critical velocity when dealing with complex slurries is simply plugging the mass median diameter of the sieve curve into the model of choice.
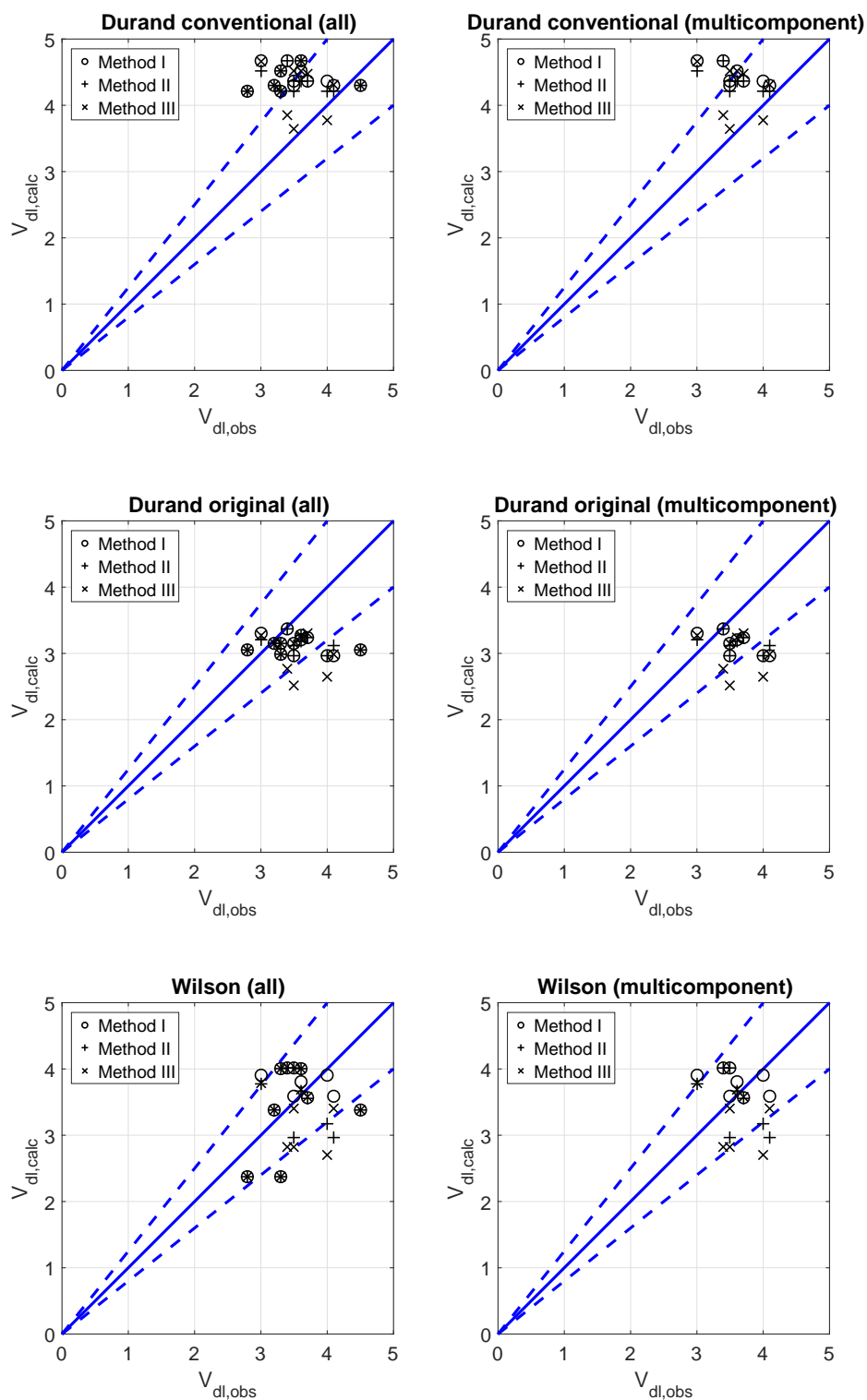
FIGURE 5.4: Comparison of the calculated V_{dl} to the observed V_{dl}. The left column shows all experiments including the ones with only one component. The right column shows only those experiments where multicomponent mixtures were used. The dotted lines indicate a 20% relative error.

5.3 Analysis of 4 component model results

Objective number one of this study is to determine in what degree the 4 component model is accurate in determining the hydraulic gradient of a wide variety of slurries. The accuracy of the individual models making up the 4 component model is analyzed and comparisons between various mixtures are made.

5.3.1 Interpretation of the 4 component model results.

The results of the 4 component model calculation serve to determine the accuracy of the current version of the 4 component model in predicting the pressure gradient over a long straight section. The full results visualized in the same manner as figure 4.3 can be found in appendix E. This section only serves to discuss the findings of these graphs.

Test 1a; 1.00 X_p , C_{vd} = 4.8%: Figure E.1 and E.2. The model seems to predict pressure losses in the X_p fraction with excellent accuracy. A slight underestimation is present throughout the entire velocity interval but nothing of note. In run 2 the underestimation becomes slightly more noticeable but this is most likely due to the absence of ultrasonic density meter data. Run 1 is calculated with an average of the ultrasonic and U-loop data and run 2 is calculated only with U-loop data. Overall the error made by the model is quite manageable. Then again, concentrations are so low that these results are not to very interesting to anyone.

test 1b; 0.33 X_p + 0.67 X_h , C_{vd} = 17.1%: Figure E.3 and E.4. The model again predicts with remarkable accuracy the pressure losses. Only below the limit deposit velocity do the experimental losses deviate in a notable manner from the calculated losses. There is quite a large difference between the concentrations measured by the U-loop and by the ultrasonic density meter. When averaging the results of both the expected accuracy of the calculation is to within a few percent so no major problems should be expected here.

test 2a; 0.33 X_p + 0.67 X_h , C_{vd} = 6.6%: Figure E.5 and E.6. Both show exactly the same behavior. It starts with a slight over prediction of the pressure loss at high velocities. The calculation is more or less on point until a stationary deposition formed. When a stationary deposit forms the calculation underpredicts losses by a lot. This is a well known attribute of basically all known models.

test 2b; 0.25 X_p + 0.50 X_h + 0.25 X_s , C_{vd} = 7.3%: Figure E.7 and E.8. When X_s-particles are added to the slurry of test 2a the calculation makes a heavy underestimation of the losses. Delivered concentrations as indicated by the U-loop and ultrasonic move closer together giving a hint of changing behavior of the slurry. At high velocities the model should be usable, underpredicting the pressure losses at about 20%. But because a stationary deposition forms quite quickly when X_s-particles are present in the flow, the model quickly becomes unusable when velocities drop below the critical velocity.

One thing that is noteworthy is that the slurry behaves exactly the same way in both runs. There seems to be order here and fixing the model to give more accurate results could be done by introducing additional empirical coefficients. The real question is whether the introduction of even more (semi-) empirical coefficients is desirable in an already very complex model.

test 3a; 1.00 X_s , C_{vd} = 4.0%: Figure E.9 and E.10. Completely opposite to what one would expect after the behavior of the slurry in test 2b, where the experimental losses were lower than calculated after adding X_s-particles. Here the model severely overpredicts the pressure losses. This leads to the suspicion that the interaction between the different fractions is not accurately captured by the model. When only X_s-particles are present in the system the losses are lower than expected but when they are combined with X_h and X_p particles like in experiment 2b, they are higher than expected.

test 3b; 0.67 X_h + 0.33 X_s , C_{vd} = 6.7%: Figure E.11 and E.12. The accuracy of the model is accurate up until a stationary bed forms. This seems strange as the similarly wide slurry of test 2b resulted in quite inaccurate results. Strangely enough, the results are almost identical in accuracy when compared to test 2a, with a slight overestimation at the highest velocity and than predicting with good accuracy around medium velocities until giving large underestimations when a stationary bed forms. This leads to the suspicion that the X_h-particles dictate for the most part how the slurry behaves.

test 4a; 1.00 X_s , C_{vd} = 6.4%: Figure E.13 and E.14. Like test 3a; Massive overestimations over the entire velocity interval. The error becomes more severe the deeper into the stationary bed regime the flow enters. Like in test 3a, a thing that should be noted is that only the ultrasonic density meter seems to work when pumping X_s-particles at low concentrations. This leads to the concentration being calculated from only the ultrasonic data. When this slurry is to be calculated with a working U-loop, the concentration would likely be slightly lower leading to less severe overestimations. Still, the model does not seem to predict losses accurately when only X_s-particles are present in the slurry.

test 4b; 0.67 X_h + 0.33 X_s , C_{vd} = 16.7%: Figure E.15 and E.16. The addition of X_h-particles appears to drastically change the behavior of the slurry. It is remarkable how accurate the model becomes when adding the medium sized X_h-particles. A minor overestimation remains, but everything stays well within 20%. Like always, the effect of a stationary deposition can be seen very well reflected in the data. Also note the measured delivered concentration of the U-loop and ultrasonic. When a stationary deposition forms they seem to converge towards each other. Indication almost the exact same values at the lowest velocity of run1.

test 5; 1.00 X_p , C_{vd} = 9.3%: E.17 and E.18. Results are more or less accurate falling mostly within 10% accuracy. Strangely enough, this slurry composition seems to be predicted less accurately at high velocities. This is completely opposite to the other slurry composition which are usually more accurately predicted by the 4 component model at high velocities and are drastically mispredicted once a stationary deposition forms. This slurry composition does not suffer from this phenomenon because a stationary deposition was not observed during this test.
Also not that the U-loop and ultrasonic concentration measurements diverge with decreasing velocity, this is also in opposition to the previous experiments.

remarks on experiments 6 through 8 : Results of the lower fraction and upper fraction of the X_h-fraction are ideally compared against each other as well as the whole fraction. The experiments on the whole X_h-fraction have been done by J. de Ridder

some months before the experiments of this thesis. The U-loop was not yet available during these experiments making the comparing of these results a little more challenging. The U-loop concentration measurements seem to lower the concentration at which the calculations are executed a little bit at the lower concentration. At the high concentrations of test 6c and 8c, the U-loop data increases the averaged concentration a little bit.

test 6a; 1.00 X_{hl} , C_{vd} = 8.0%: Figure E.19. Results are accurate throughout the entire velocity interval, falling within 20% accuracy at all times. The 4 component model seems to slightly overestimate the losses of the small particles of the X_h-fraction. Like with basically all low concentrations the ultrasonic and the U-loop indicate quite different concentrations so keep this in mind when interpreting the results.

test 6b; 1.00 X_{hl} , C_{vd} = 13.2%: Figure E.20. Like test 6a the 4 component model overestimates the losses slightly over the velocity interval. The effect of a stationary deposition is more pronounced in the higher concentration variant of this slurry composition. At a velocity of 3.6 m/s it can be clearly seen that the measured losses start to increase significantly. The concentration measured by the U-loop and ultrasonic also start to diverge at this velocity. Overall the prediction made by the 4 component model is more or less accurate over the entire velocity interval staying within roughly 10% relative error.

test 6c; 0.67 X_{hl} + 0.33 X_{hu} , C_{vd} = 19,6%: Figure E.21. Very similar results to test 6a and 6b. The Wilson V_{50} model, which is used on the heterogeneous fractions, seems to work extraordinarily well in predicting pressure losses of medium sized particles. For this higher concentration composition it works almost perfectly at higher velocities. Something to note might be that the error line did move downward slightly indicating that the larger particles within the X_h-fraction contribute more to the pressure losses than the smaller particles, since losses in test 6a and 6b were consistently overpredicted.
The effect of a stationary deposition is still clearly visible in the data. The losses increase significantly around 3.1 meters per second. Something else to note is the U-loop is now indicating higher concentrations than the ultrasonic. This has likely to do with the higher concentration within the pipe and not with the slurry composition.

test 7; 0.50 X_{hl} + 0.50 X_{hu} , C_{vd} = 14.4%: Figure E.22 and E.23. Very accurate results over the entire velocity interval. The effect of a stationary deposition is visible like before. The losses seem to slightly decrease in the velocity range just before a stationary deposition is observed. The cause of this is unknown. The ultrasonic seem to agree on the concentration.

test 8a; 1.00 X_{hu} , C_{vd} = 10.2%: Figure E.24. A similar shape in the calculation error as in test 6a appears to take place. Some erratic behavior in the measured losses can be seen at the highest velocities, this was also the case in test 6a. The cause of this is still unknown. In this concentration a stationary deposition was observed extraordinarily early. The earliest of any experiment performed during this research in fact. This seems like a very strange slurry composition for this outlier result. Due to time constraint test 8a could only be performed once, which is regretful since it would be interesting to see if this strange behavior would repeat itself.

Something else to note is that usually with the establishment of a stationary deposition the measured losses increase drastically. In this experiment the losses actually seem to decrease. Strange behavior all around in this test.

test 8b; 1.00 X_{hu} , C_{vd} = 15.4%: Figure E.25. Very accurate results over the entire velocity interval again. The most interesting thing is that similar to test 6c, the pressure loss seems to decrease (with regards to the expected pressure loss) right before a stationary deposition is formed. Then once a bed is formed the pressure losses increase significantly again.
Pressure losses seem to be a little bit higher than test 6b where particles at the lower part of the X_h-fraction were tested. So there does seem to be some divergent behavior within the X_h-fraction but nothing too serious.

test 8c; 0.33 X_{hl} + 0.67 X_{hu} , C_{vd} = 22.8%: Figure E.26. Very similar results to test 8b. The same strange behavior where the measured losses seem to be lower than the calculated losses right before a bed is formed is observed here again. Overall the model seems to predict pressure losses quite well over the entire velocity interval never falling outside of 20% relative error.
Like test 6c the U-loop indicates concentrations a little higher than the ultrasonic.

test 9; 1.00 X_s , C_{vd} = 11.0%: Figure E.27. When pumping X_s-particles in high concentrations the pump could not get the velocity above 3 m/s. A bed was immediately formed although some density waves remained in the system. For a report on the slurry behavior near the critical velocity during the experiments appendix C can be consulted.
Completely unexpected when looking at test 3a and 4a, the pressure losses are predicted almost perfectly. Lowering the pump rpm seems to mostly reduce delivered concentration instead of velocity, but the measured and calculated results fall mostly within 5% relative error.

5.3.2 Comparison of slurry composition on accuracy of the model

In figure 5.5 a couple of different slurry compositions are displayed. The top row 'a' displays slurries around 5% concentration, and row 'b' and 'c' display slurries around 10% and 15% concentration respectively. What can be seen is that especially at low concentrations the model does not seem to accurately predict pressure losses. Test 3a shows a large overprediction, while JdR1 shows an underprediction which increases with decreasing velocity. Something to note once again, is that the JdR experiments were performed when the lab did not have all the equipment available yet. Errors because the lab was not set up to completion could have sneaked into the measurements. A comparison of a JdR experiment to an experiment carried out at a later date in a complete lab is displayed in figure 5.6. The shape of the experimental data are identical. There is however a displacement in the measurements, where a larger hydraulic gradient was measured by J. de Ridder. An easy explanation for this phenomenon is that the actual concentration during the JdR experiments were higher than indicated by the ultrasonic density meter. No concrete proof can be given for this explanation.
The middle row 'b', shows slurries at around 10% concentration. Very accurate results have been found around this range. Even the X_s fraction which showed massive overpredictions at lower concentrations as can be seen in figure 5.7 row 'e' was predicted with astonishing accuracy. This leads to the suspicion that concentration

should play a more important role in calculating the hydraulic gradient of the X_s fraction. Test 5 and 8a, also shown in row b), both show some fluctuation around the expected hydraulic gradient but nothing of note is observed in these two experiments.

The bottom row in figure 5.5 shows concentrations around 15%. What can be clearly seen is that the formation of a bed starts to play an important role at lower velocities. All three experiments show a characteristic leap in the hydraulic gradient when approaching 3 m/s mean velocity. Generally the accuracy of the model is quite good at velocities above 4 m/s. Like in row 'a'.

5.3.3 Effect of concentration on the accuracy of the model

Many of the experiments were performed using the same mixture composition at different concentrations. This was done so the accuracy of the 4 component model in predicting the hydraulic gradient at different concentrations could be studied. To get a better overview on the slurry compositions and their concentrations the experiment matrix (table 5.1) is rearranged in a more logical order. The experiments by J. de Ridder (table 4.3) are also included in the new rearranged test matrix (table 5.7). This table only includes experiments done at different concentrations.

	1a	5	6a	6b	JdR1	JdR2	JdR3	8a	8b	3a	4a	9	2a	1b	3b	4b
X_p	1	1											.33	.33		
X_{hl}			1	1												
X_h					1	1	1						.67	.67	.67	.67
X_{hu}								1	1							
X_s										1	1	1			.33	.33
$C_{vd,u}$	6.4	8.5	10.3	13.5	4.5	12.7	15.1	12.4	16.6	4.0	6.4	10.8	8.3	19.9	8.9	15.2
$C_{vd,l}$	3.2	10.0	5.7	12.9				8.0	14.2			11.1	4.8	14.2	4.5	18.2

TABLE 5.7: Test matrix showing slurry composition and delivered concentrations in percentage according to the ultrasonic $C_{vd,u}$, and the U-loop $C_{vd,l}$. See chapter 3 for more information on the contents of this table.

Partial results, showing only the measured hydraulic gradient and the calculation error of the single sediment experiments, are plotted in figure 5.7 and 5.9 in row 'a' through 'e'. These results aim to show trends in the behavior of the model when increasing concentrations. What can be seen in these graphs is that generally the accuracy in predicting the hydraulic gradient increases with increased solids concentration. Calculation errors fall mostly within 20% relative error which is reasonable for any model. Something that can be seen is that when velocities fall below the critical velocity, the actual pressure loss is significantly higher than calculated. This is a known limitation of the 4 component model, or any model for mixture flow for that matter.

The model does seem to consistently under-predict the pressure losses in the pure heterogeneous fraction (row 'c'). While the relative error still is around 20%, it does seem a little bit suspicious when comparing it to the other heterogeneous fractions X_{hl} and X_{hu} (row 'b' and 'd'). The calculations of the X_{hl} and X_{hu} fractions are based on concentrations measurements of both the U-loop and the ultrasonic, while the X_h fraction calculations are based only on the ultrasonic concentration measurements. The ultrasonic concentration measurements are generally a little bit higher than the U-loop measurements which makes the under-prediction of the model even stranger. The general trend in the calculation error does follow the expected route where the measured losses are significantly higher than the calculated losses once a

a)

b)

c)
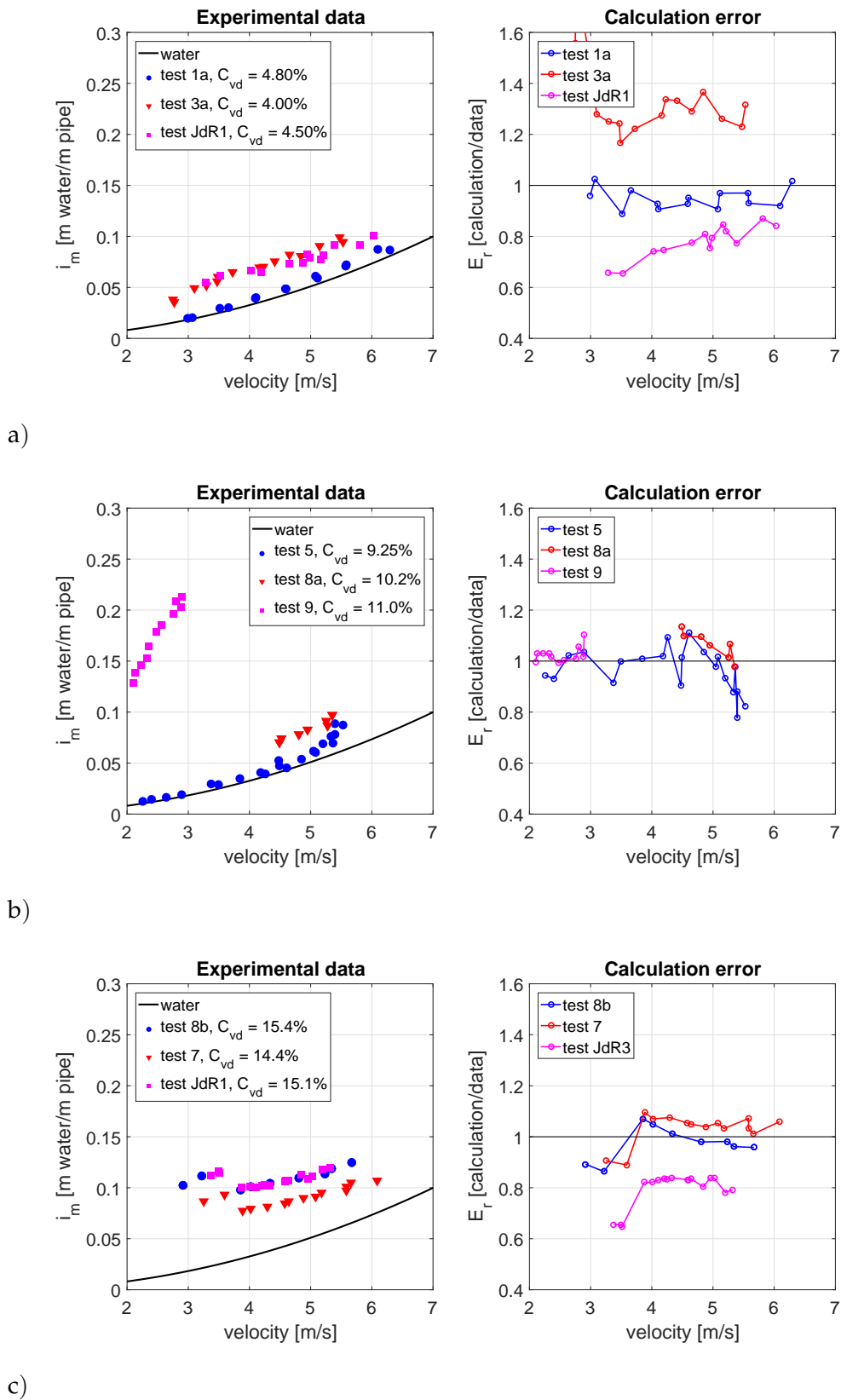
FIGURE 5.5: Comparisons of different slurry compositions around the same solids concentrations.
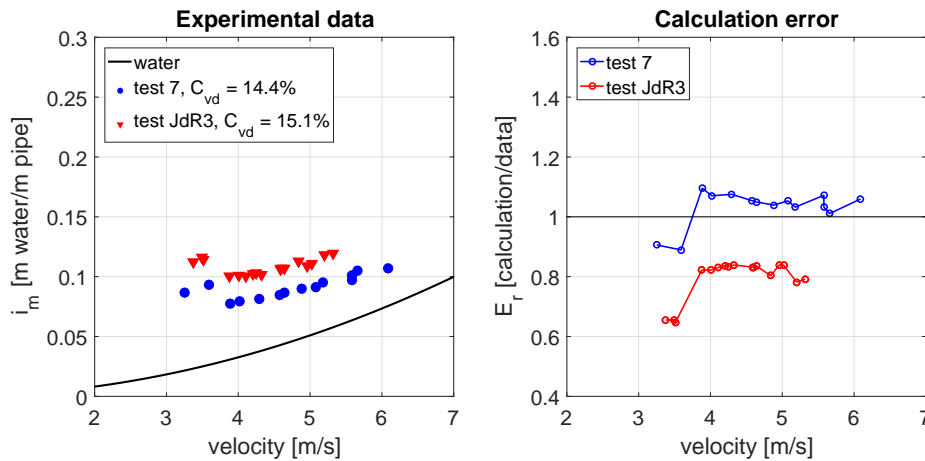
FIGURE 5.6: Comparison of composite X_h fraction and the X_h used by Jelte de Ridder.

stationary bed forms.

The X_s fraction pressure losses, shown in row 'e', are significantly overpredicted at low concentrations. This is easily explained when looking at the definition of the stratified fraction. The whole idea is that the particles in the stratified fraction travel as contact loads. In both of the lower concentration experiments of the X_s fraction (experiment 3a and 4a) no stationary bed or even a really explicit sliding bed were observed. The equation that calculates the hydraulic losses of the stratified fraction does not deal well with suspended sediments. Maybe a term that lowers the pressure losses at concentrations below 10% could be included in the Δi_s equation.

What is surprising when considering the large over-predictions in the low concentration X_s experiments, is the incredible accuracy in the higher concentration X_s experiment. The concentration used in experiment 9 as indicated in figure 4.3 is deceiving as it varies wildly. When lowering the pump rpm the velocity decreases only slightly, mostly the delivered concentration just decreases. For a more accurate report on the experiment one can refer to appendix E. An explanation for the accurate results of test 9 is that at every tested velocity a perfectly defined bed was observed. Thus meeting the definition set for the equation used for the X_s fraction.

When considering concentration in multi-component slurries the effects can be linked without too much imagination to the single component slurries. Row 'f' through 'i' show the experiments with multiple components at more than one concentration. The 0.33 X_p + 0.67 X_h slurry seems to increase in accuracy with increased concentration like X_p particles and the bed development can be easily spotted like in the X_h fraction experiments. Similarly the over-prediction of the X_s fraction can be spotted at the higher concentration of the 0.67 X_h + 0.33 X_s slurry experiments.

5.3.4 Effect of combined slurries on hydraulic gradient

The 4 component model aims to make accurate predictions on the hydraulic gradient for very wide slurries. The individual fractions interact with each other resulting in very dynamic behavior with regard to the hydraulic gradient. The multicomponent slurries can be viewed in the bottom row of figure 5.8 and in figure 5.9. What
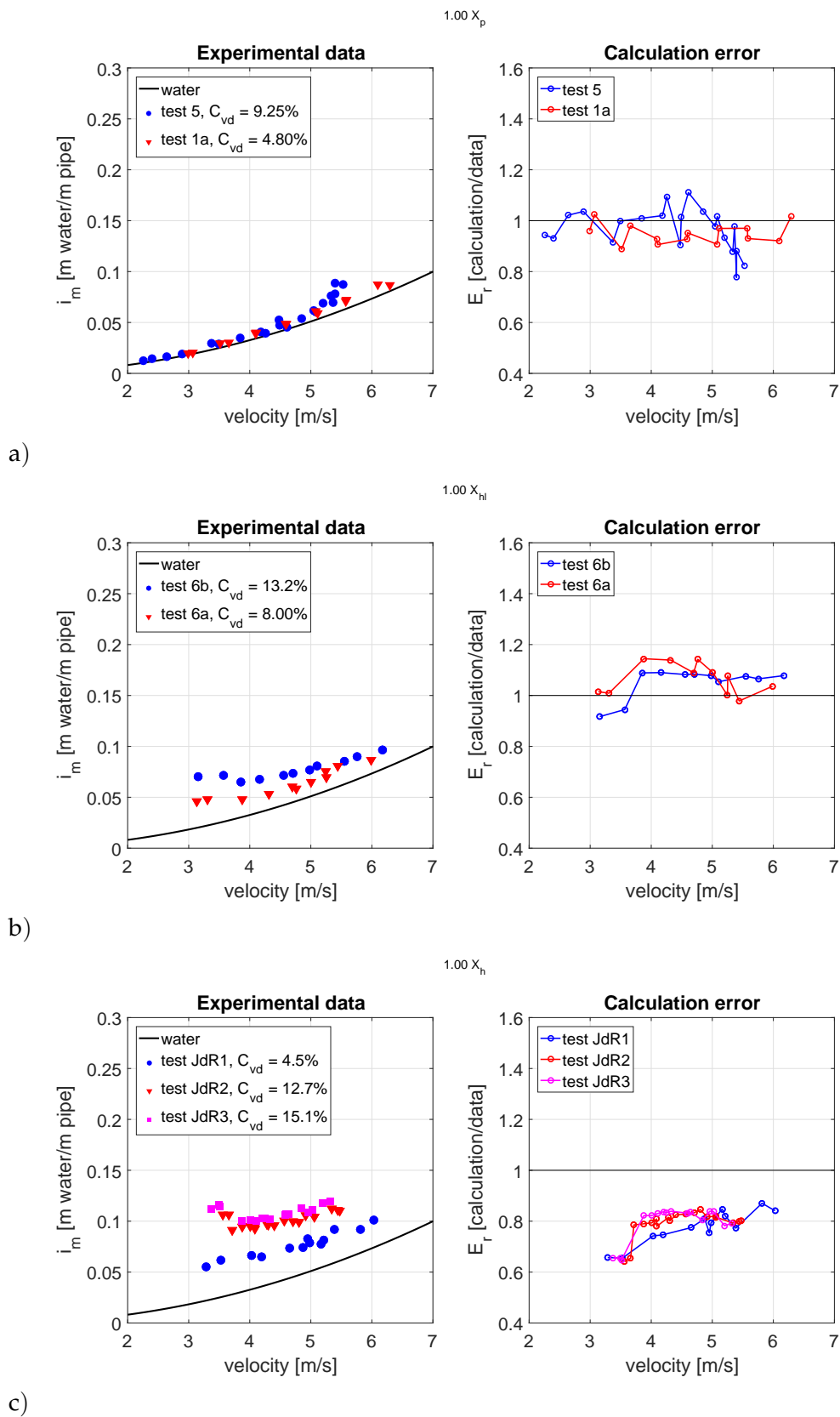
FIGURE 5.7: Comparisons of slurry compositions at different concentrations. Part 1 of 3.
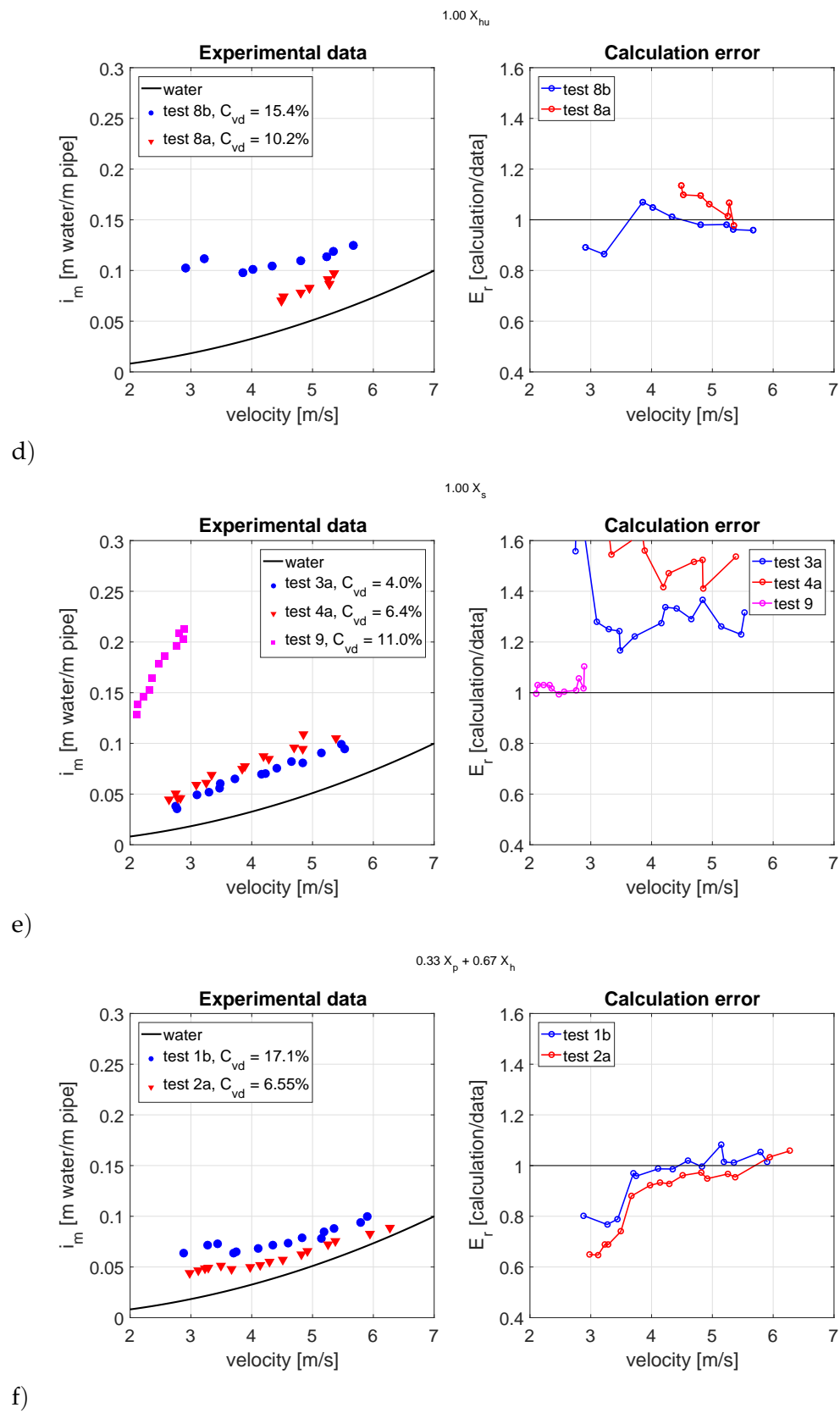
FIGURE 5.8: Comparisons of slurry compositions at different concentrations. Part 2 of 3.

$0.67\,X_h + 0.33\,X_s$

g)

test 6c: $0.67\,X_{hl} + 0.33\,X_{hu}$, test 8c: $0.33\,X_{hl} + 0.67\,X_{hu}$, test 7: $0.50\,X_{hl} + 0.50\,X_{hu}$

h)

test 2b: $0.25\,X_p + 0.50\,X_h + 0.25\,X_s$

i)
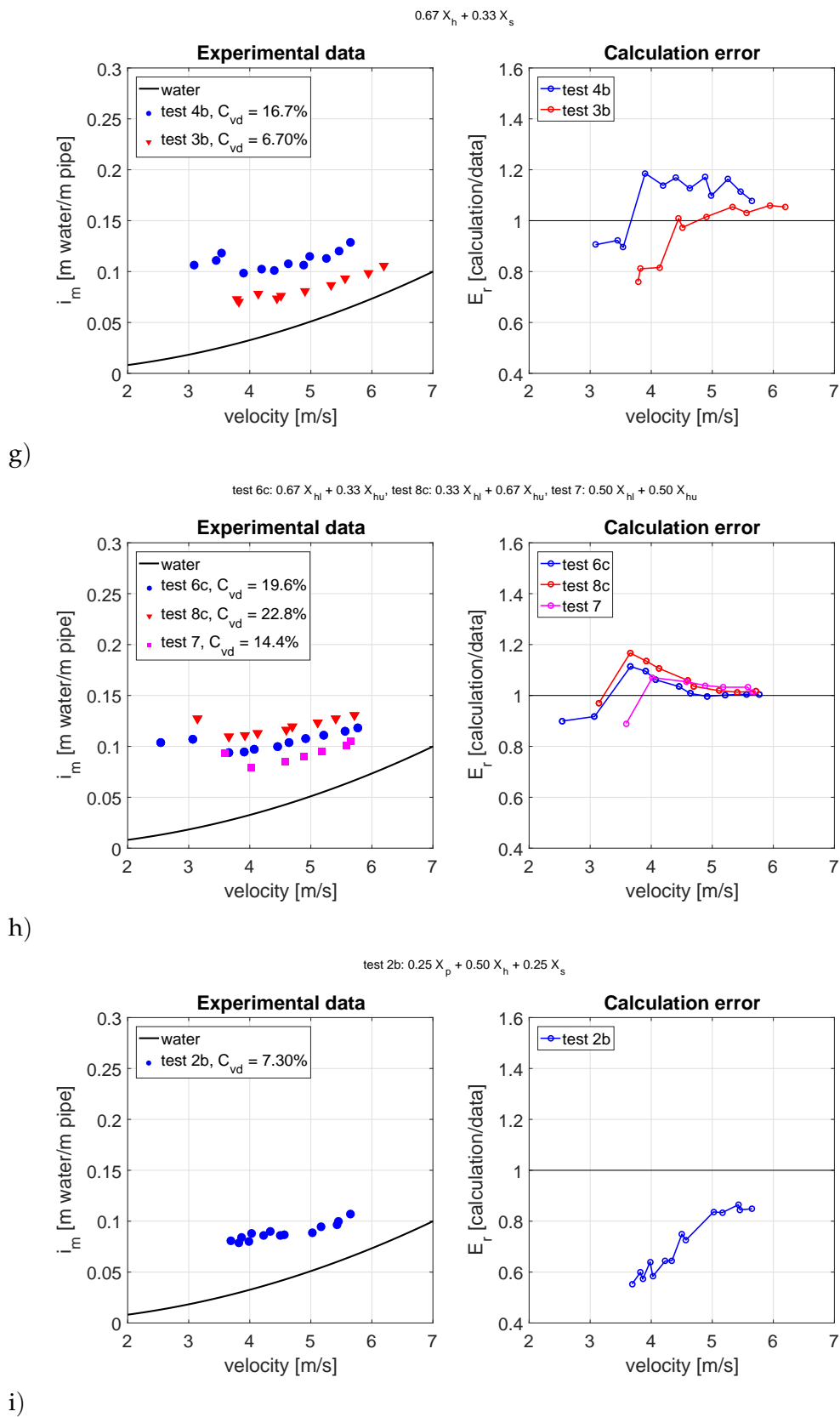
FIGURE 5.9: Comparisons of slurry compositions at different concentrations. Part 3 of 3.

can be seen is that for most of the mixtures the hydraulic gradient is reasonably predicted over the velocity interval. The widest tested slurry of test 2b seen in row 'i' in figure 5.9 does leave something to be desired. For high velocities the accuracy is reasonable like for all of the wide slurries. At even moderate velocities, only slightly below 5 m/s, the accuracy begins to fall drastically though. In the measurements the pressure gradient does not seem to fall much below 5 m/s.

5.3.5 pressure losses in the upper and lower part of the heterogeneous fraction

In the theory section of this research it has been hypothesized that the pressure losses due to the heterogeneous fraction are no longer accurately predicted in large diameter pipes. This is because of the definition of the upper bound of the heterogeneous fraction which is linked linearly to the pipe diameter. A good portion of the experiments were done to validate this hypothesis. The heterogeneous fraction was split into a lower part (0.2mm to 1mm) and an upper part (1mm to 4.5mm) and experiments were ran using these newly created fractions. When looking at the results of the X_{hl} and X_{hu} fractions, figure 5.7 row 'b' and figure 5.8 row 'd', it can not be said that the suspicion was confirmed. Results of both fractions remained wholly within 20% relative error and even the establishment of a stationary bed was at around the same velocity for both fractions. The experiments of the X_{hu} particles at around 10% concentration did result in a stationary bed at a velocity that is higher than expected. Strangely enough this behavior was not seen again at the increased concentration so this could just be a freak occurrence.

5.3.6 Usage of V_{50} model in the stratified fraction

One thing that has stood out during the analysis of the results is that the stratified model used on X_s-particles does not accurately predict the pressure losses at low velocity. Possibly this is due to the fact that most of the X_s-particles are in suspension when transported at low concentrations. A hypothesis is that the V_{50} model is more suited to predict pressure losses in the stratified fraction when the sediment is not transported in a stratified manner. Row 'a' in figure 5.10 gives a comparison of the calculation error that is made when applying the stratified flow model and the V_{50} model on test 3a and 4a. What can be seen immediately is that the V_{50} model is significantly more accurate at velocities above roughly 3.5 m/s. At lower velocities the accuracy does suffer, but not more so than when using the stratified flow model. Using the V_{50} model on experiments with more than one sediment can show to improve the accuracy somewhat. Row 'b' and 'c' show experiments with a minor fraction of X_s-particles present in the slurry. Especially experiment 3b and 4b show a noticeable improvement in accuracy, especially at the higher tested velocities. Experiment 2b, which really has only a very minor presence of X_s-particles does not seem to benefit very much from applying the V_{50} model.
More extensive results of all the experiments containing X_s particles can be found in appendix F.
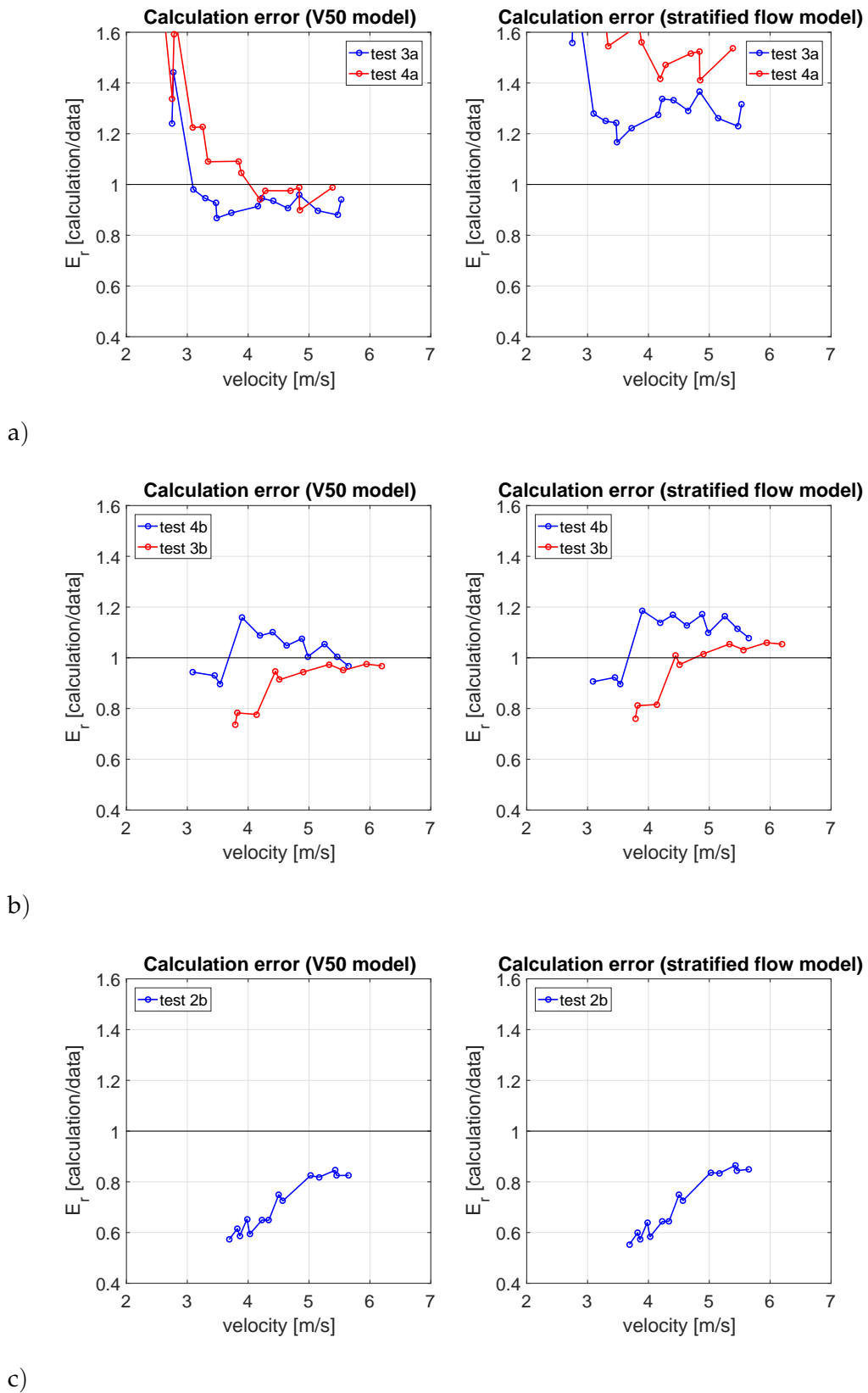
FIGURE 5.10: Comparison of hydraulic gradient calculation when using stratified flow model and V_{50} model.

Chapter 6

Conclusions and recommendations

In this chapter conclusion of this research are drawn, and recommendations for further research will be made.

6.1 Conclusions

The objective established at the beginning of this research was to gather insight in the performance of the 4 component model. Many results of experiments done in small diameter pipelines are known and the results of these studies have shaped the model into what it currently is. The results of the research done for this study will help to validate whether the 4 component model is also accurate when predicting hydraulic gradients in larger diameter pipes like the 300mm pipe used in this research.

In addition to the 4 component model research, the experiments proved an excellent opportunity to provide data on stationary bed development in wide graded slurries. The Durand model and the Wilson model for critical velocity were tested on accuracy. Three methods of accounting for the wide sieve curves were also considered.

6.1.1 Conclusions regarding the 4 component model research

When applying the 2017 version of the model as described by Visintainer et al. (2017) in a 300mm diameter pipeline the accuracy of the model falls mostly within 20% relative error. When considering small and intermediate sized particles (10μm < d < 5 mm) and concentrations below 20% at velocities used in conventional dredging practices, the error can often be considered to be within 10% relative error.

Pressure losses of slurries containing particles belonging to the stratified fraction were calculated the most inaccurate. The presence of X_s particles (particles larger than 0.015 times the pipe diameter) in the slurry reduces the performance of the model universally. The usage of the V_{50} model instead of the stratified flow model to calculate pressure losses of X_s particles in low concentrations did seem to be promising, reducing the relative error to below 20% for velocities above 3.5 m/s.

The hypothesis that the V_{50} model does not work correctly when used on a wide heterogeneous fraction is not substantiated by the results of this research. Hydraulic gradients using only the lower (X_{hl}) or the only the upper (X_{hu}) portion of the heterogeneous fraction are calculated equally well. Slurries made out of a variety of different ratios of these fractions were also seen to behave similarly and losses were predicted well in these combined slurries.

6.1.2 Conclusions regrading stationary deposition research

When using the Durand model to predict the deposit limit velocity, the original 1952 version of the Durand graph was shown to be slightly more accurate. The more widely known 1953 version of the Durand graph does show some merit in being more conservative in its predictions.

Comparing the Durand model to the Wilson model, it was shown that the Wilson model is most accurate overall. The Wilson model also suffers from the largest scatter in the results. This large scatter means that the Durand model may prove to be more useful for particles around a certain diameter range.

Incorporating a wide or multi-component sieve curve into the stationary deposition prediction models was best done by simply taking the d_{50}. The more sophisticated methods of incorporating a wide sieve curve were universally proven to be less accurate.

6.2 Recommendations

The experiments done in this research are mostly done at intermediate and low concentrations. To get results that are more relevant to real world dredging operations it is recommended to test the performance of the 4 component model at higher concentrations. Knowing at which velocities a stationary bed can be expected is also much more important at higher concentrations. For the lab to be able to handle these high concentrations a larger pump must be purchased. The maximum capacity of the pump has already been reached when loading only about 15% X_s-particles.

Some problems with the lab were encountered while carrying out the experiments for this research. Due to these problems one has to be cautious when drawing conclusions from the results. It is recommended to do some experiments to check on the behavior of the lab equipment. This makes it easier to recalibrate some of the measuring devices and can save a lot of time for future users of the lab.

It was shown in this research that the most inaccurate results by far are in the stratified fraction of the 4 component model. To get more insight into the behavior of this part of the model it is recommended to do more experiments using particles larger than 1.5% the pipe diameter. It was also shown that the V_{50} model makes more accurate predictions of the hydraulic gradient than the stratified flow model when transporting low concentrations of X_s-particles. It could be useful to do a study using multiple models to calculate pressure losses for large particles. What could also be useful is incorporating solids concentration into the definition of the boundary between heterogeneous particles and stratified particles. This boundary is currently defined as 0.15D.

Bibliography

Durand, R., Condolios, E. (1952). Étude expérimentale du refoulement des matériaux en conduite, 2émes Journées de I'Hydralique, SHF, Grenoble, France.

Durand, R. (1953). Basic relationships of the transportation of solids in pipes - experimental research. Proc. IAHR Minnesota International Hydraulic Convention, 1-4 September 1953, Minneapolis, Minnesota, U.S.A.

Matousek, V. (1997). Flow Mechanism of Sand-Water Mixtures in Pipelines. PhD Thesis, Delft University of Technology, Delft, The Netherlands.

Matousek, V. (2006). Solids Distribution in Current Above Stationary Bed in Slurry Pipe. Proc. 13th Int. Conf. on Transport and Sedimentation of Solid Particles. 18-20 Sept 2006, Tbilisi, Georgia.

Matousek, V., Visintainer, R., Furlan, J., McCall II, G., Sellgren, A. (2017). Deposition limit velocity: effect of particle size distribution. Proc. 18th Int. Conf. on Transport and Sedimentation of Solid Particles. 11-15 Sept. 2017, Prague, Czech Republic, pp 217-224.

Miedema, S.A., (2016). Slurry Transport: Fundamentals, A Historical Overview & The Delft Head Loss & Limit Deposit Velocity Framework (R. C. Ramsdell, Ed.) Miami, Florida, USA, Delft University of Technology, Delft, The Netherlands.

Newitt, D.M., Richardson, J.F., Abbot, M. & Turtle, R.B. (1955). Hydraulic conveying of solids in horizontal pipes. Trans. Inst. of Chem. Engrs., Vol. 33, London, United Kingdom.

Sanders, R.S., Sun, R., Gullies, R.G., McKibben, M.J., Litzenberger, C. & Shook, C.A. (2004). Deposition velocities for particles of intermediate size in turbulent flow, Proc. Hydrotransport 16. BHR Group, Cranfield, United Kingdom, pp 429-442.

Sellgren, A., Wilson, K.C. (2007). Validation of a four-component pipeline friction-loss model, Hydrotransport 17, 7–11 May 2007, Cape Town, South Africa.

Sellgren, A., Visintainer, R., Furlan, J., Matousek, V. (2016). Pump and Pipeline Performance when Pumping Slurries with Different Particle Gradings. Can. J. Chem. Eng., Vol. 94, pp 1025-1031.

Thomas, A.D. (1979). The role of laminar/turbulent transition in determining the critical deposit velocity and the operating pressure gradient for long distance slurry pipelines, Proc. Hydrotransport 6, BHRA Fluid Engineering, Cranfield, United Kingdom, pp 13-26.

Visintainer, R., Furlan, 1., McCall II, G., Sellgren, A., Matousek, V. (2017). Comprehensive loop testing of a broadly graded (4-component) slurry. Proc. 20th Int. Conf. on Hydrotransport, 3-5 May 2017, Melbourne, Australia.

Wilson, K.C., Horsley, R.R., Kealy, T., Reizes, J.C. & Horsley, M. (2003). Direcct prediction of fall velocities in non-Newtonian materials. int'l J. Mineral Proc., Vol. 71/1-4 pp 17-30.

Wilson, K.C., Addie, G.R., Sellgren, A., Clift, R. (2006). Slurry Transport Using Centrifugal Pumps, 3rd Ed., Springer, New York, U.S.A.

Appendix A

Dredge pump curves

性 能 试 验 记 录

试验编号：	ASP1050-300-7000030W		合同号：			试验日期：		2015.10.12

泵名称：	离心泵	泵型号：	ASP1050-300-700	出厂编号：	15102058

保证值	流量(m³/h)	1600	扬程(m)	25	转速(rpm)	740
	泵输入功率(kW)	151.4	泵效率(%)	72	必须汽蚀余量(m)	

检测条件	大气压力(hPa)	1008	入口测压截面直径(m)	0.35	入口表位差(m)	0
	试验水温(℃)	25	出口测压截面直径(m)	0.35	出口表位差(m)	0.2

测量结果

序号	测 定 数 据						换算到规定转速下的值			泵效率(%)
	流量(m³/h)	转速(r/min)	入口压力(MPa)	扬程(m)	泵输入功率(kW)	泵输出功率(kW)	流量(m³/h)	扬程(m)	泵输入功率(kW)	
1	611.1	748.5	-0.0125	36.11	94.3	60	604.2	35.29	91.1	63.6
2	997.7	748.1	-0.0149	32.27	119.7	87.5	986.9	31.57	116	73.1
3	1209	747.9	-0.0167	30.53	133.5	100	1196	29.89	129	75.1
4	1417	747.2	-0.0199	28.31	145.7	109	1403	27.77	142	74.8
5	1623	746.8	-0.0244	25.71	156.8	113	1608	25.24	153	72.3
6	1809	746.5	-0.0309	23.06	164	113	1793	22.66	160	69.1
7	2024	746.1	-0.0462	20.22	173.7	111	2007	19.89	169	64.0
8										
9										
10										
11										
12										
13										
14										
15										

试验结论	流量、扬程： 合格　　　　效率： 合格

检测：		校核：		试验主管：	

安徽三联泵业股份有限公司

检 测 报 告

（性能曲线）

试验编号：	ASP1050-300-7000030W	合同号：		试验日期：	2015.10.12
泵名称：	离心泵	泵型号：	ASP1050-300-700	出厂编号：	15102058
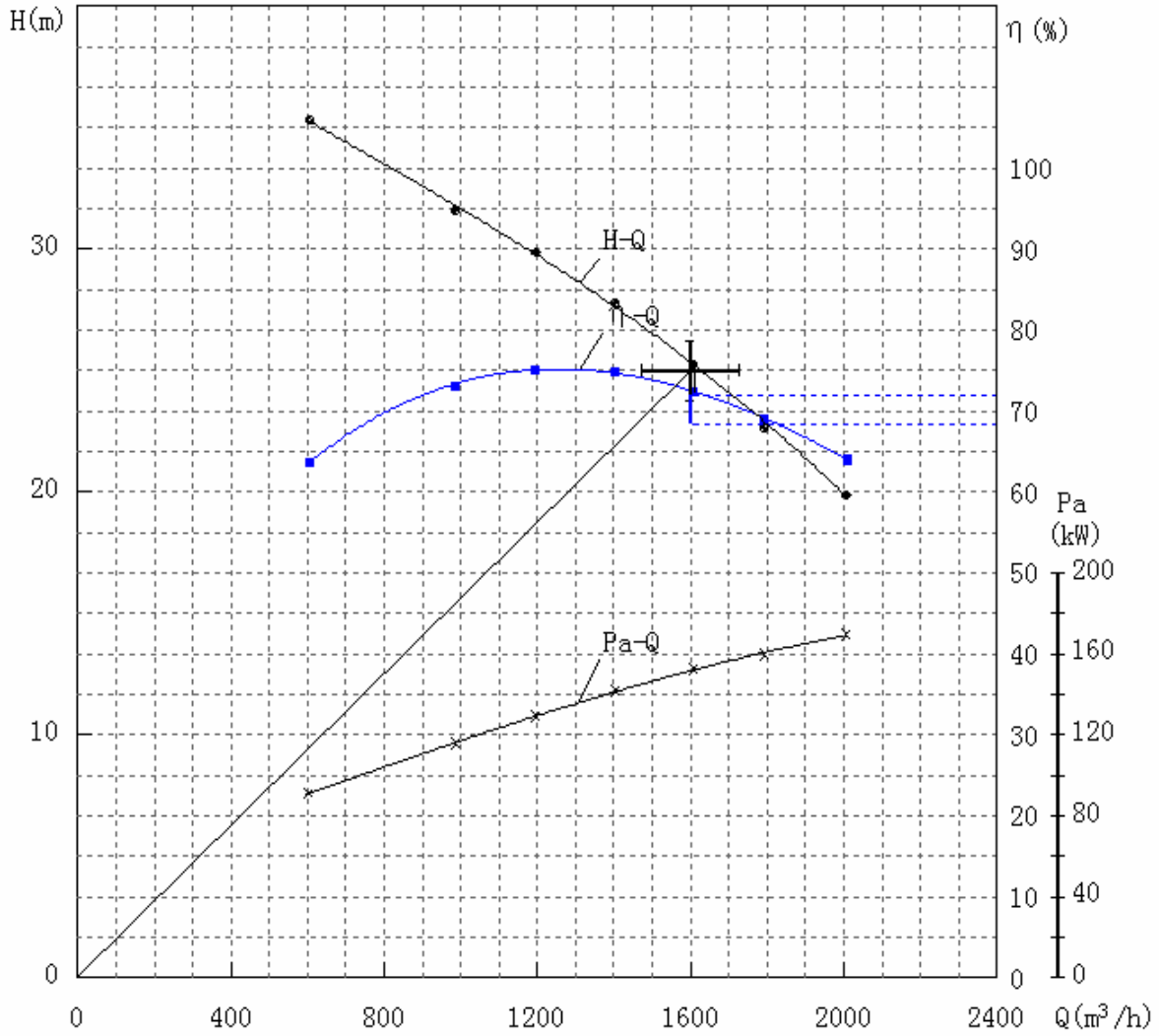
保证点性能参数测试结果

参数名称	流量(m³/h)	扬程(m)	转速(r/min)	输入功率(kW)	泵效率(%)	
测量数据	1600	25.35	740	151.6	72.5	

检测：		校核：		试验主管：	

安徽三联泵业股份有限公司

Appendix B

Flow meter information

3、性能简介

LDG—S电磁流量传感器   LDG—/K高压电磁流量传感器

口　　　径	DN10～2000	DN10～500
电极材料	1Cr18Ni9Ti　0Cr18Ni12Mo2Ti Ti　Ta　Hb　Hc　Pt 等	1Cr18Ni9Ti 等
内衬材料	聚四氟乙烯、氯丁橡胶、 聚氨酯橡胶	氯丁橡胶、聚氨酯橡胶
介　　　质	导电性液体（含固液二相）	导电性液体（含固液二相）
介质电导率	＞20μS/cm	＞20μS/cm
配套精确度等级	0.5、1.0	0.5、1.0
流速范围	0.5m/s～10m/s	0.5m/s～10m/s
工作温度	－25℃～＋150℃（橡胶衬里 ≤ 80℃） （聚氨酯衬里 ≤ 45℃）	≤80℃（橡胶衬里） ≤45℃（聚氨酯衬里）
工作压力	4.0MPa～0.6MPa（按口径分）	32MPa～6.3MPa（按口径分）
防护等级	标准型 IP65（防喷水） 特殊型 IP67（防浸水） IP68（潜水型）	标准型 IP65（防喷水） 特殊型 IP67（防浸水）
配　　套 转换器型号	LDZ—4B型 LDZ—6型、LDZ—7型	LDZ—4B型 LDZ—6型、LDZ—7型
输出信号	0～10mA DC 或 4～20mA DC Max.5K或10KHz（配LDZ—型、LDZ—7型）	0～10mA DC 或 4～20mA DC Max.5K或10KHz（配LDZ—6型、LDZ—7型）
通迅接口	＊ RS485/232C HART、Modbus	＊ RS485/232C HART、Modbus
防爆标志	Exdmia Ⅱ BT4	—
适用电源	传感器由转换器供电 转换器电源　220VAC 50Hz 24V DC（配LDZ—6型）	传感器由转换器供电 转换器电源　220VAC 50Hz 24V DC（配LDZ—6型）
应　　　用	酸碱等腐蚀液；矿浆、泥浆、 纸浆等两相液；给排水系统	高压注水、高压条件下泥浆、 水泥浆测量
连接法兰	机标JB/T81—94　　　　（口径250～2000） 国标GB/T9119—2000（口径10～200） 或按用户需要	由任连接 法兰连接　国标GB／T9116.4—2000(DN10~50) 国标GB／T9115.4—2000(DN80~150) 或按用户需要
产品标准	Q/YXYS 13—2002	Q/YXYS 13—2002
安装形式	分体式	分体式，一体式（LDY-/K型）

＊ 选择件

Appendix C

Stationary deposition notes

The experiments started with the loading of the sediments at the highest pump rpm. Gradually the rpm was lowered until a stationary bed was formed. Oftentimes rpm was lowered slightly into the stationary bed regime. This gives some extra info into the behavior of the bed. During the experiments

test 1a: No stationary deposition has been observed

test 1b: A continuous stationary bed was observed at around 3.4 m/s. A sliding bed which would occasionally come to a halt was observed from around 4.4 m/s.

test 2a: A stable stationary deposition was established at around 3.5 m/s.

test 2b: A somewhat stable bed appears at around 4.4 m/s. The bed occasionally completely erodes. The bed by the looks of it consists mostly of X_h particles.
At below 4 m/s the bed is mostly stable. In a 10 minute time frame the bed eroded only once. The bed still appears to consist mostly of X_h particles.

test 3a: Even at 5.5 m/s, the highest tested velocity, A sliding bed occasionally forms. The sediments are almost all located in the bottom half of the pipe.
At 3.5 m/s a fragile sliding bed has formed which is occasionally completely stationary for a short while.
At the lowest tested velocity, 2.7 m/s, a stable stationary bed has still not formed.
An interesting observation is that due to particle degradation in the second run a more wide spectrum of particles has formed. Particle segregation appears to take place, where small particles occupy the lower part of the sliding bed. Another observation is that a flux of small particle appear to infiltrate into the bed. Maybe the pressure in the bed is lower than in the mixture above the bed?

test 3b: A thin but stable stationary bed has formed at around 4.1 m/s. The stationary part of the consists of mostly small particles by the looks of it. On top of the stationary part of the bed is a sliding bed consisting mostly of rolling large particles. Like in test 3a, a flux of small particles infiltrate into the bed as if the pressure int he bed is lower than above it.

test 4a: At around 4.2 m/s clusters of sediment can be seen which form a slow moving plug. Velocity of the plug may slow down occasionally but never completely stops. The plug accelerates quickly when coming almost to a halt.
At around 3.3 m/s a fragile stationary bed has formed. Dramatic density waves filling almost the entire cross section in heterogeneous suspension enters the perspex section and washes away the stationary deposition. A thin streak of fine particles

occupies the bottom of the pipe. This thin streak of small particles seems to slowly move against the flow direction.

at 3 m/s a stable stationary bed has formed. A huge density wave washed away the bed once but it was instantly reestablished.

When lowering the velocity past 3 m/s the flow initially becomes significantly more unstable. At 2.8 m/s the density waves appear to become larger. Heterogeneous, sliding bed, and stationary bed regimes follow each other in rapid succession. Sometimes it looks like you are almost pumping water. This is then followed by a huge density waves which you can hear coming from a large distance.

test 4b: A very stable stationary bed has formed at around 3.5 m/s. The heterogeneous fraction appears to have a stabilizing effect on the slurry. When lowering the velocity past 3.5 m/s to 3 m/s the bed remains stable unlike when pumping only X_s fraction where an island of stability was formed which was followed by chaos when lowering the velocity past this stable point.

test 5: A very uniformly moving bed is formed at around 2.4 m/s. No stationary deposition has been observed.

test 6a: A stable stationary bed has formed at 3.3 m/s.

test 6b: A stable stationary bed has formed at around 3.6 m/s.

test 6c: A stable stationary bed has formed at around 3 m/s. The bed reaches up to $\frac{1}{4}D$ in height. This is the highest bed that has been observed up to now.

test 7: A stable stationary bed has formed at around 3.6 m/s.

test 8a: A stable stationary bed has formed at around 4.5 m/s. This seems extraordinarily early.

test 8b: A stable stationary bed has formed at around 3.2 m/s. Much later than when pumping only half the volume of X_{hu} particles.

test 8c: A stable stationary bed has formed at around 3.7 m/s.

test 9: With this very high concentration of X_s particles we couldn't get the flow velocity very high. The velocity range of the performed experiments were between 2.8 and 2.0 m/s. At 2.8 m/s the flow might as well be considered in the stationary deposition regime. Occasionally the stationary bed is washed away by a density wave but it instantly reestablishes. When lowering the rpm of the pump not much changes. Almost all of the sediments appear to be laying on the bottom of the pipe.

Appendix D

U-loop recalibration process

The U-loop that was used in the Shanghai experiments has not been set up correctly. To get correct information on the concentration that can be used in the analysis of the results, the data must be recalibrated.

D.1 Introduction

The U-loop has been used in previous research by M. de Vreede. It was during his research that it was discovered that the raw data of the U-loop was flawed. As a result most of the recalibration process described in this appendix has been developed by M. de Vreede.

For the recalibration to work the assumption is made that the trend in the error is the same for water flow experiments as they are for slurry experiments. It is suspected that a misalignment of the pressure taps leads to an unaccounted for influence of the dynamic pressure on the differential pressure data. Another installation error that has been discovered is an incorrect static pressure in the pressure sensors. This can be seen by the sizable offset of the measured pressure when compared to the theoretical pressure (Darcy-Weisbach curve) at a velocity of 0 m/s. To correct for the calibration errors the measured data profile must be aligned to the theoretical data profiles for water flow.
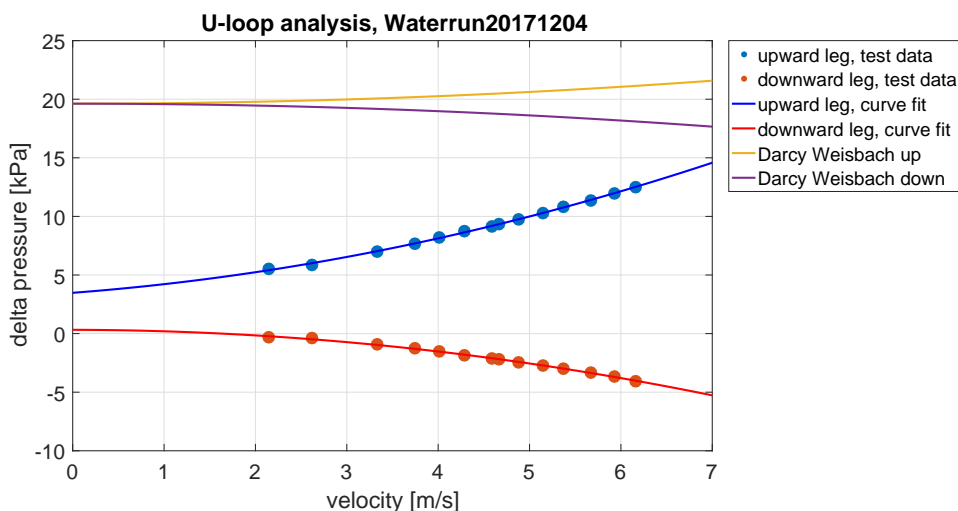
FIGURE D.1: Raw U-loop data of water compared to theoretical data curves.

D.2   Theory for water data

To get a good understanding of the data we are working with, the first thing that should be done is decompose the pressure differential term into a static and a dynamic term:

$$\Delta p = p_{static} + p_{dynamic} = \rho g \Delta z + \frac{1}{2}\rho v^2 \tag{D.1}$$

The static pressure differential is quite sizable since we are dealing with a vertical flow. The pressure sensors are located 2m apart resulting in a static pressure differential of 19.62 kPa when pumping water. The second term quantifies the influence of velocity of the pressure differential. It was already stated that the assumption must be made that the shape of the error is independent of slurry composition. This means that the hydraulic gradient is calculated by an equivalent liquid model for every experiment, in vertical flow this assumption will not result in too much of an error since no stratification will take place. The Darcy-Weisbach equation is only to be corrected for the density of the slurry. With the dynamic part of the pressure differential replaced with the Darcy-Weisbach equation, the following equation is established:

$$\Delta p = \rho g \Delta z + f \frac{\rho}{2}\frac{v^2}{D}L \tag{D.2}$$

In figure D.1 the Darcy-Weisbach theoretical losses are displayed with the experimental data and a curve fit of the experimental data. It can be seen that there is a rather large difference between the theoretical data (Darcy-Weisbach curve) and the actual data. The shape does somewhat resemble the theoretical curves. The first step is to correct for the large offset. The offset is easily corrected by adding the difference at v=0 to the experimental data:

$$p_{offset} = p_{Darcy-Weisbach}(v = 0) - p_{experimental}(v = 0) \tag{D.3}$$

The result of this first correction can be seen in figure D.2.
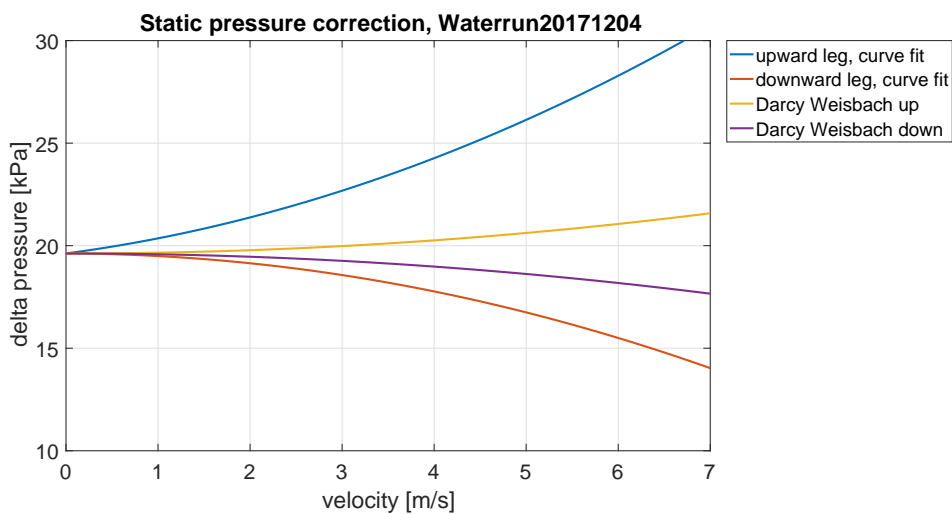
FIGURE D.2: In the upward leg the offset is 16.14 and in the downward leg the offset is 19.30.

It appears the effect of increased velocity is exaggerated in the experimental data. A correction must now be made for this error. To do this the velocity dependent term must be multiplied by a correction factor. To come up with a correction factor we subtract the static pressure (pressure at v=0) from the curves leaving only the velocity dependent dynamic pressure. The next step is to determine the velocity at which we want to correct. A velocity of 6 m/s is deemed reasonable since this is the highest velocity for most of the experiments. The correction factor is obtained by dividing the dynamic pressure of the Darcy-Weisbach equation at 6 m/s by the dynamic pressure of the curve fit at 6 m/s. The results of this can seen in figure D.3.
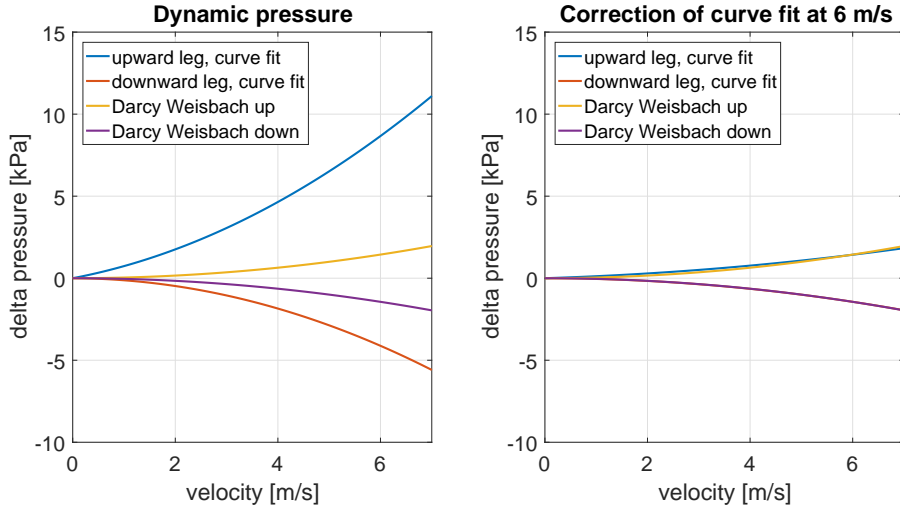
FIGURE D.3: The curve fit data of waterrun20171204 is multiplied by a correction factor to fit the theoretical data. Upward correction factor = 0.1360, downward correction factor = 0.3456.

It can be seen that the Experimental data follows the theoretical data exactly like expected in the downward leg of the U-loop. In the upward leg the shape of the experimental and the theoretical data is slightly different. There must be a secondary phenomenon affecting the data. Correcting for the secondary effect is outside of the scope of this correction method.

The curve fit data is now corrected to the theoretical data. Let's see how the actual experimental data is corrected:

$$final corrected dataset = p_{offset} + p_{static} + (data - p_{static}) * correction factor \quad \text{(D.4)}$$

When the actual data is corrected like described in this section, the results will be like shown in figure D.4.

D.3 Theory for slurry data

The goal of the correction is to correct the U-loop data so a concentration can be extracted from the data. The concentration will be calculated using theoretical water data and corrected slurry data. The following relation will result in the mixture density at each velocity:

$$\Delta p = f \frac{\rho}{2} \frac{v^2}{D} L \quad \text{(D.5)}$$
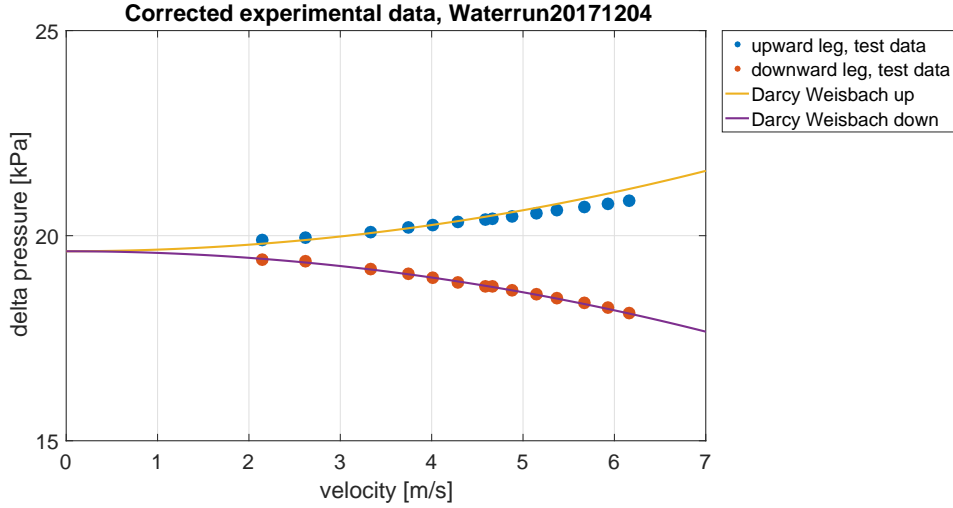
FIGURE D.4: Corrected water data when the entire process described
in this section is followed.

$$\Delta p_m - \Delta p_w = f\frac{\rho_m}{2}\frac{v^2}{D}L - f\frac{\rho_w}{2}\frac{v^2}{D}L \tag{D.6}$$

$$\rho_m = \frac{\Delta p_m - \Delta p_w}{f\frac{1}{2}\frac{v^2}{D}L} + \rho_w \tag{D.7}$$

In the above equation all data is known except ρ_m. We know Δp_w from the theoretical Darcy-Weisbach like shown in figure D.1. We know Δp_m from the experimental data. The only thing that must be done is correct the the experimental data. We correct the experimental data using the results from the water data correction of section D.2. We add a static offset like shown in figure D.2, and we subtract the exaggerated effect of the velocity dependent dynamic pressure term like shown in figure D.3. When this entire process is followed the results will look like figure D.5.
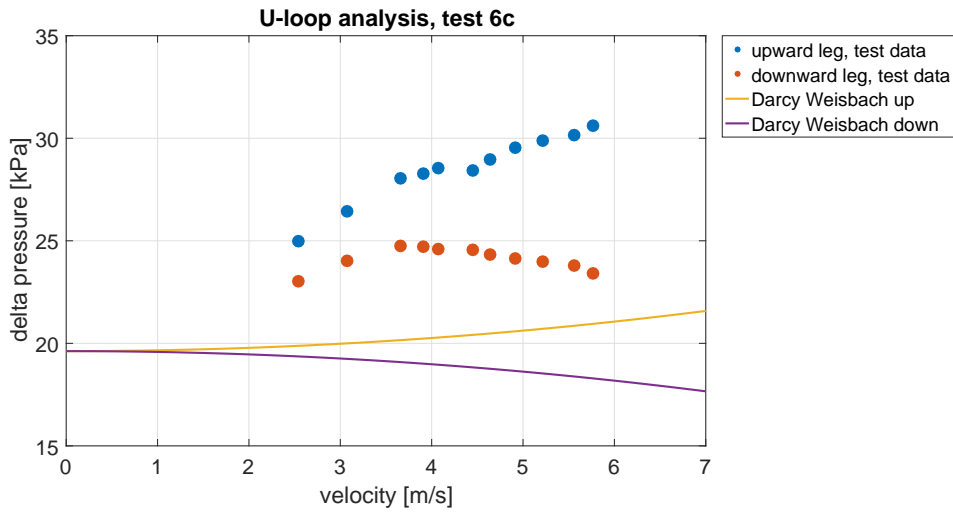
FIGURE D.5: Corrected data of test 6c with $X_{hl} = 0.67$ and $X_{hu} = 0.33$.
It can be seen that at the lowest two velocities the mixture density
starts to fall.

An in situ density of the slurry can now be calculated using equation D.7. When

adding the ρ_m calculated for the upward and downward leg of the U-loop and dividing this by two, the delivered concentration should be the result. The concentration of solids in the mixture can now be calculated according to the following equation:

$$C_s = \frac{\rho_m - \rho_w}{\rho_s - \rho_w} \tag{D.8}$$

When this whole process is followed the following concentration is found for test 6c.
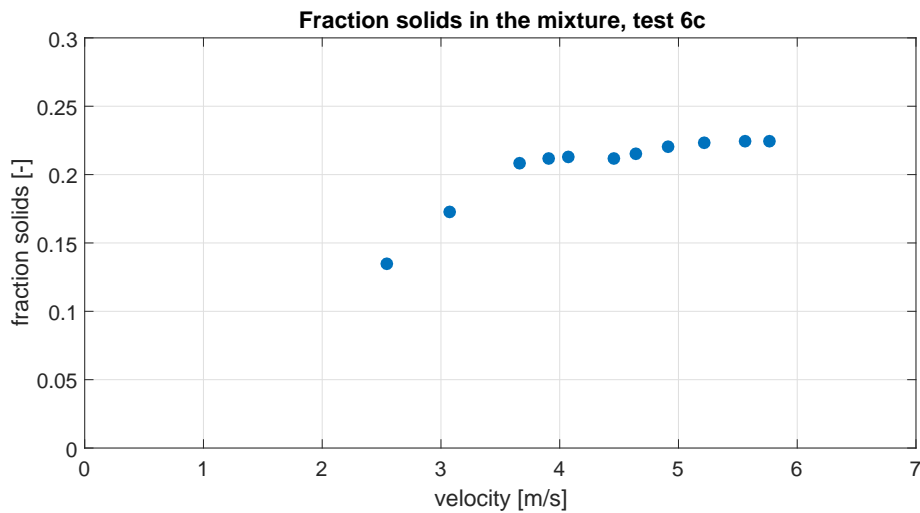
FIGURE D.6: Concentration that is calculated when the entire process described in this chapter is followed.

The concentration appears to be more or less stable up until the last two dots. This coincides with the appearance of a stationary bed which was observed at around 3 m/s in experiment 6c. A comparison with the ultrasonic concentration meter can be found in table D.1.

	1a	1b	2a	2b	3a	3b	4a	4b	5	6a	6b	6c	7	8a	8b	8c	9
X_p	1	.33	.33	.25					1								
X_{hl}										1	1	.67	.50			.33	
X_h		.67	.67	.50		.67		.67									
X_{hu}												.33	.50	1	1	.67	
X_s				.25	1	.33	1	.33									1
$C_{vd,u}$	6.4	19.9	8.3	8.1	4.0	8.9	6.4	15.2	8.5	10.3	13.5	18.6	14.9	12.4	16.6	21.0	10.8
$C_{vd,l}$	3.2	14.2	4.8	6.4	-0.5	4.5	0	18.2	10.0	5.7	12.9	20.6	13.9	8.0	14.2	24.5	11.1
C_{vd}	10	30	15	20	5	15	10	30	20	10	20	30	20	10	20	30	20

TABLE D.1: Test matrix showing slurry composition and delivered concentrations in percentage according to the ultrasonic $C_{vd,u}$, and the ucorrected U-loop data $C_{vd,l}$. The target delivered concentration is shown in the bottom row.

Appendix E

4 Component model analysis plots
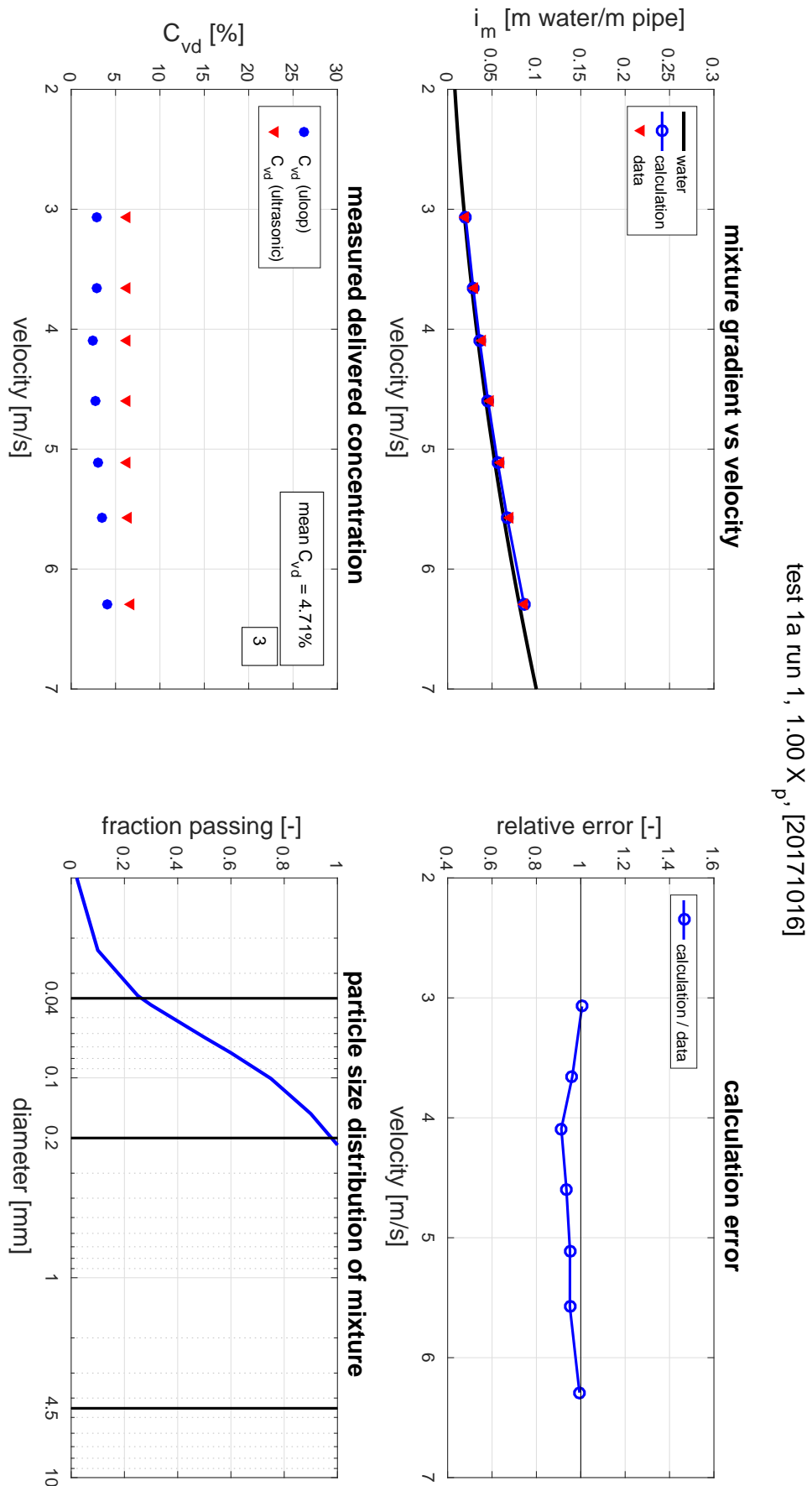
FIGURE E.1: Results of test 1a run 1.
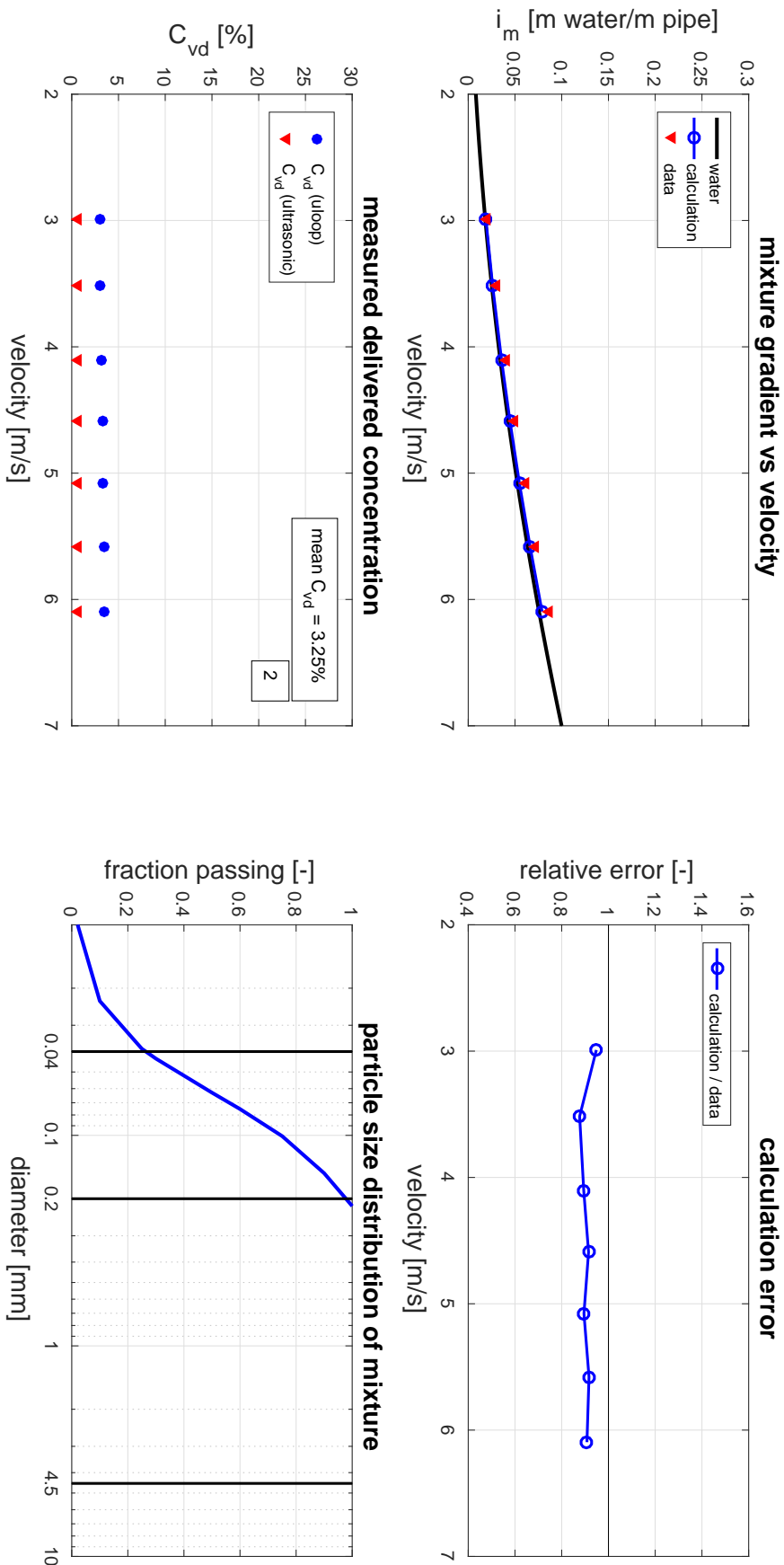
FIGURE E.2: Results of test 1a run 2.
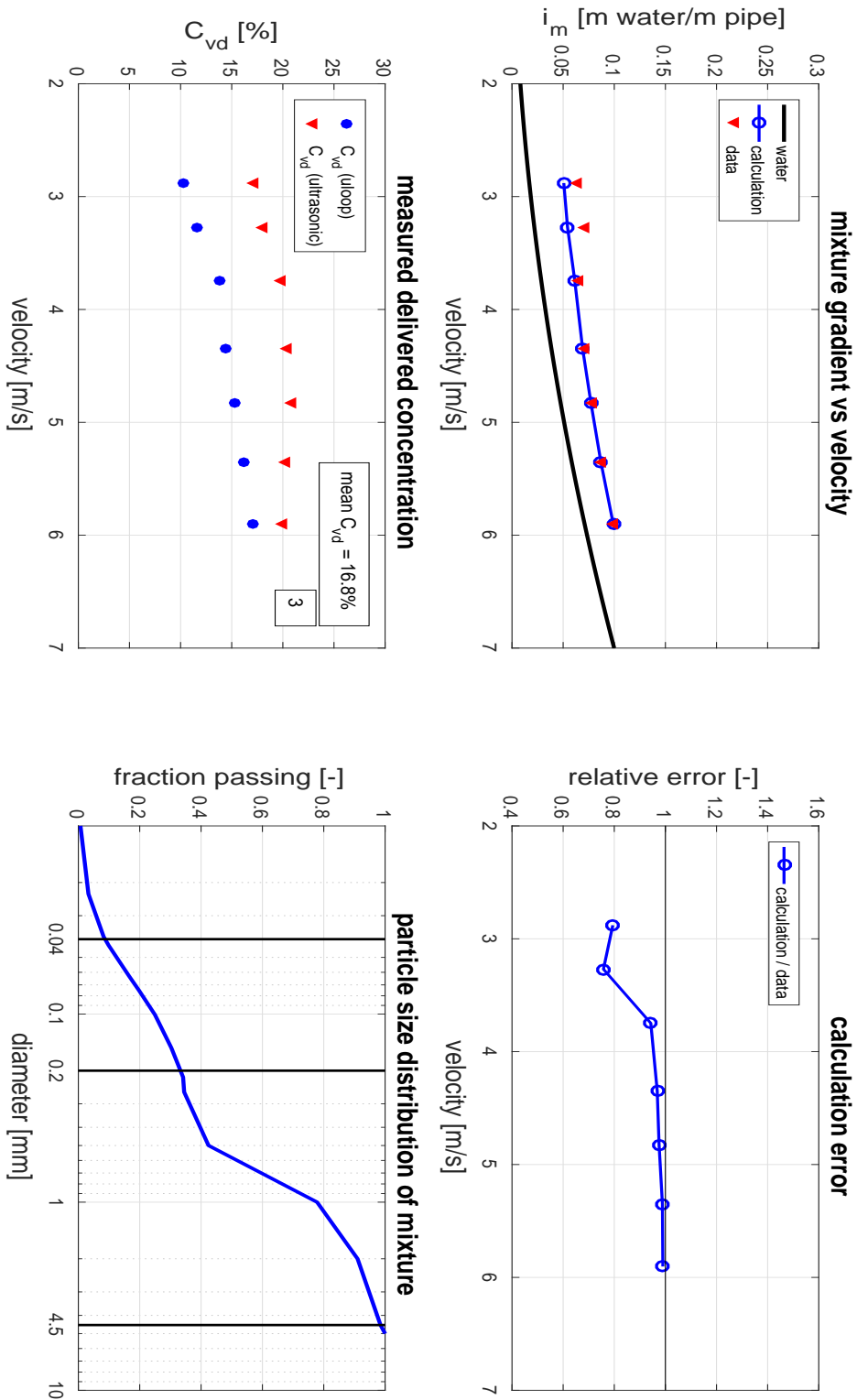
FIGURE E.3: Results of test 1b run 1.
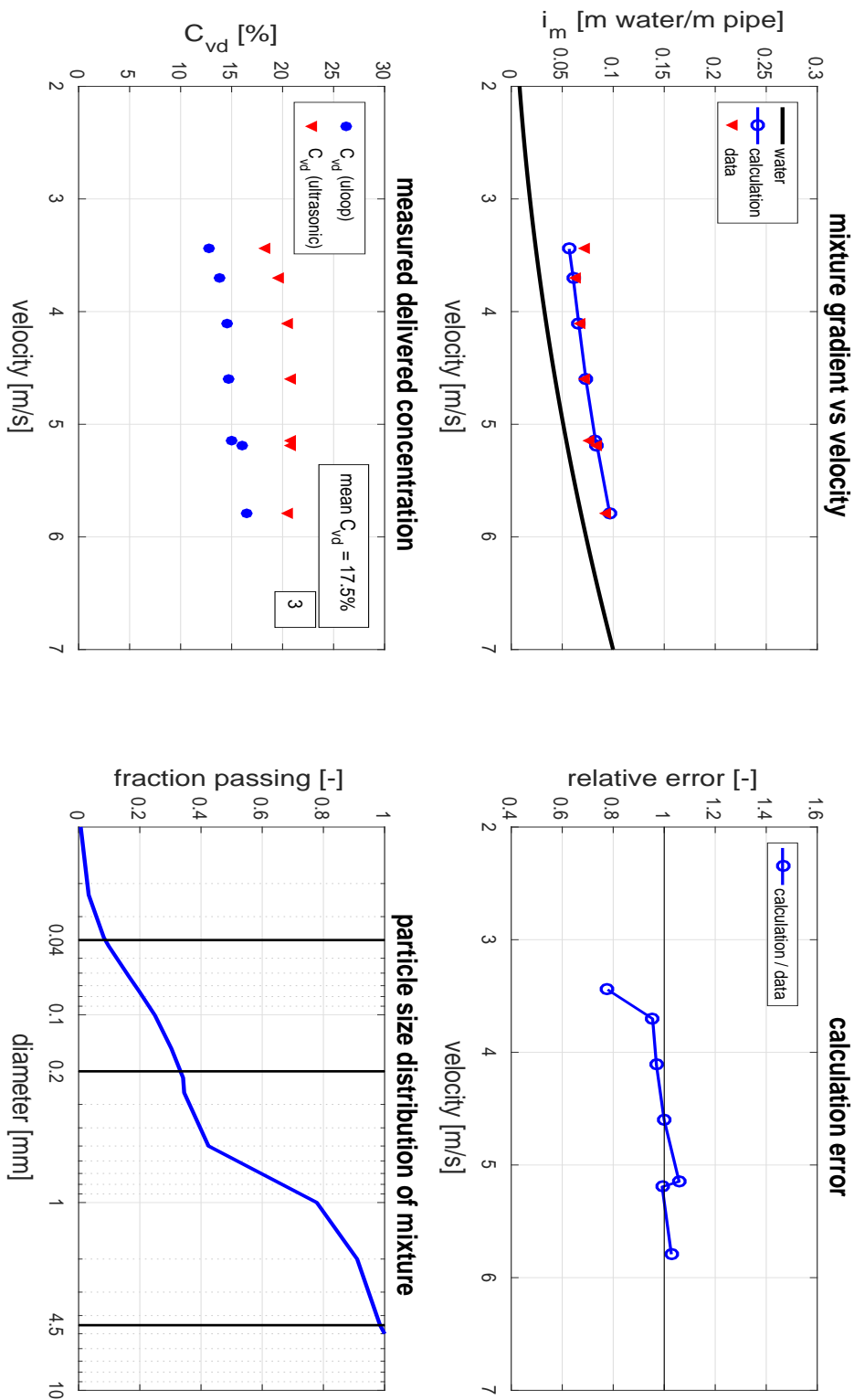
FIGURE E.4: Results of test 1b run 2.
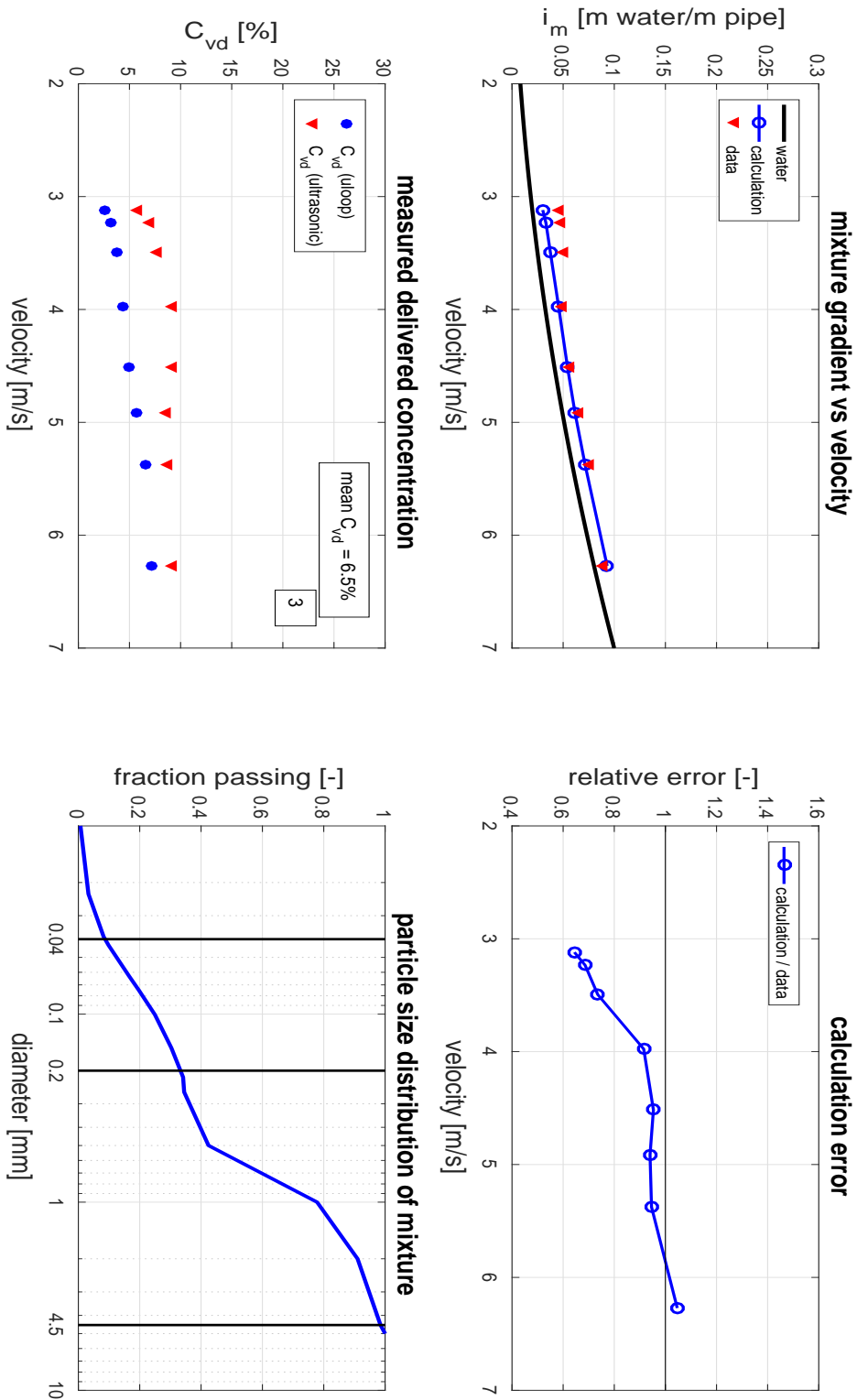
FIGURE E.5: Results of test 2a run 1.
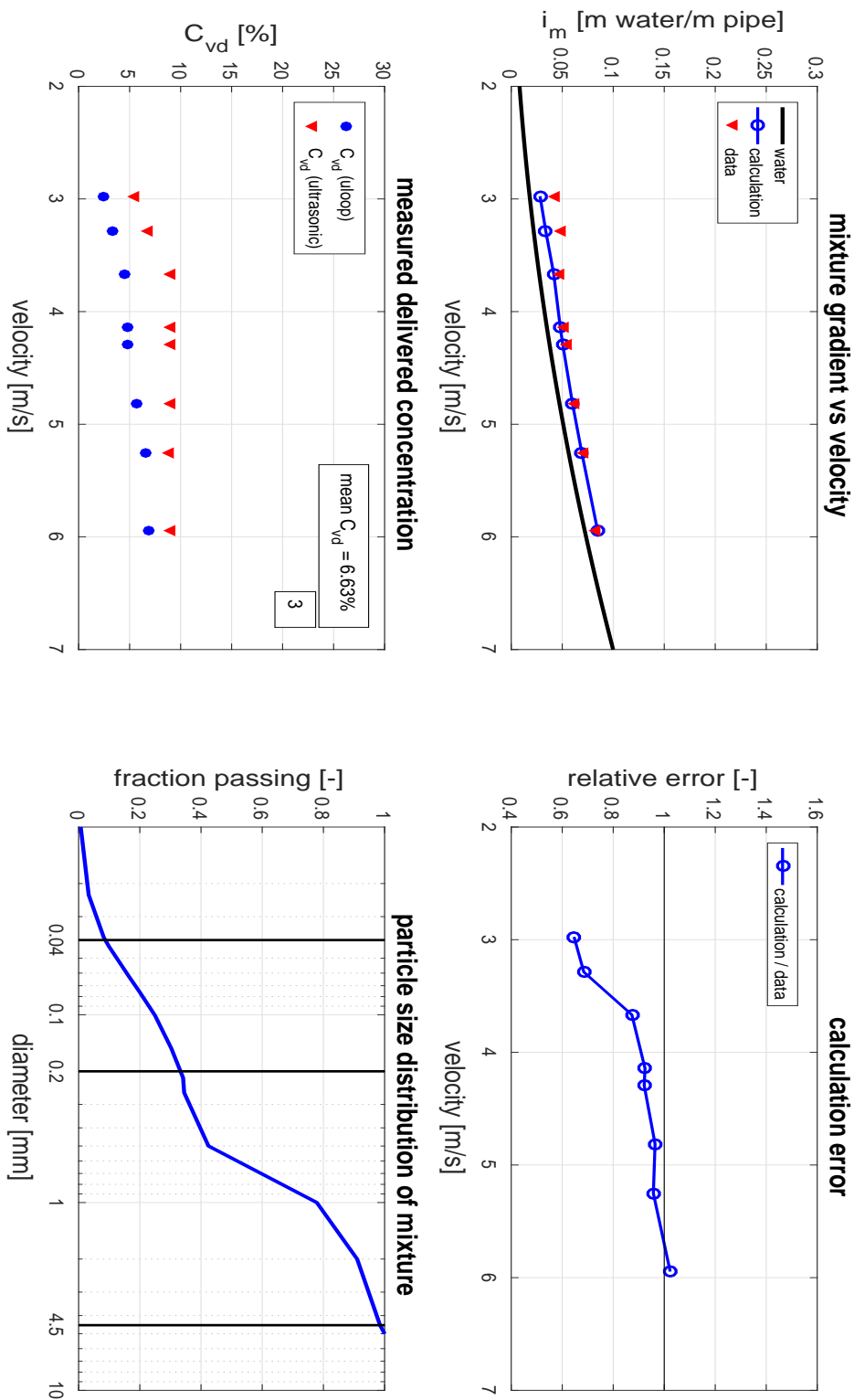
FIGURE E.6: Results of test 2a run 2.
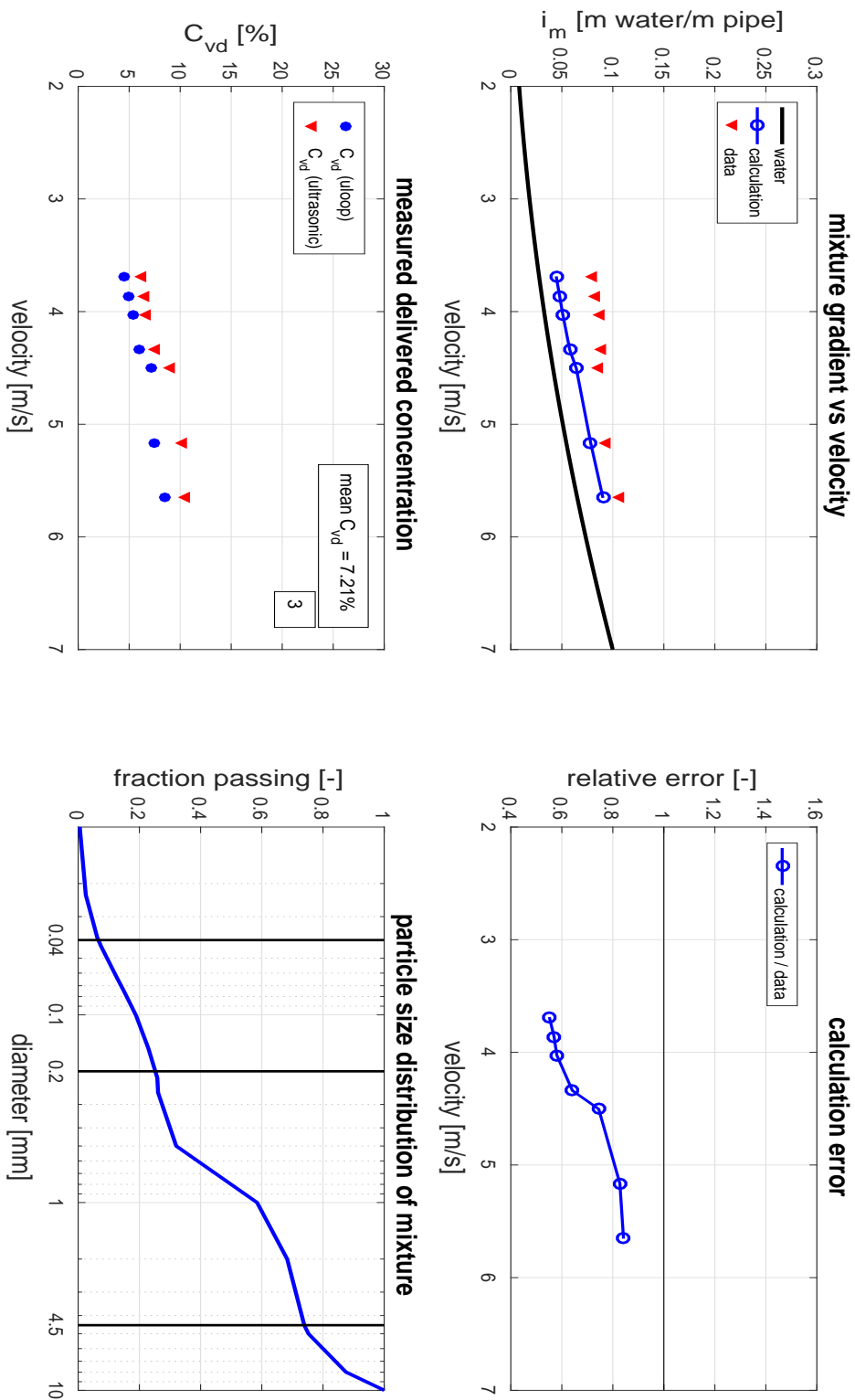
FIGURE E.7: Results of test 2b run 1.
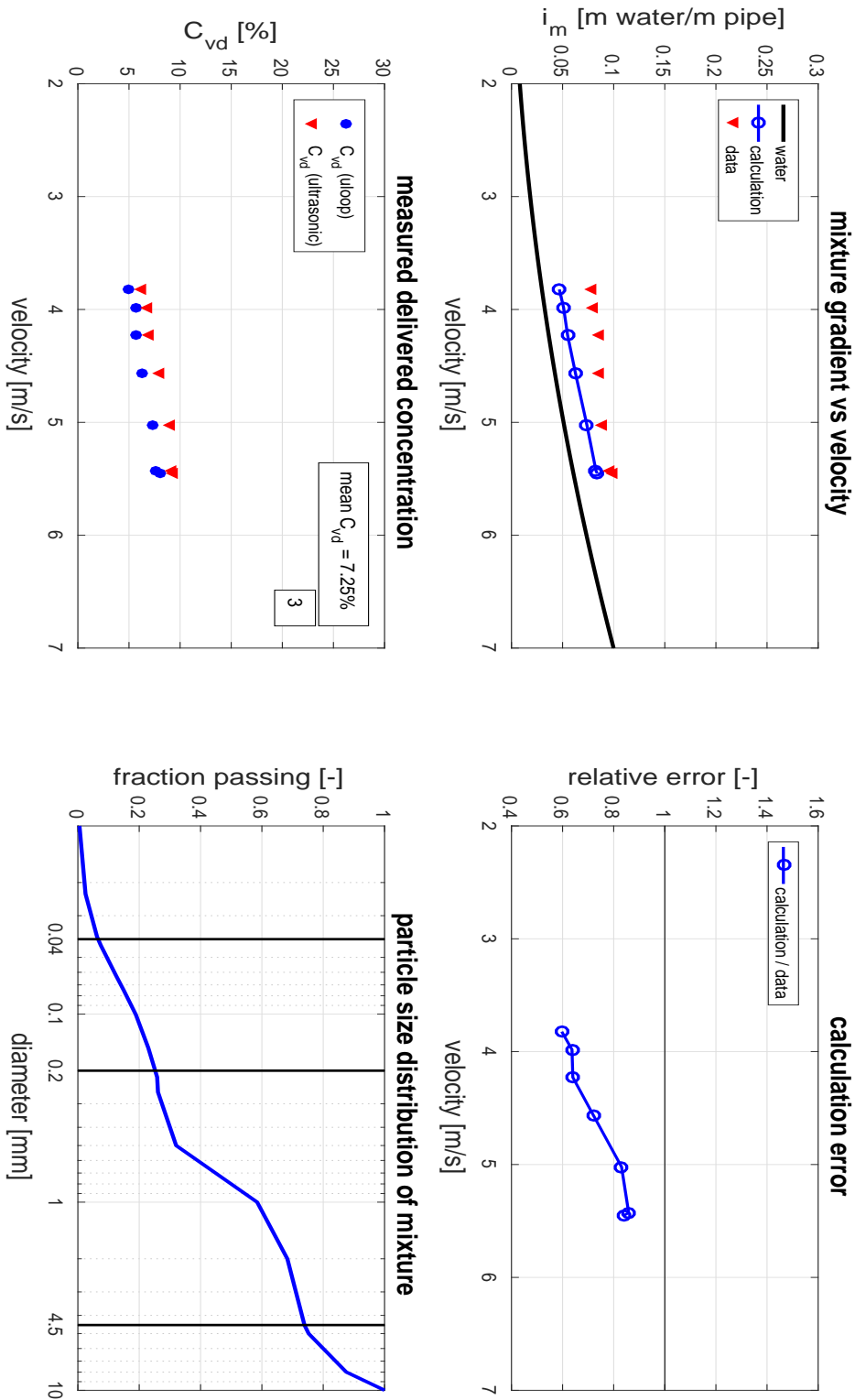
FIGURE E.8: Results of test 2b run 2.

FIGURE E.9: Results of test 3a run 1.

FIGURE E.10: Results of test 3a run 2.
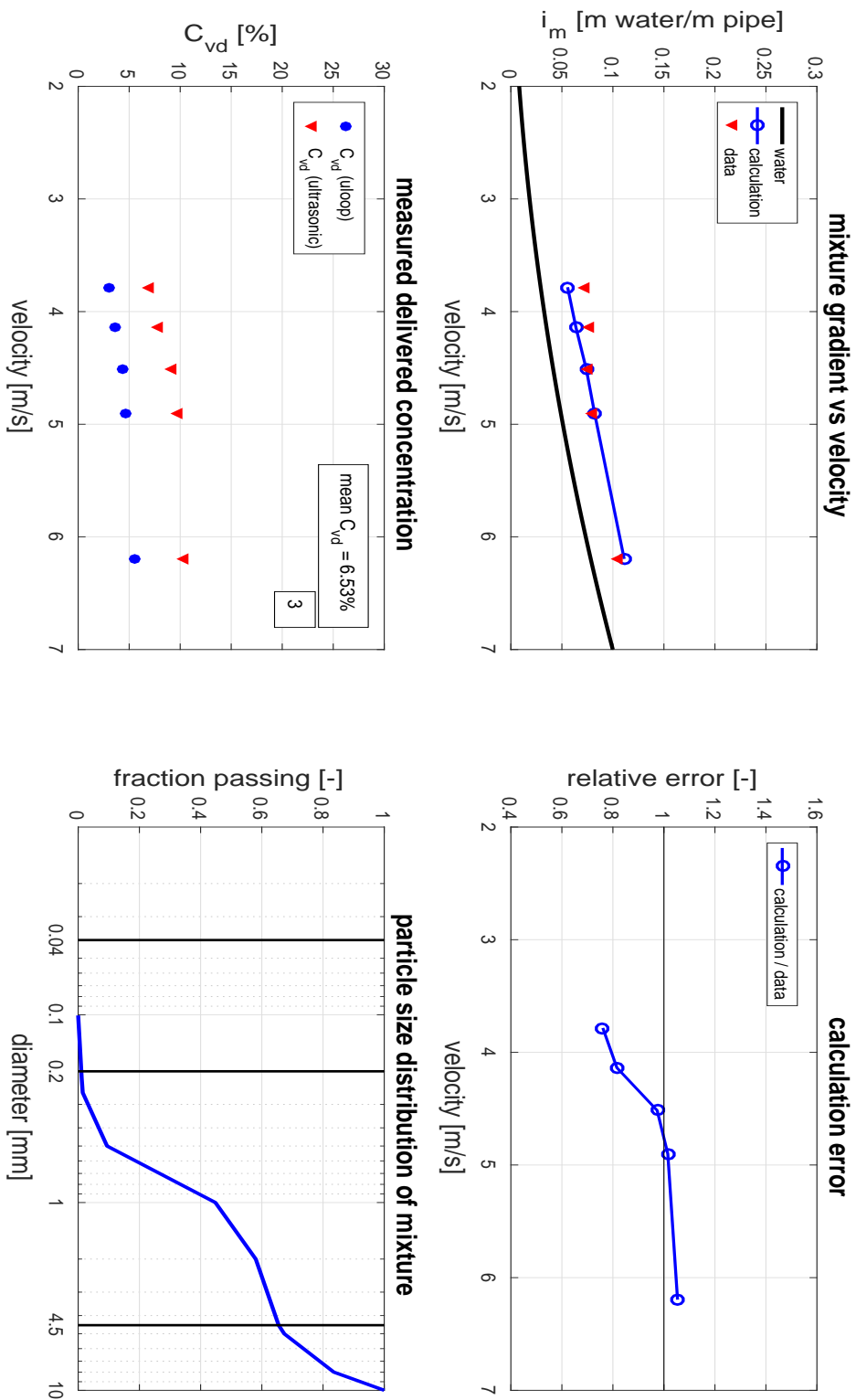
FIGURE E.11: Results of test 3b run 1.
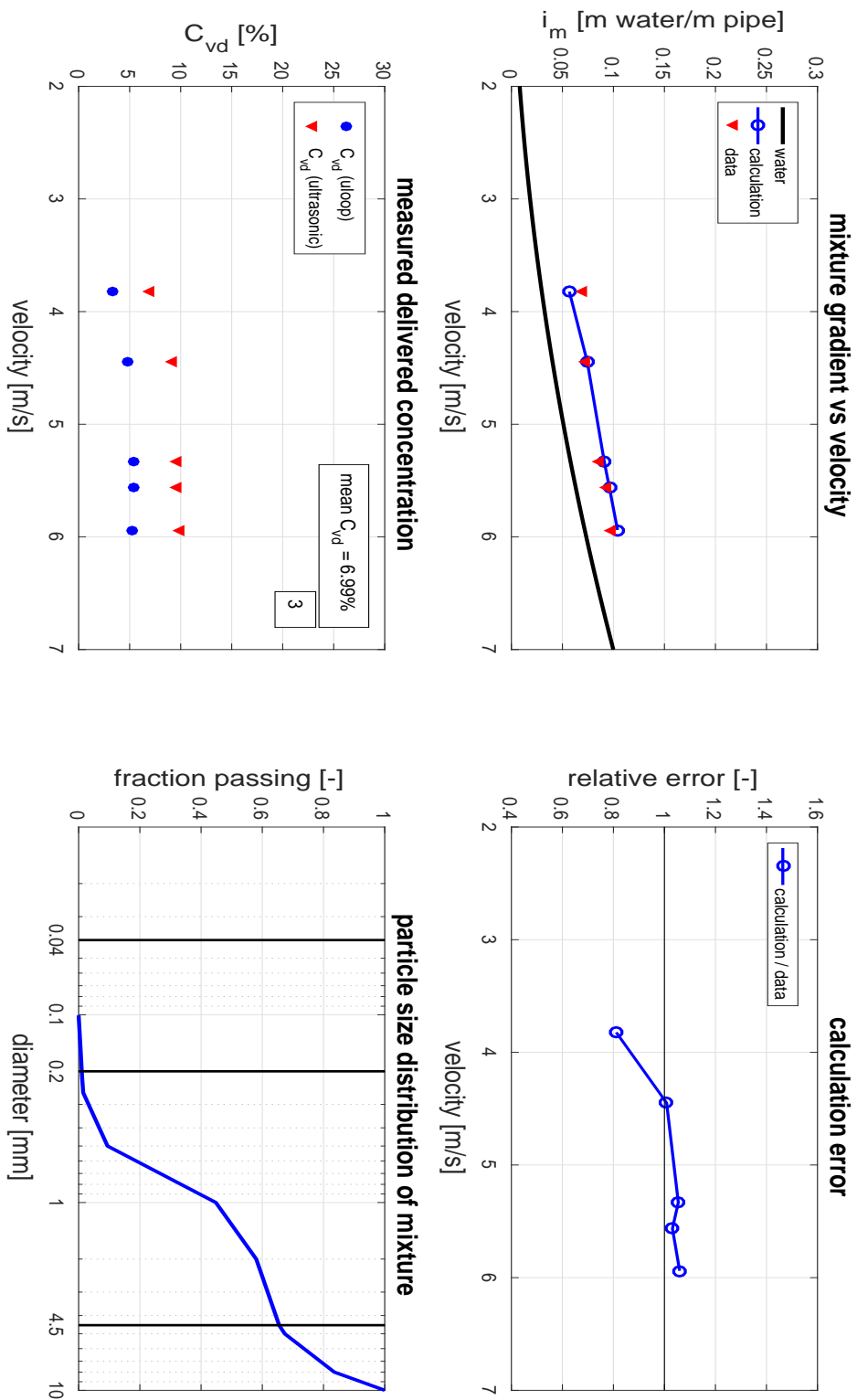
FIGURE E.12: Results of test 3b run 2.
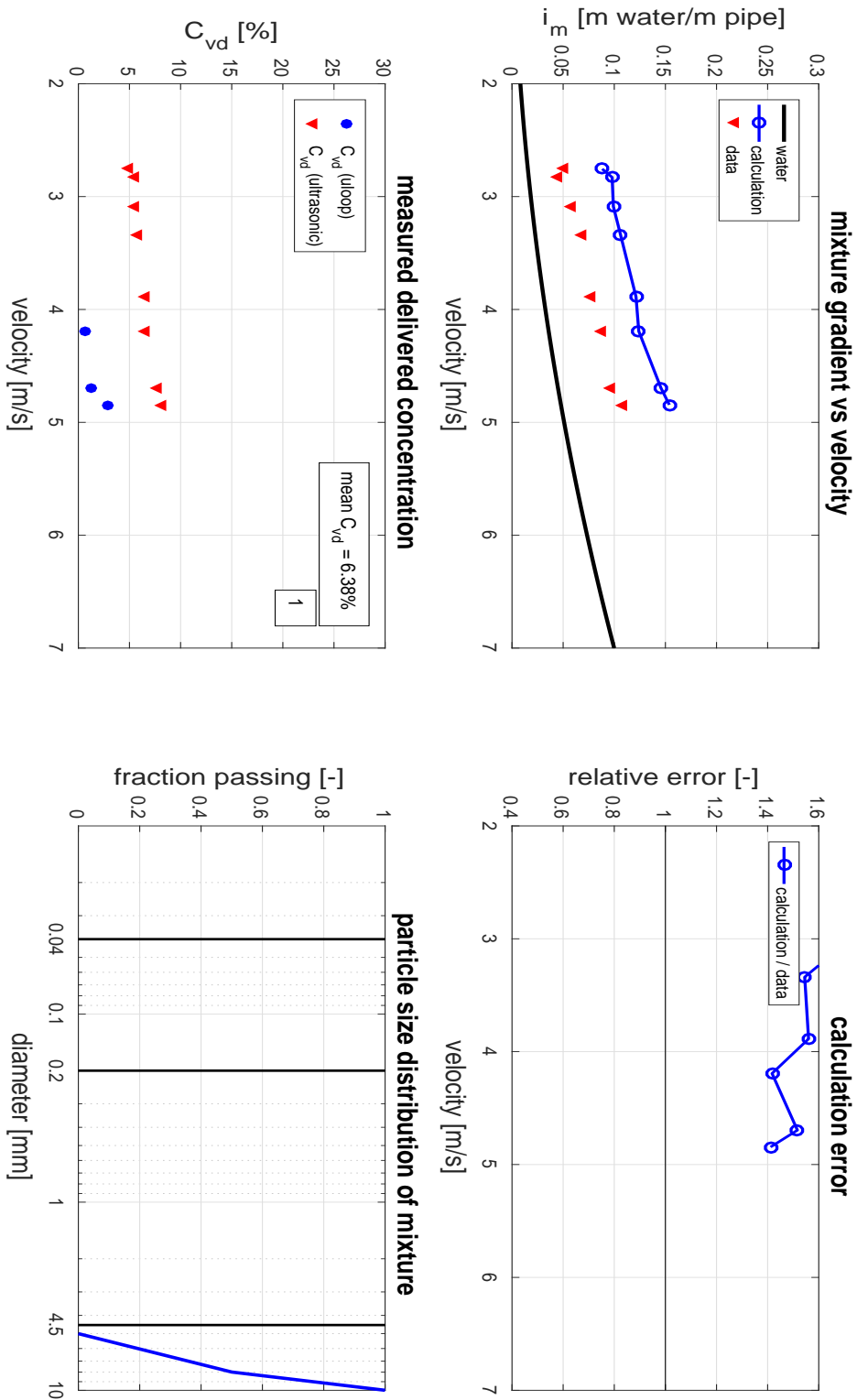
FIGURE E.13: Results of test 4a run 1.
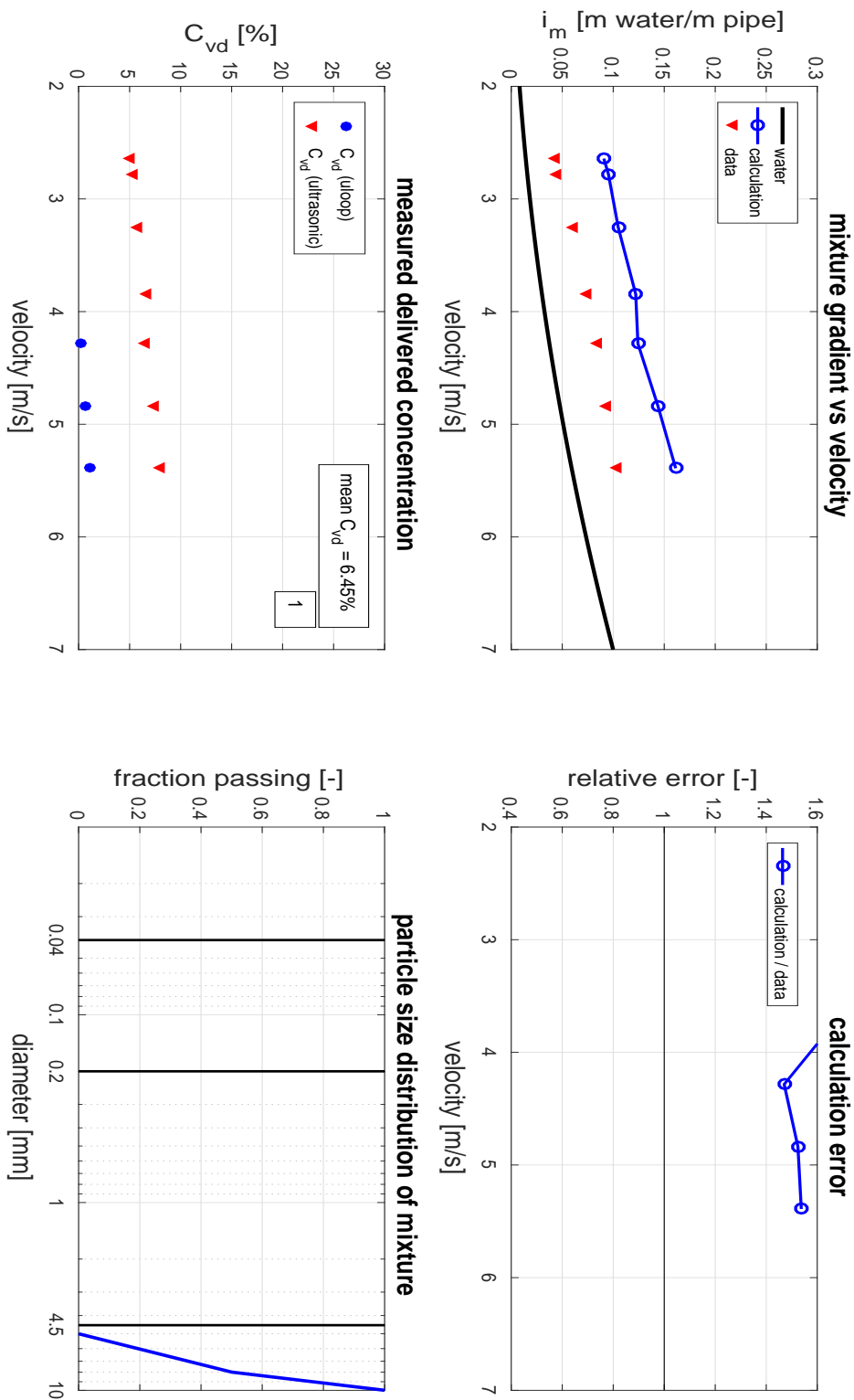
FIGURE E.14: Results of test 4a run 2.
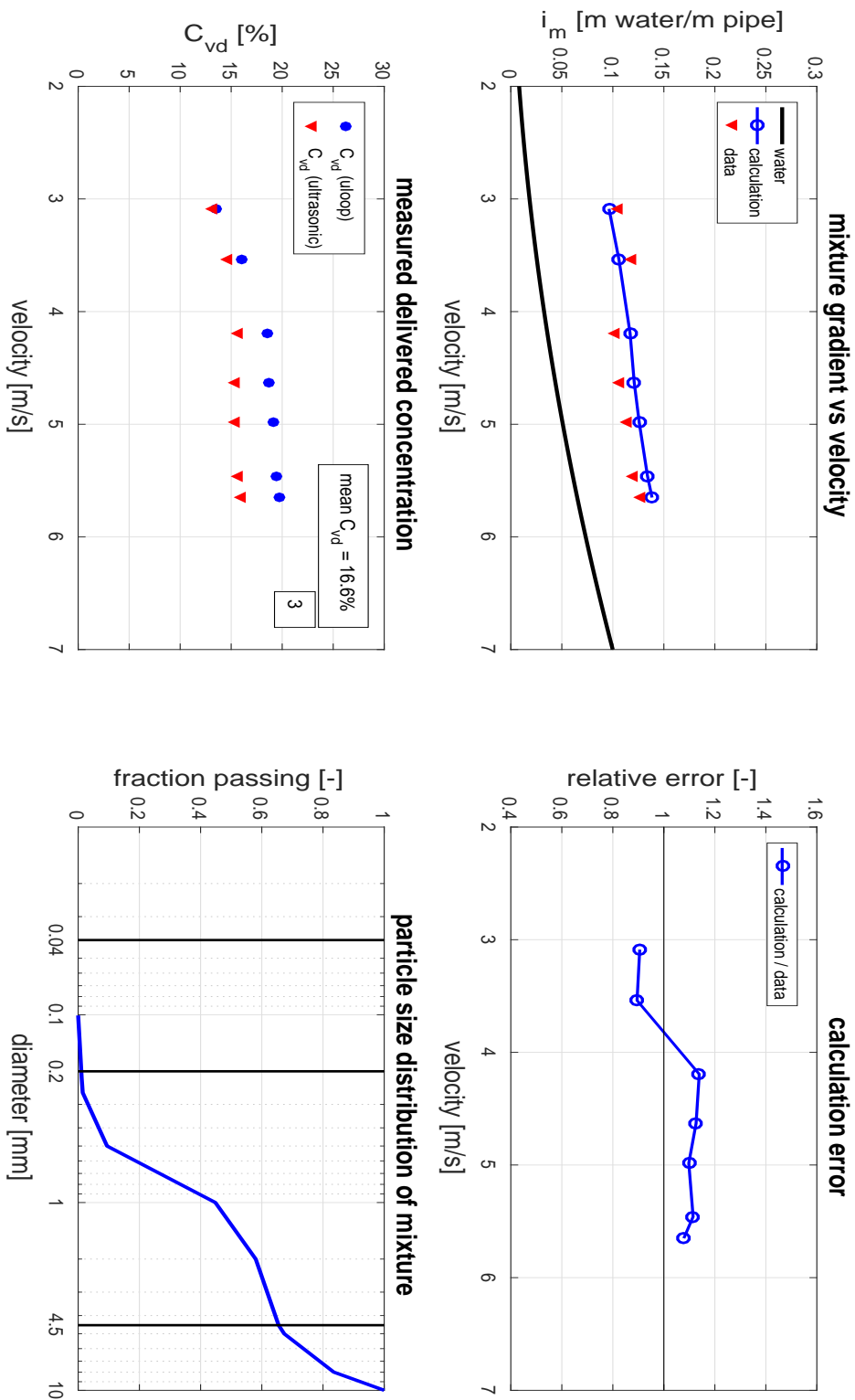
FIGURE E.15: Results of test 4b run 1.
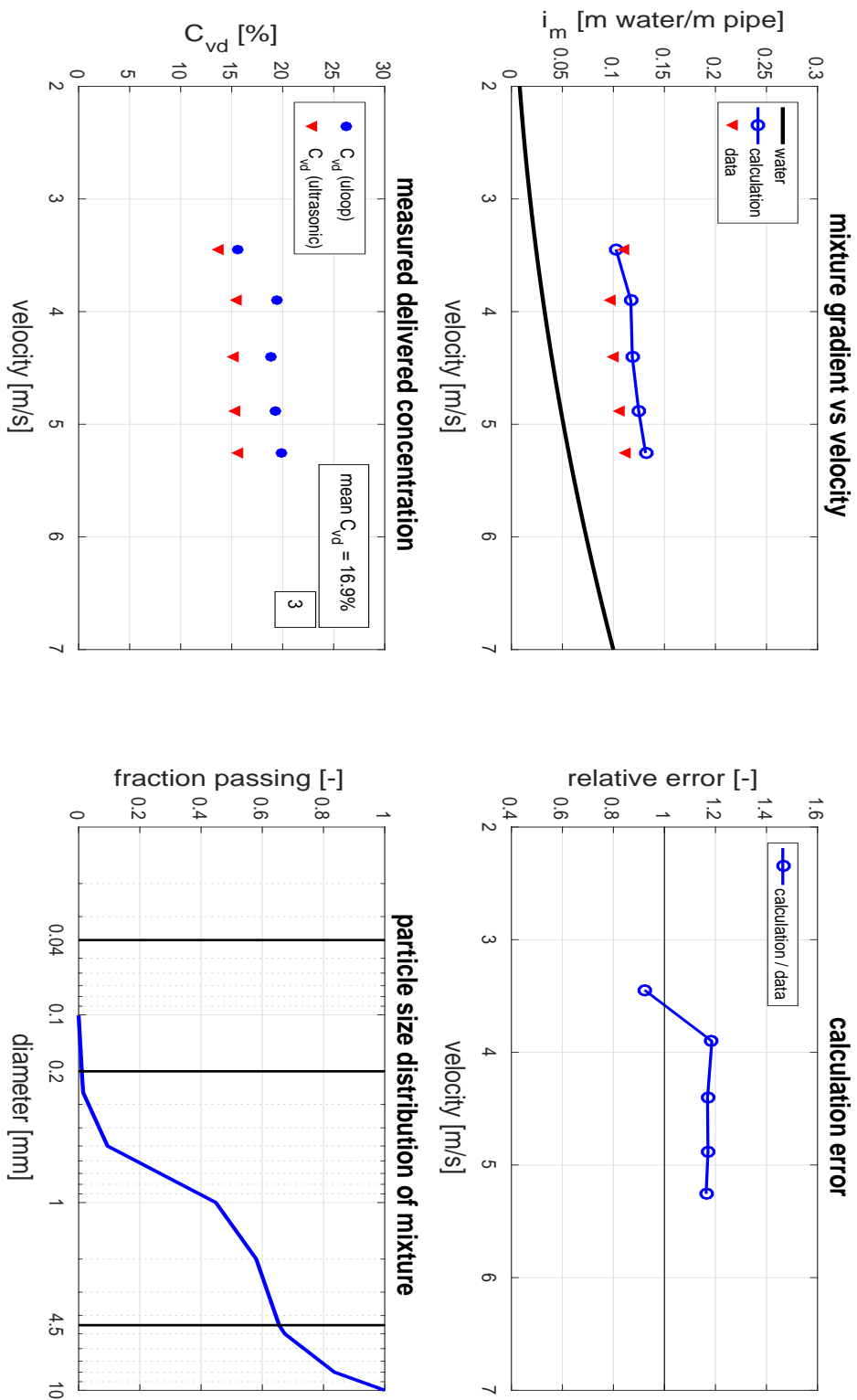
FIGURE E.16: Results of test 4b run 2.
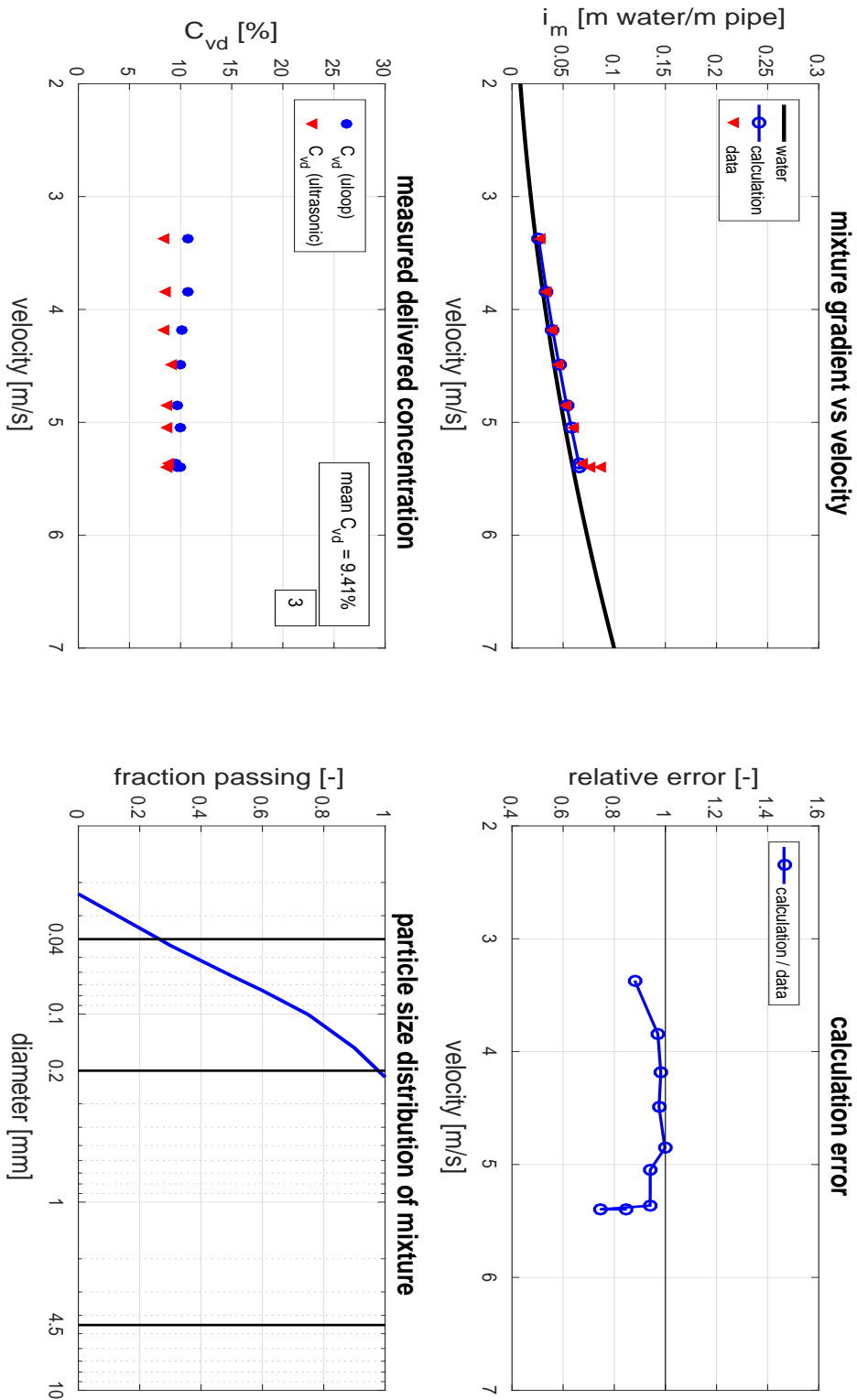
FIGURE E.17: Results of test 5 run 1.
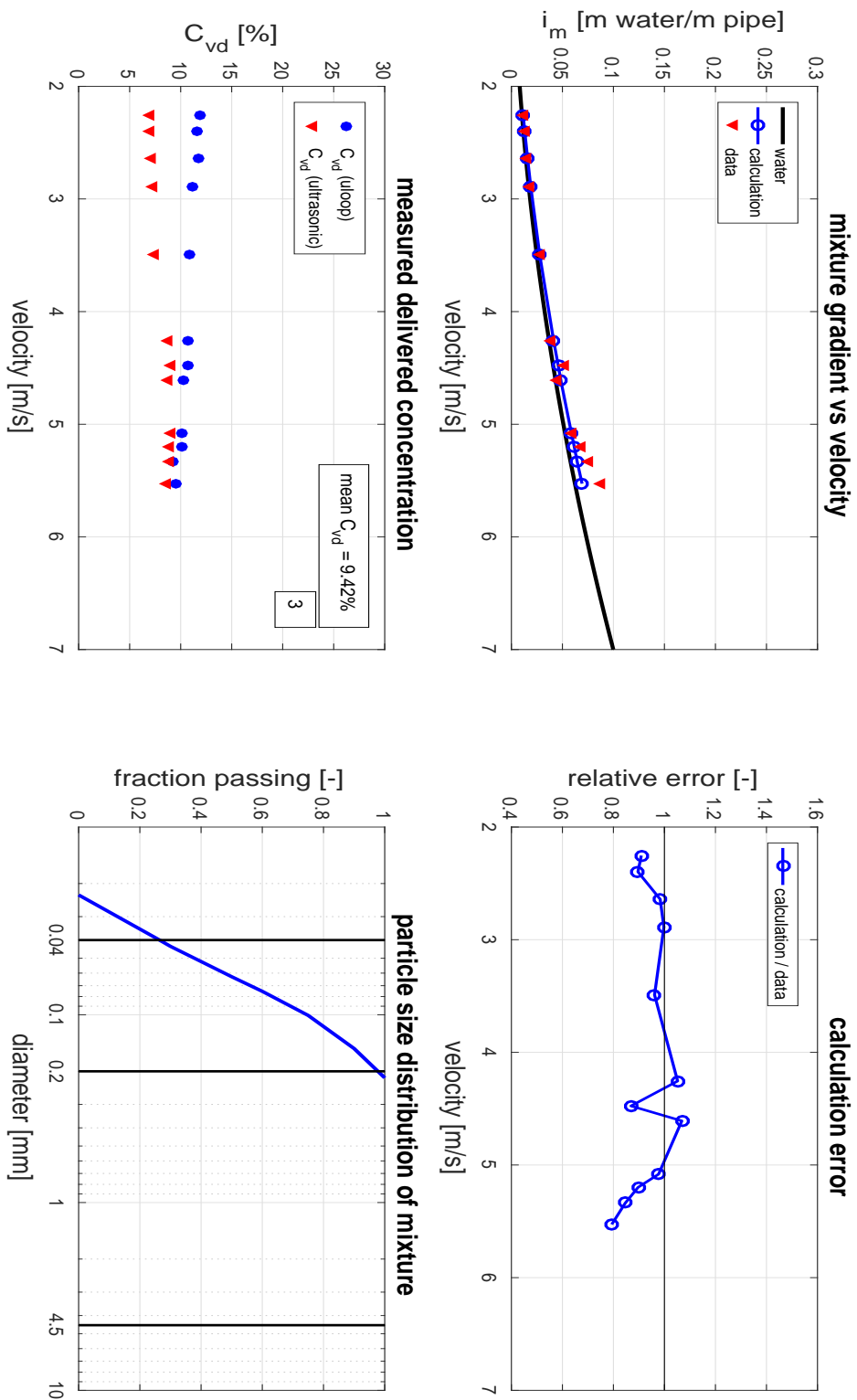
FIGURE E.18: Results of test 5 run 2.
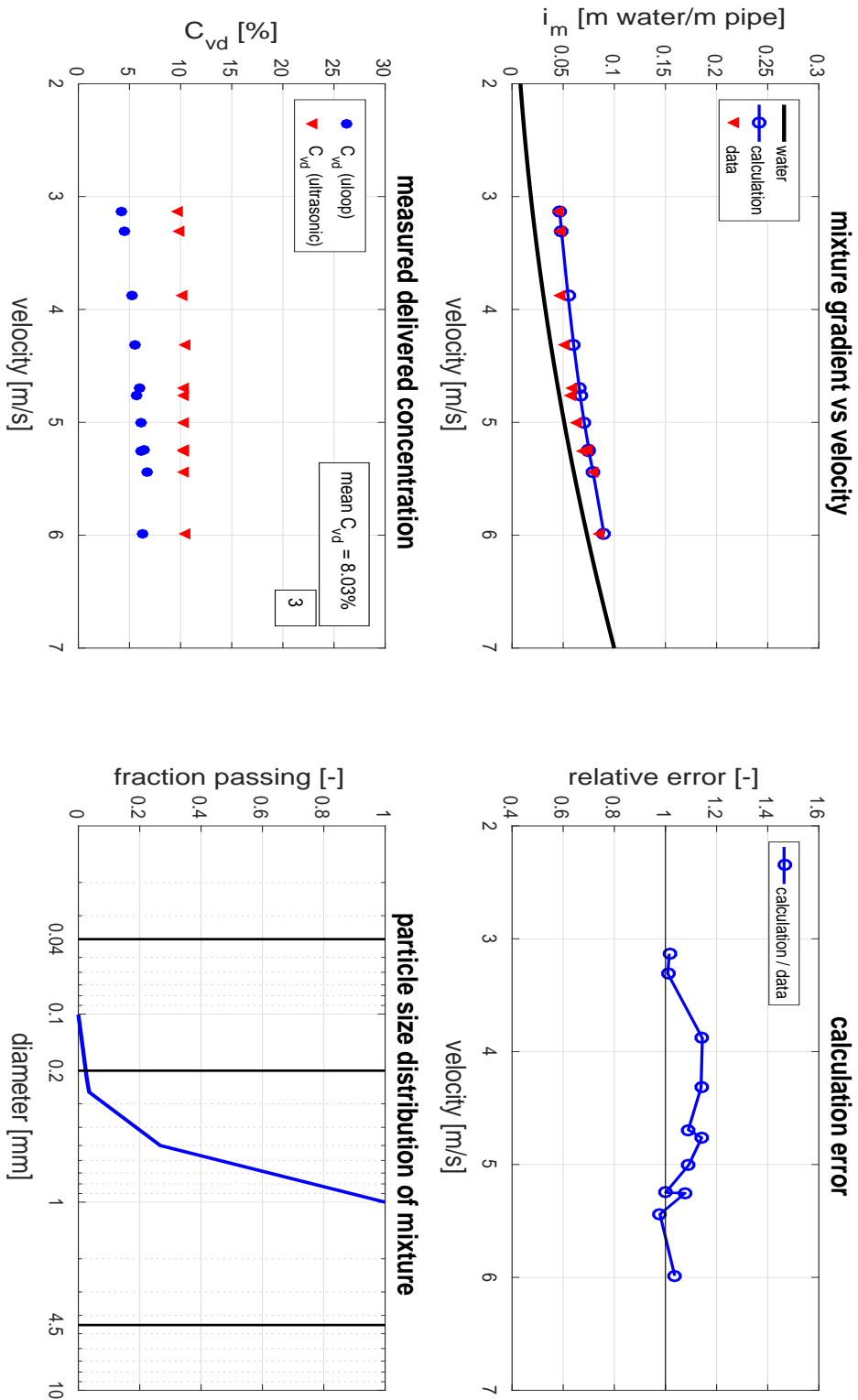
FIGURE E.19: Results of test 6a.
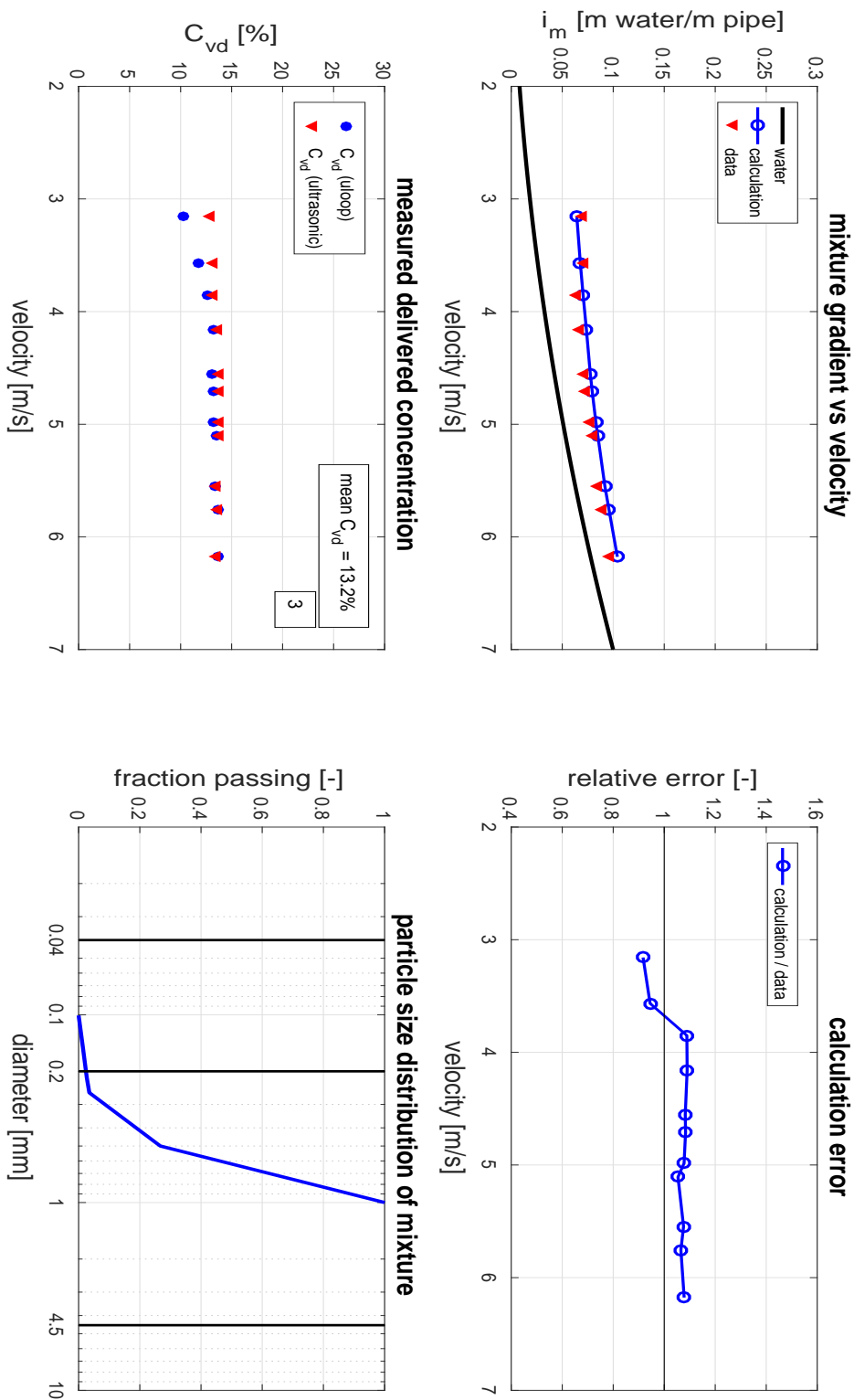
FIGURE E.20: Results of test 6b.
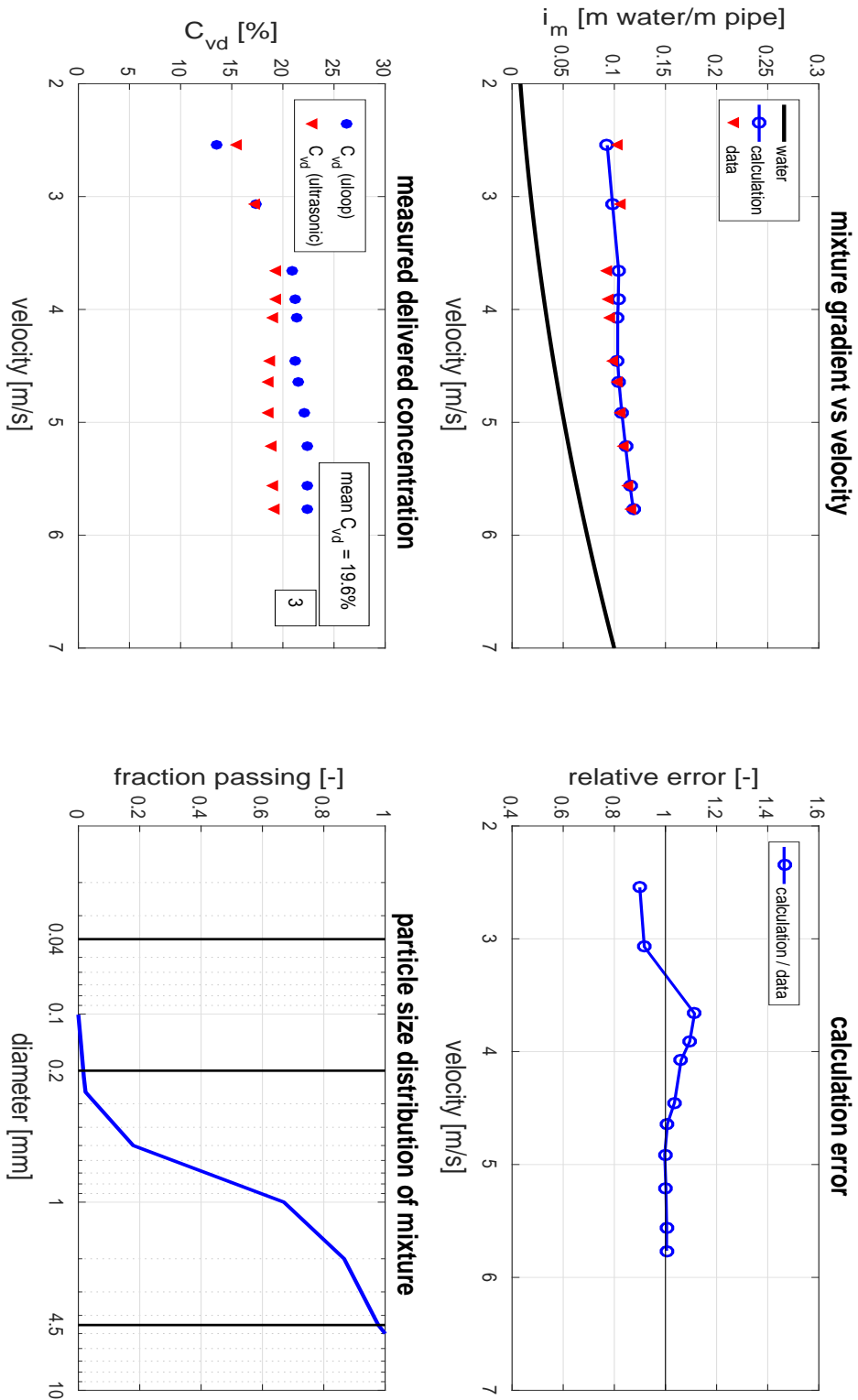
FIGURE E.21: Results of test 6c.
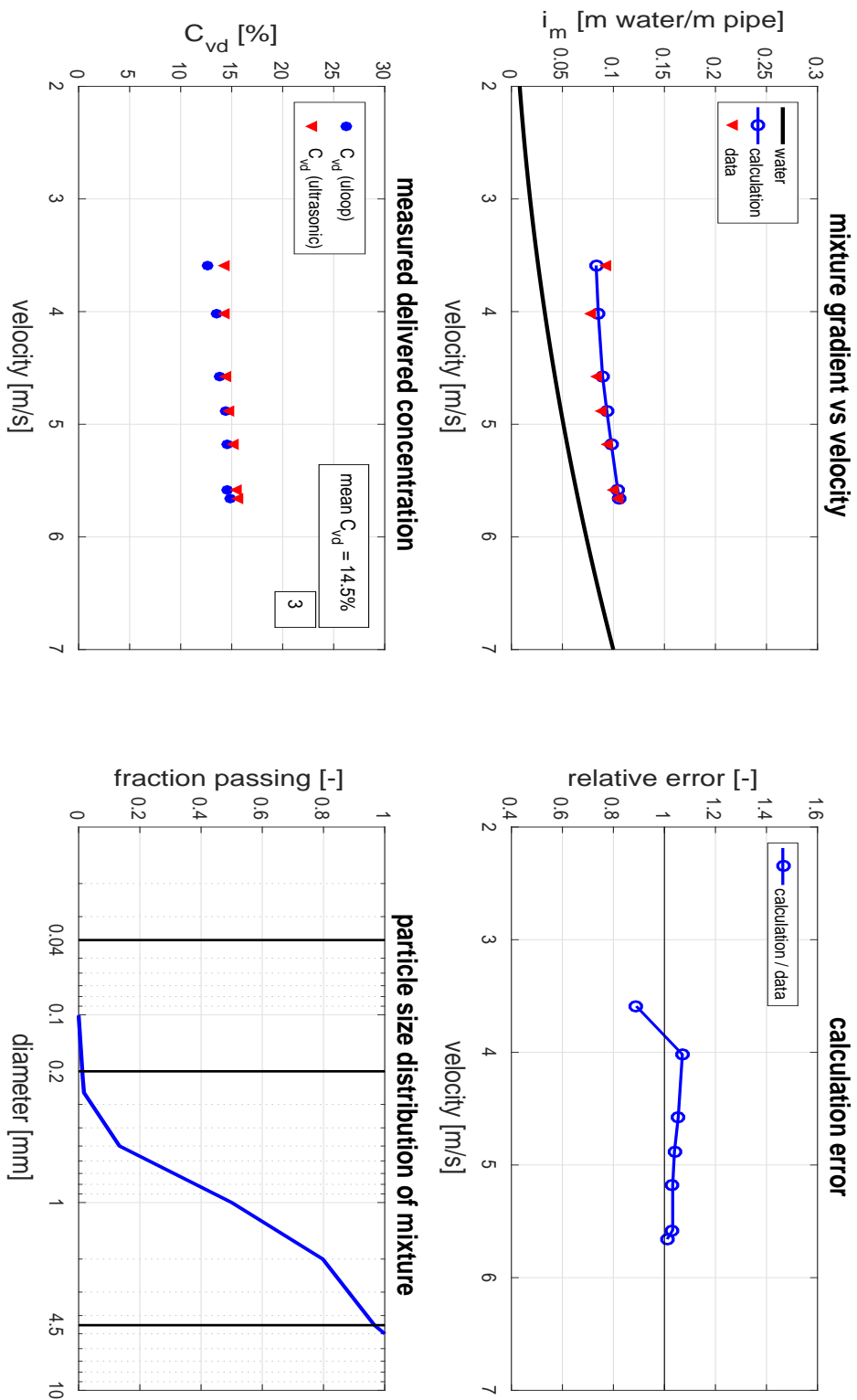
FIGURE E.22: Results of test 7 run 1.
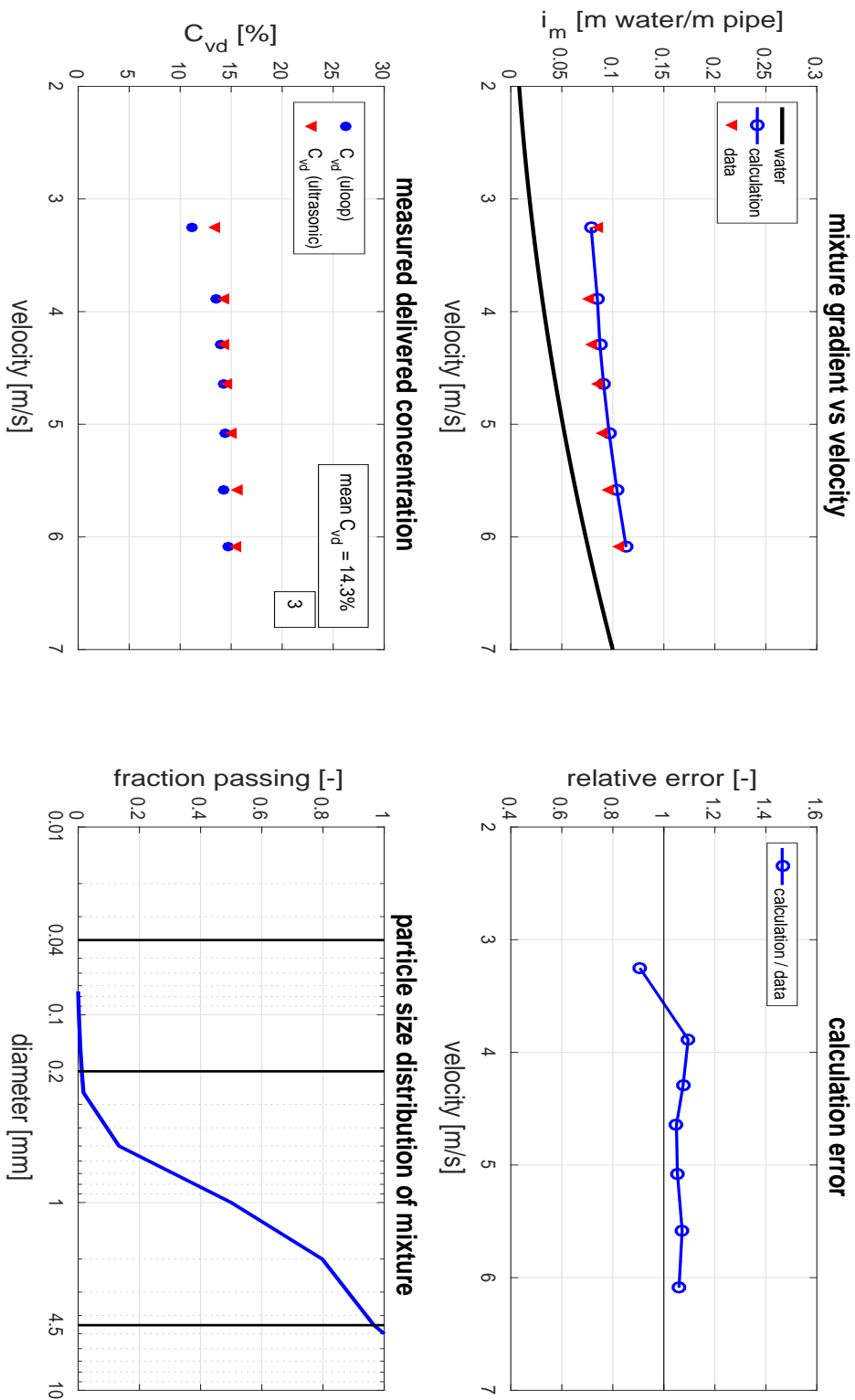
FIGURE E.23: Results of test 7 run 2.
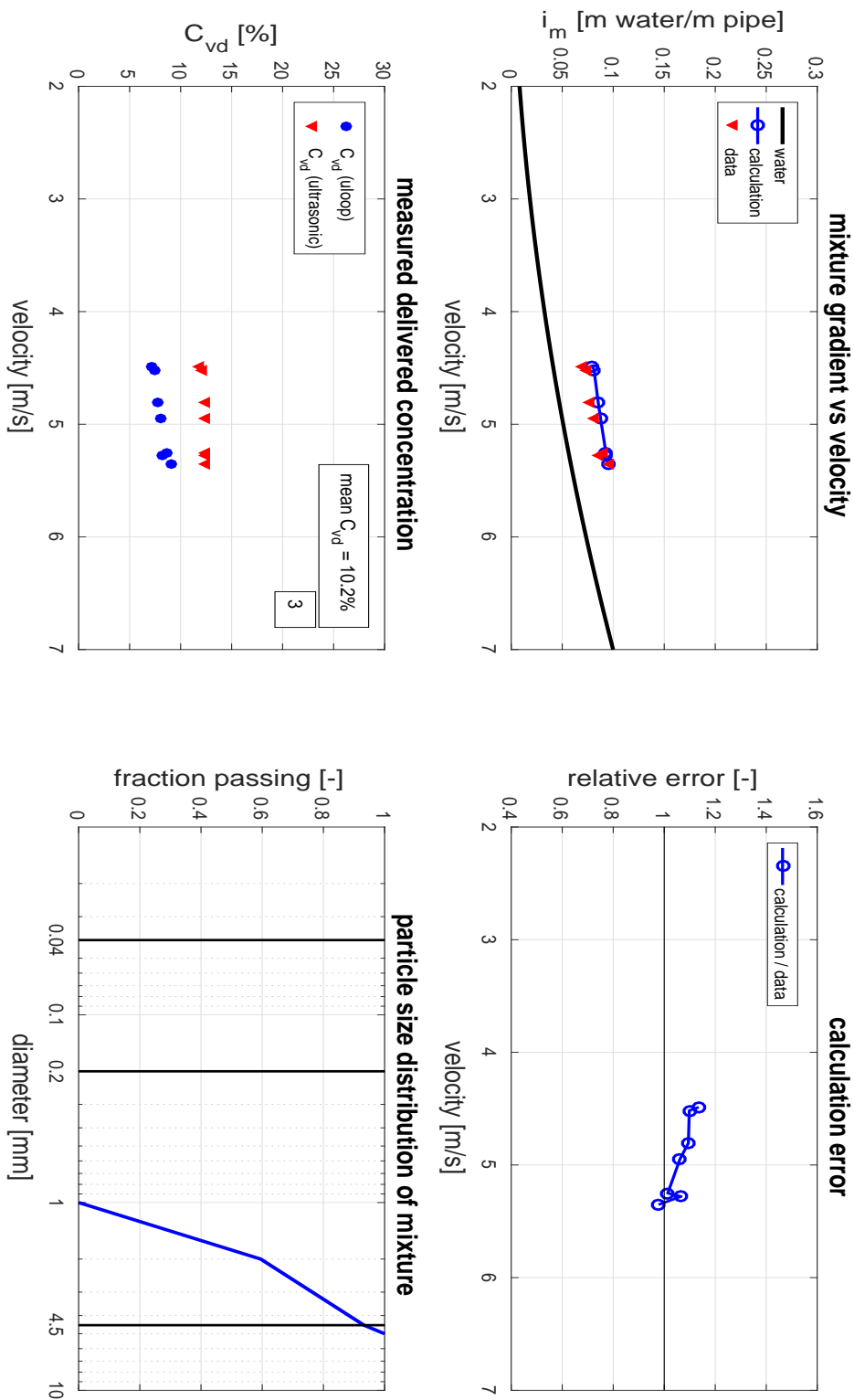
FIGURE E.24: Results of test 8a.
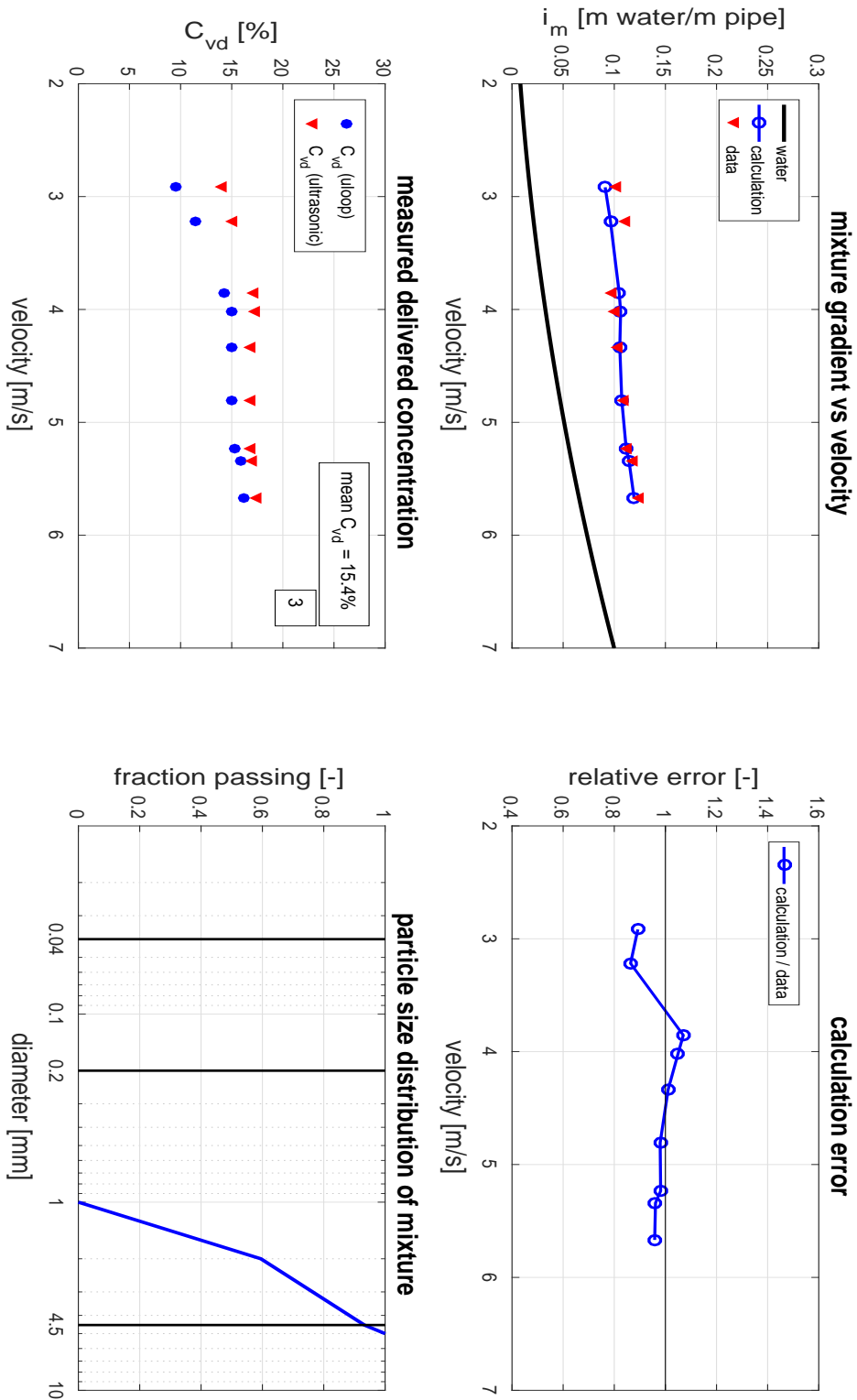
FIGURE E.25: Results of test 8b.
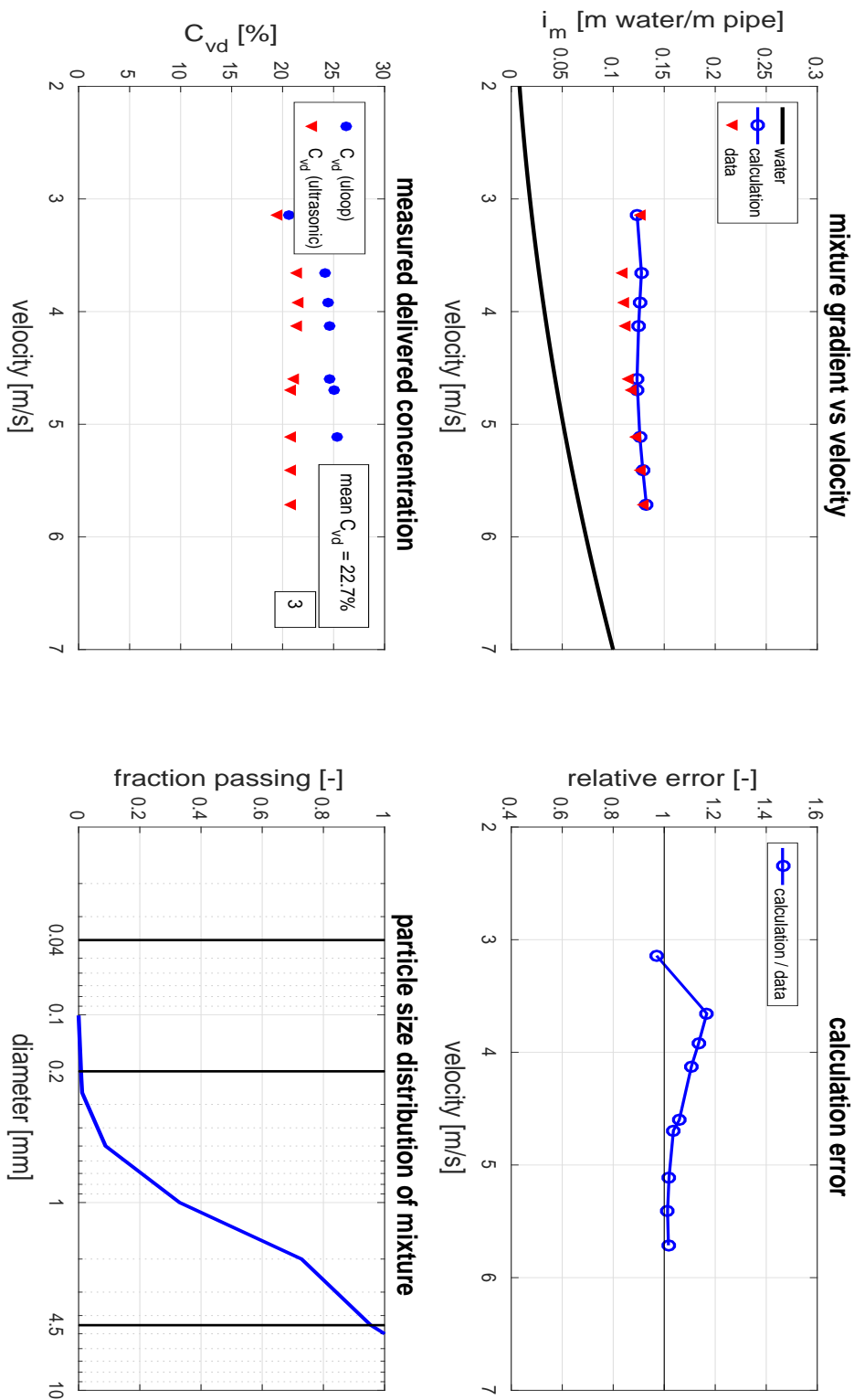
FIGURE E.26: Results of test 8c.
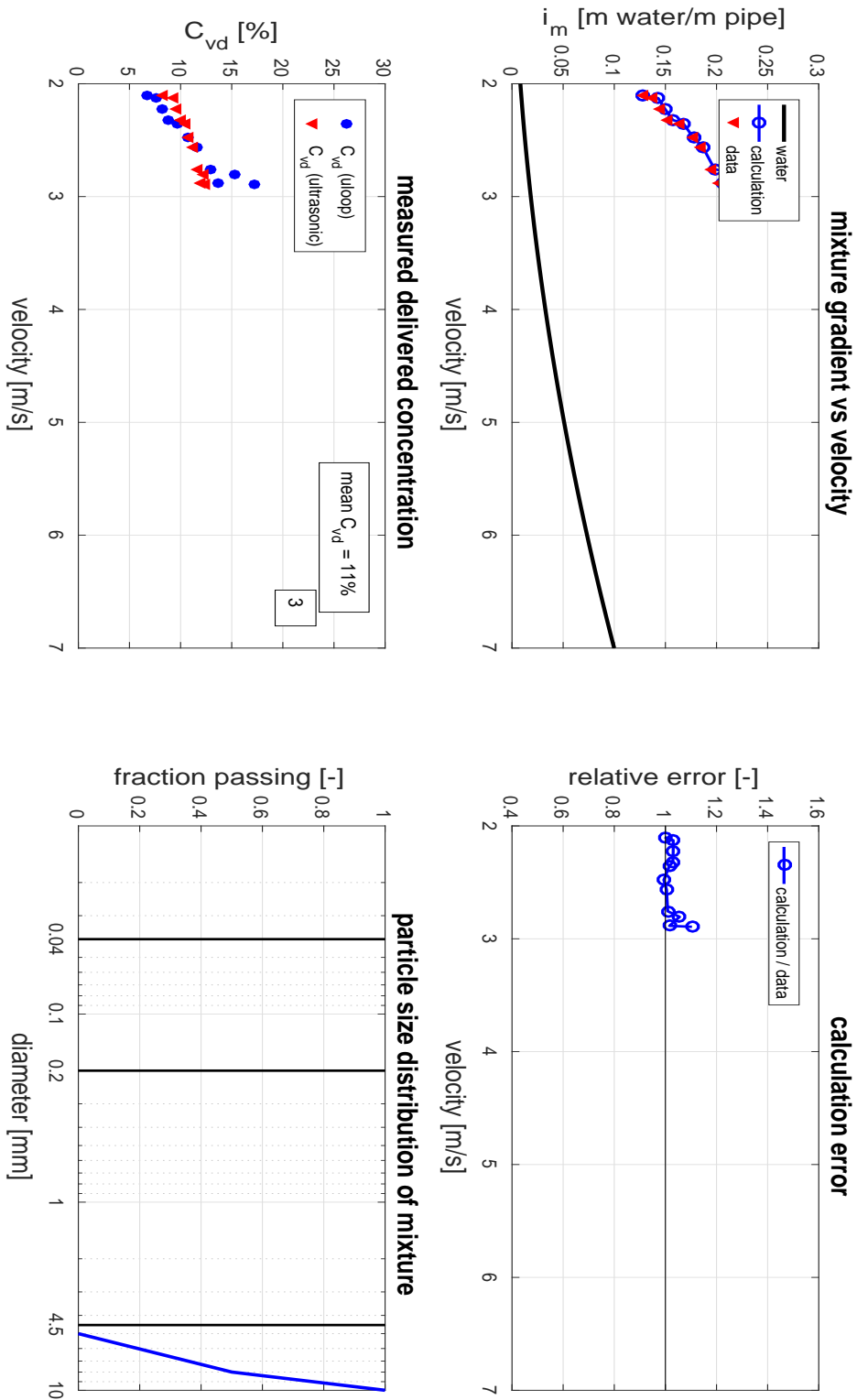
FIGURE E.27: Results of test 9.
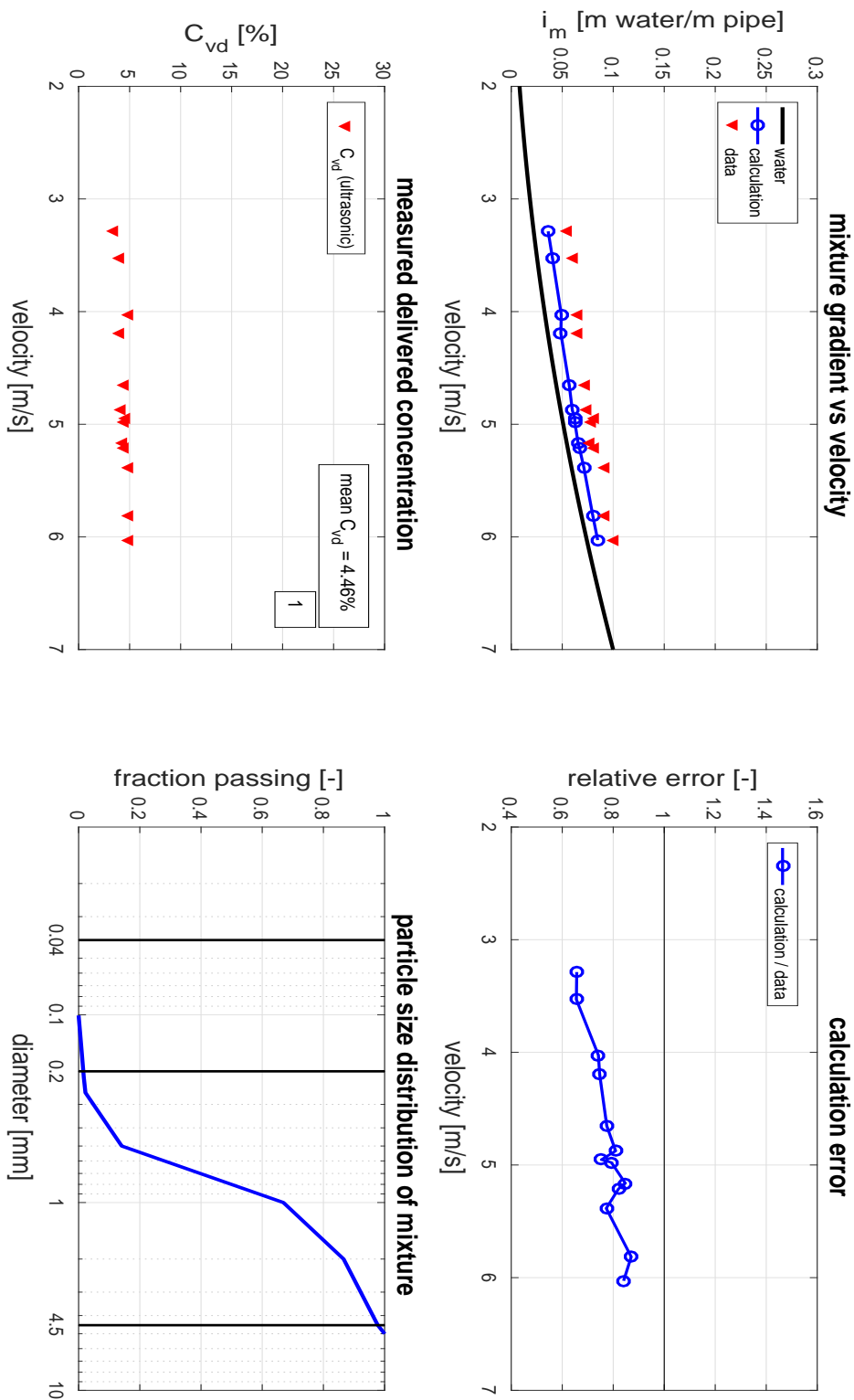
FIGURE E.28: Results of test JdR1.
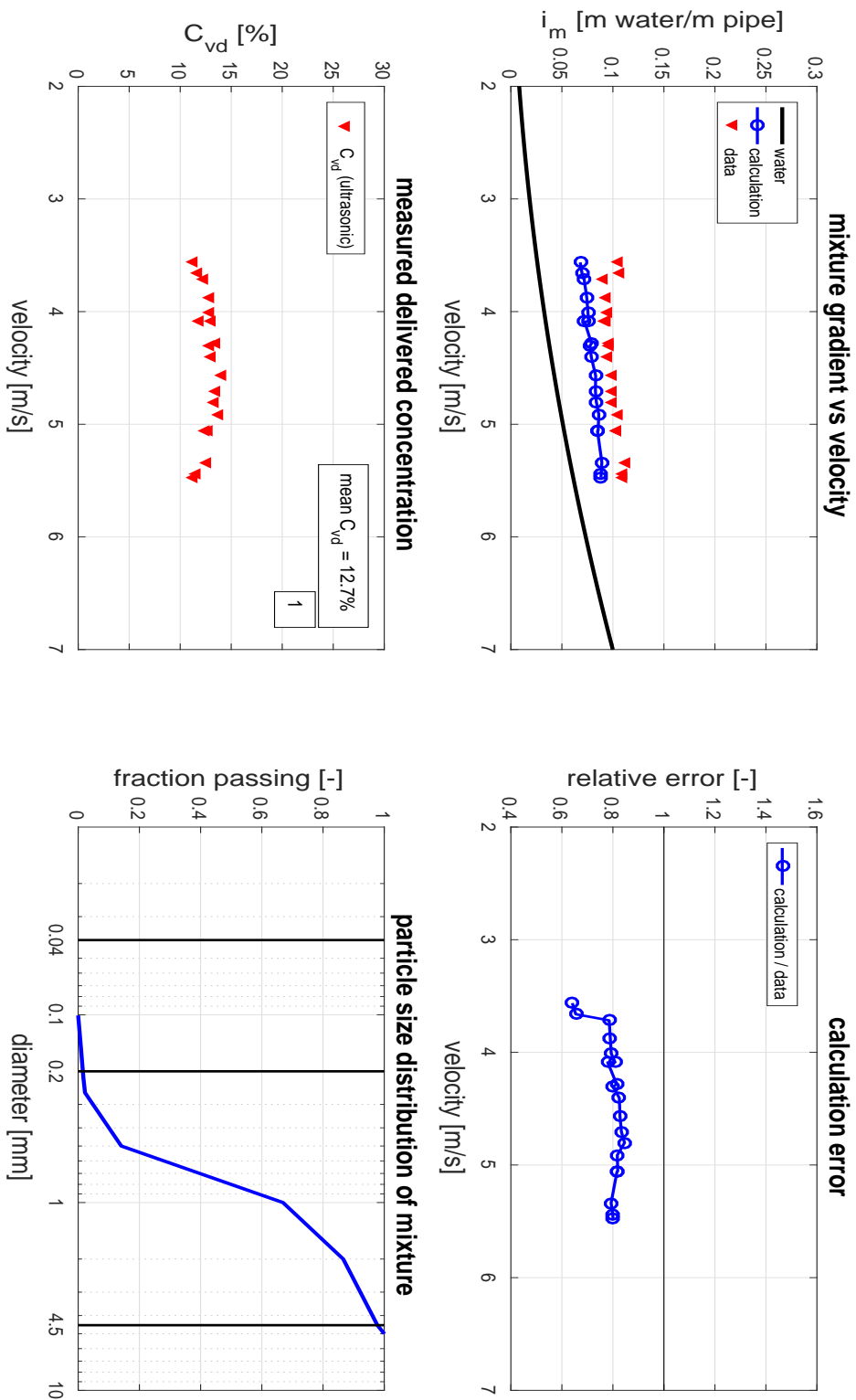
FIGURE E.29: Results of test JdR2.
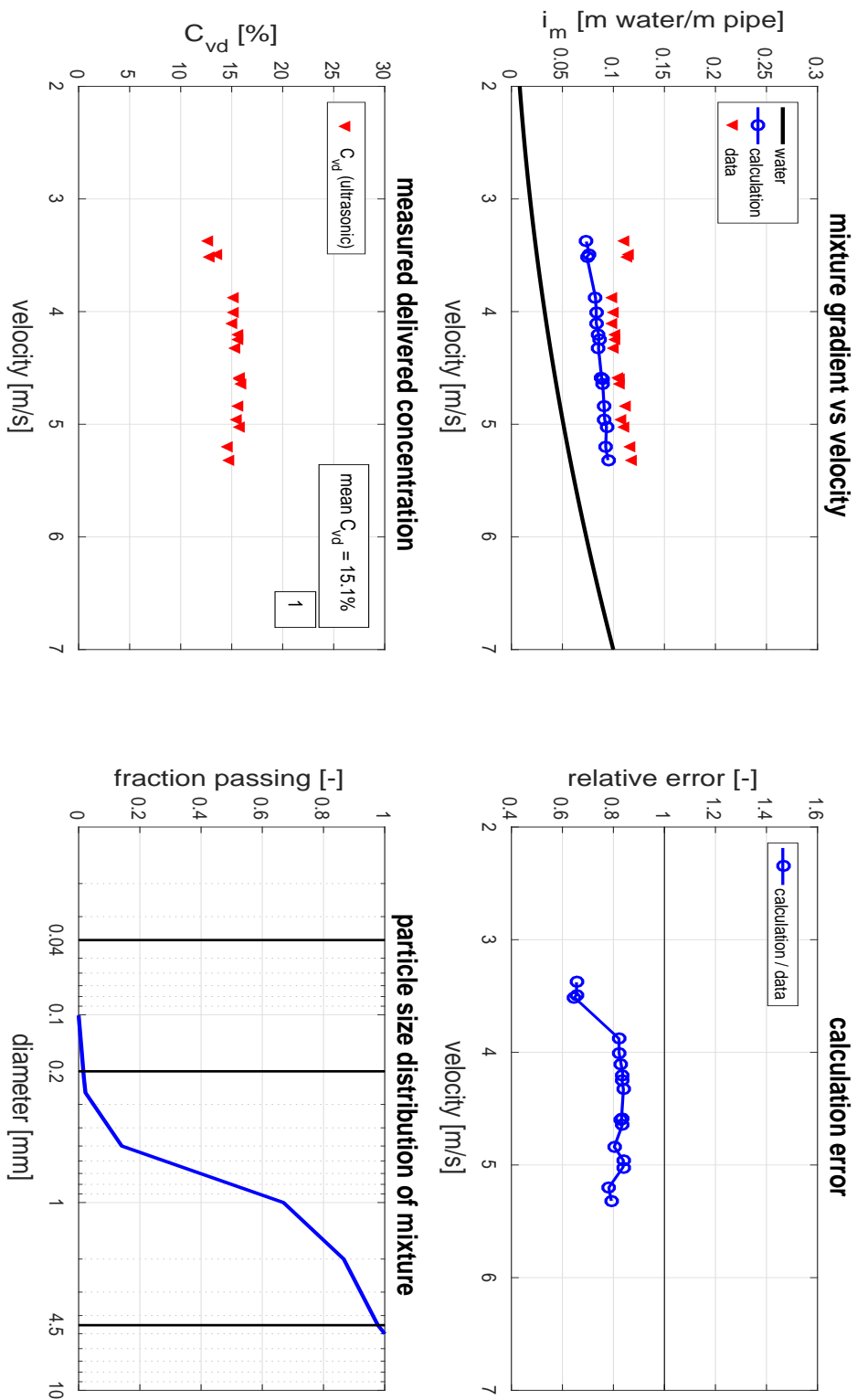
FIGURE E.30: Results of test JdR3.

Appendix F

X_s-fraction calculated using V_{50} model
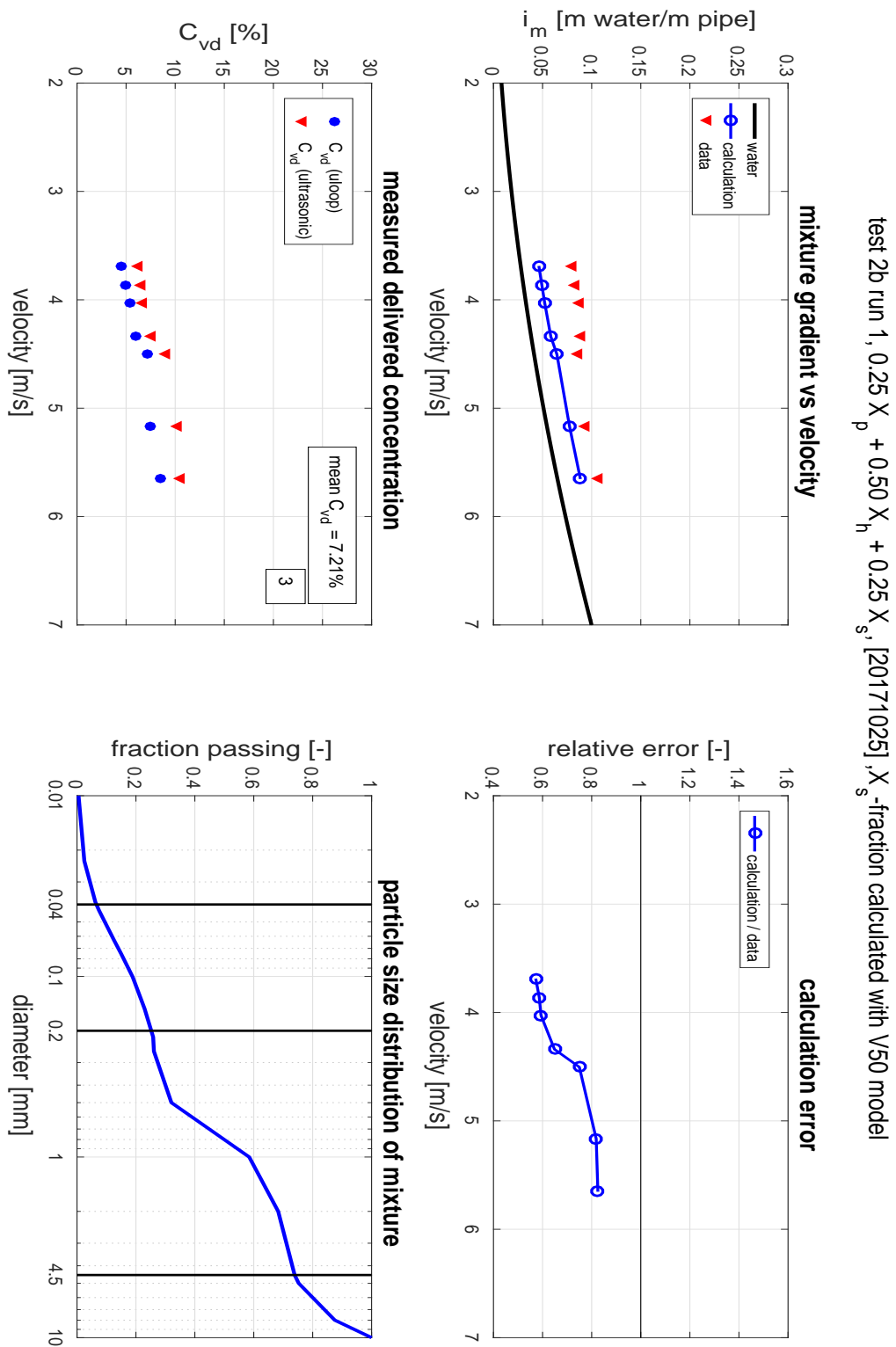
FIGURE F.1: Results of test 2b run 1 when calculating the stratified fraction with V_{50} model.
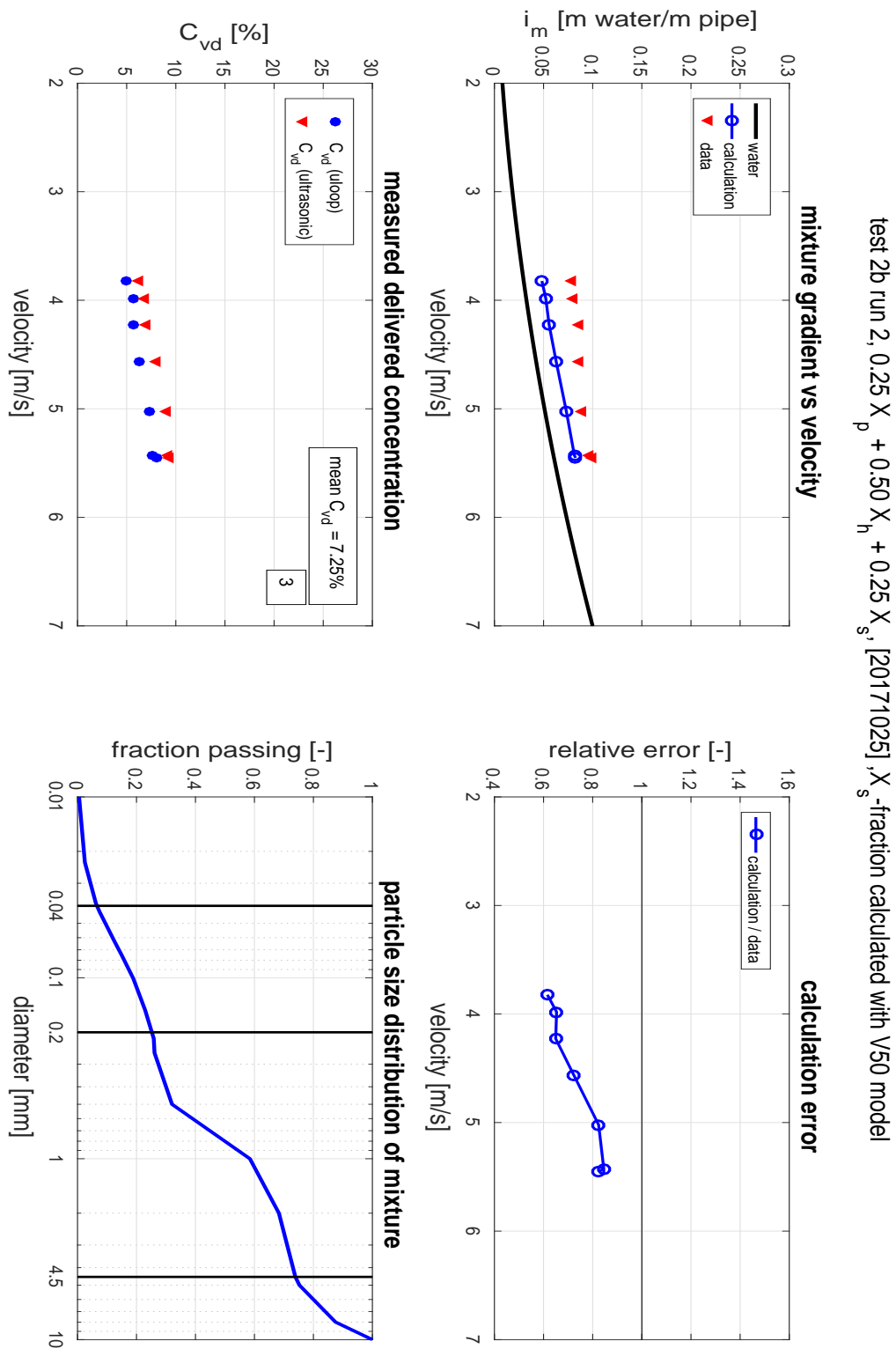
FIGURE F.2: Results of test 2b run 2 when calculating the stratified
fraction with V_{50} model.

test 3a run 1, 1.00 X_s, [20171026] ,X_s-fraction calculated with V50 model

mixture gradient vs velocity

measured delivered concentration

calculation error

particle size distribution of mixture
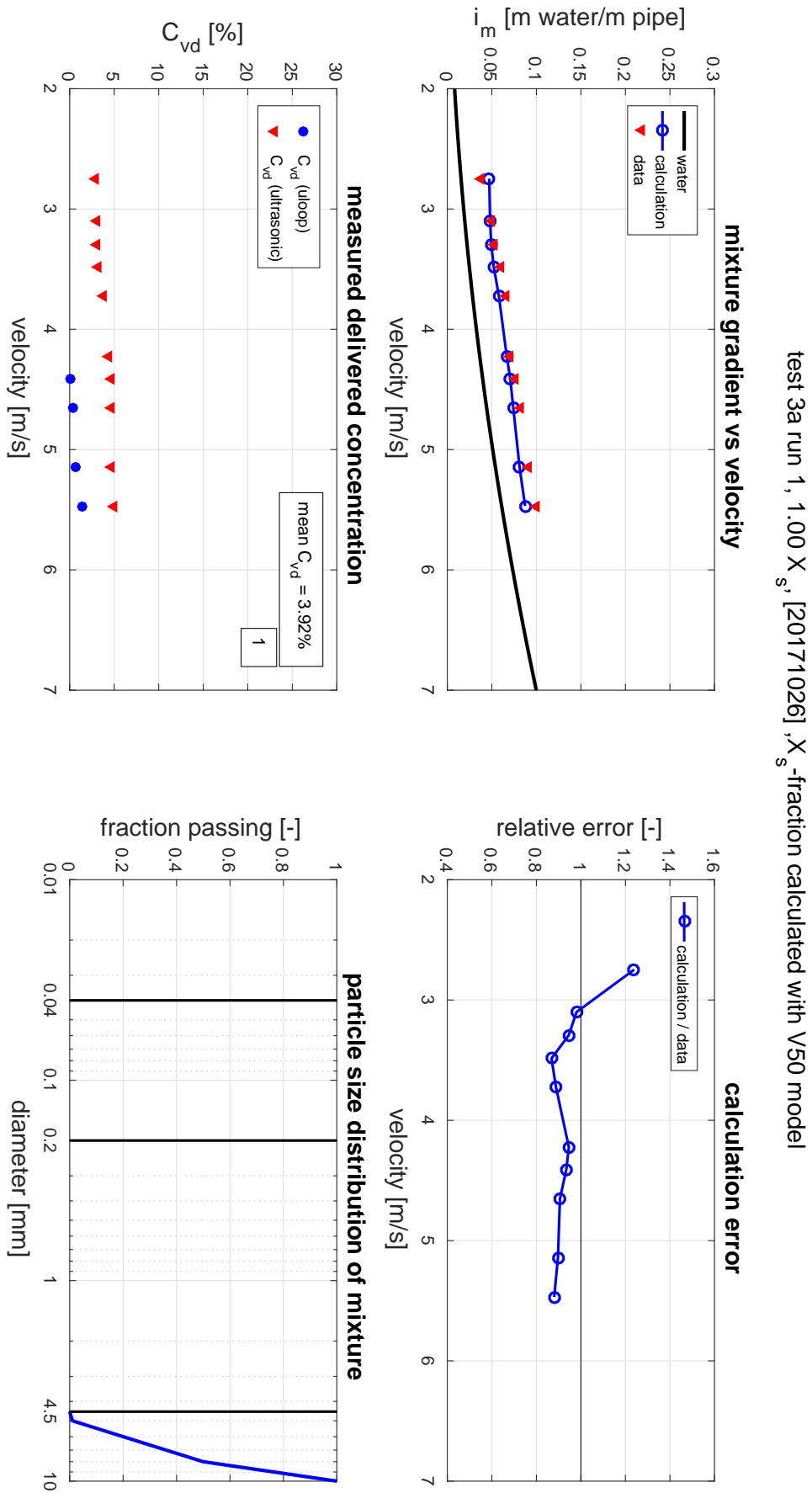
FIGURE F.3: Results of test 3a run 1 when calculating the stratified fraction with V_{50} model.

test 3a run 2, 1.00 X_s, [20171026] ,X_s-fraction calculated with V50 model

mixture gradient vs velocity

calculation error

measured delivered concentration

particle size distribution of mixture
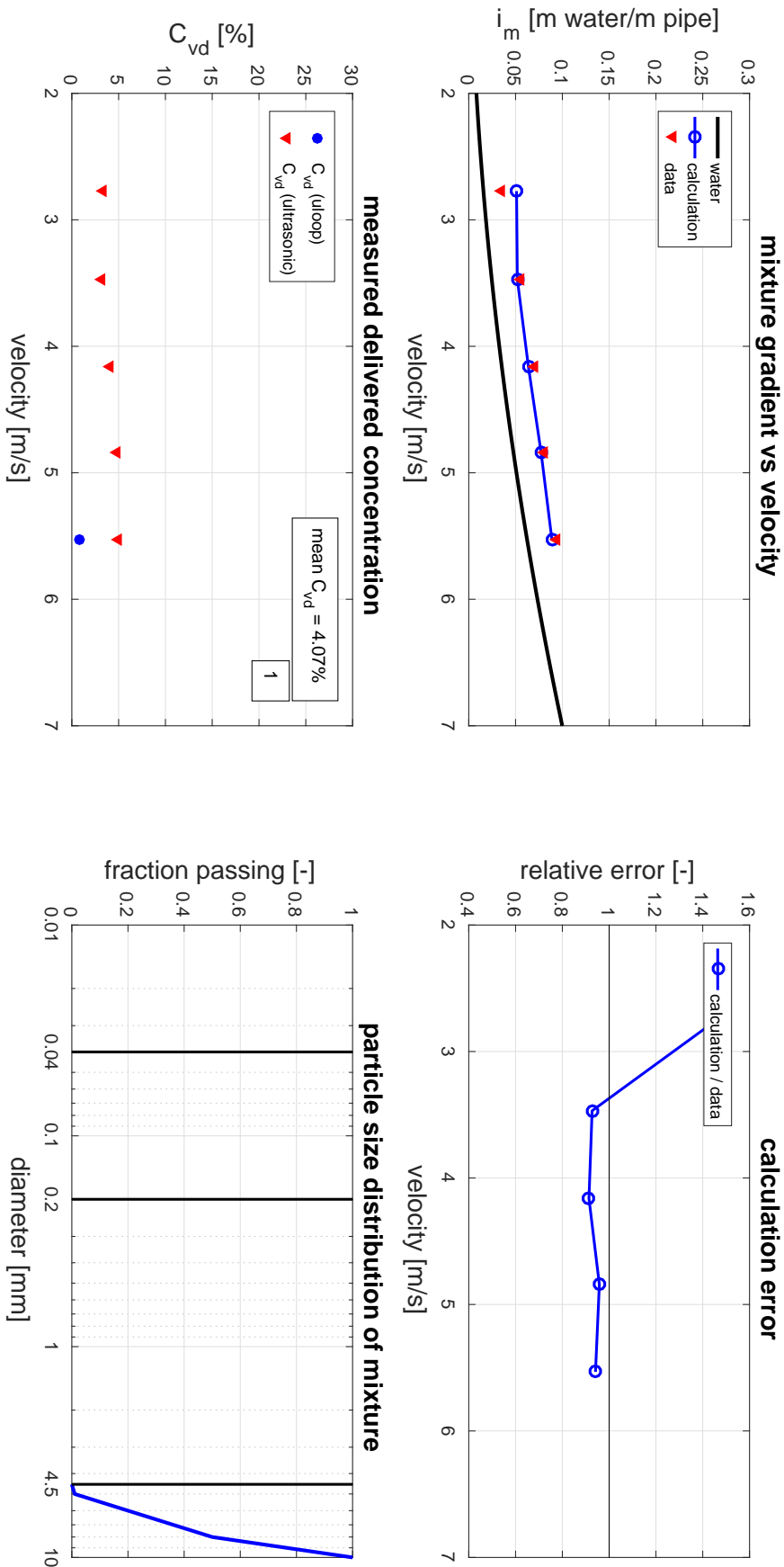
FIGURE F.4: Results of test 3a run 2 when calculating the stratified
fraction with V_{50} model.
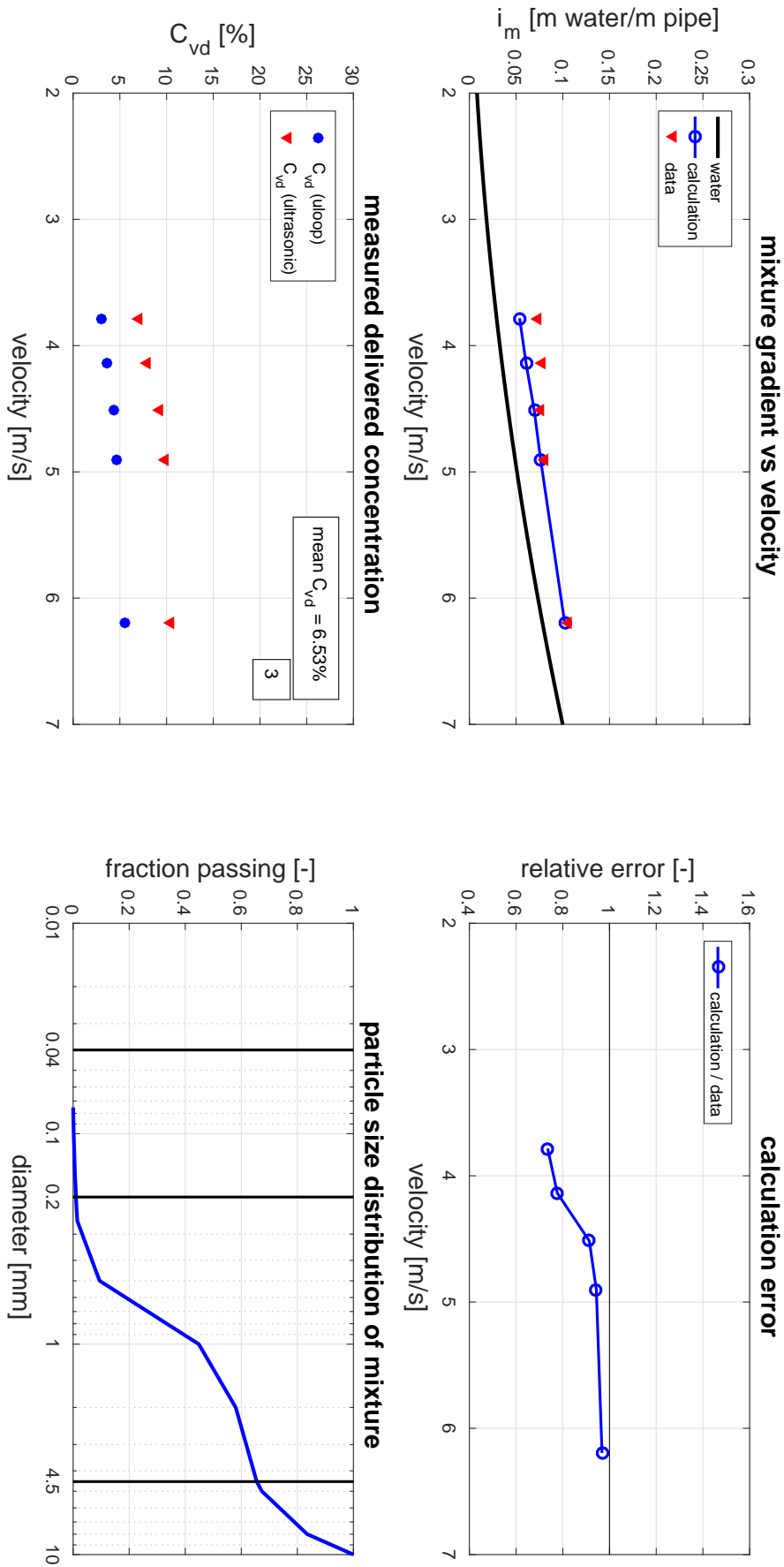
FIGURE F.5: Results of test 3b run 1 when calculating the stratified fraction with V_{50} model.
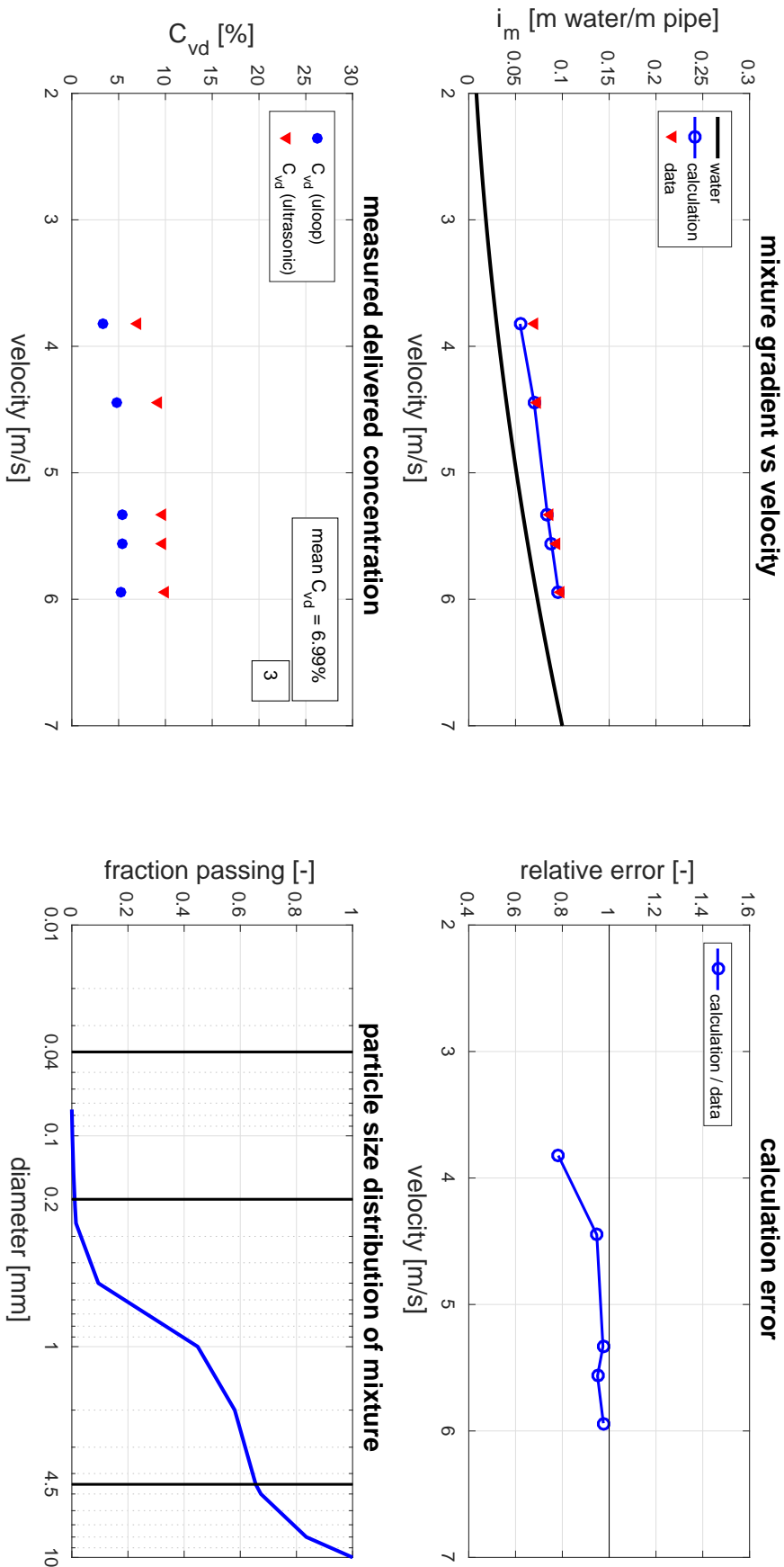
FIGURE F.6: Results of test 3b run 2 when calculating the stratified
fraction with V_{50} model.

FIGURE F.7: Results of test 4a run 1 when calculating the stratified
fraction with V_{50} model.

FIGURE F.8: Results of test 4a run 2 when calculating the stratified fraction with V_{50} model.

test 4b run 1, 0.67 X_h + 0.33 X_s, [20171027] ,X_s -fraction calculated with V50 model

mixture gradient vs velocity

measured delivered concentration

mean C_{vd} = 16.6%

3

calculation error

particle size distribution of mixture
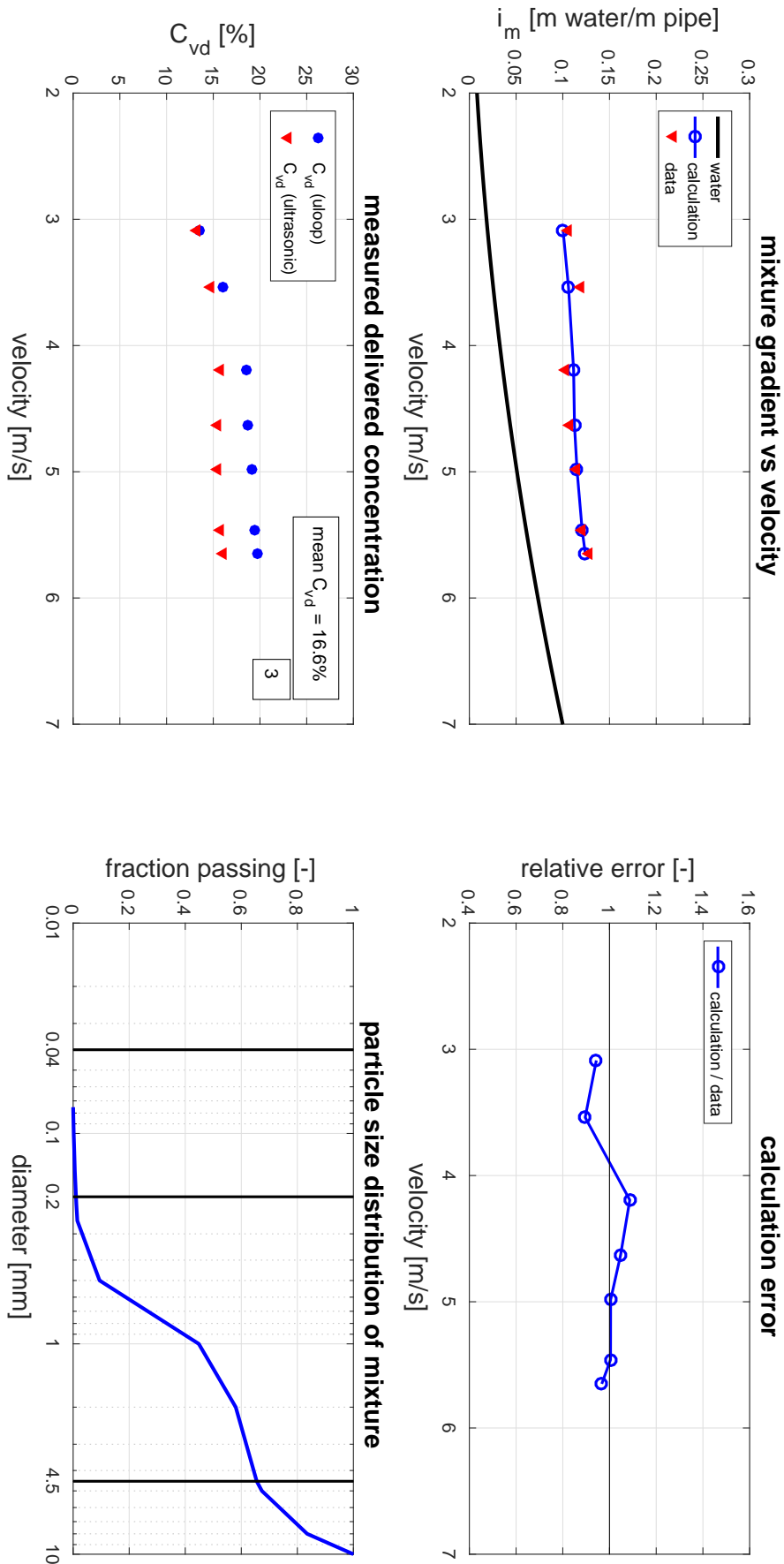
FIGURE F.9: Results of test 4b run 1 when calculating the stratified fraction with V_{50} model.
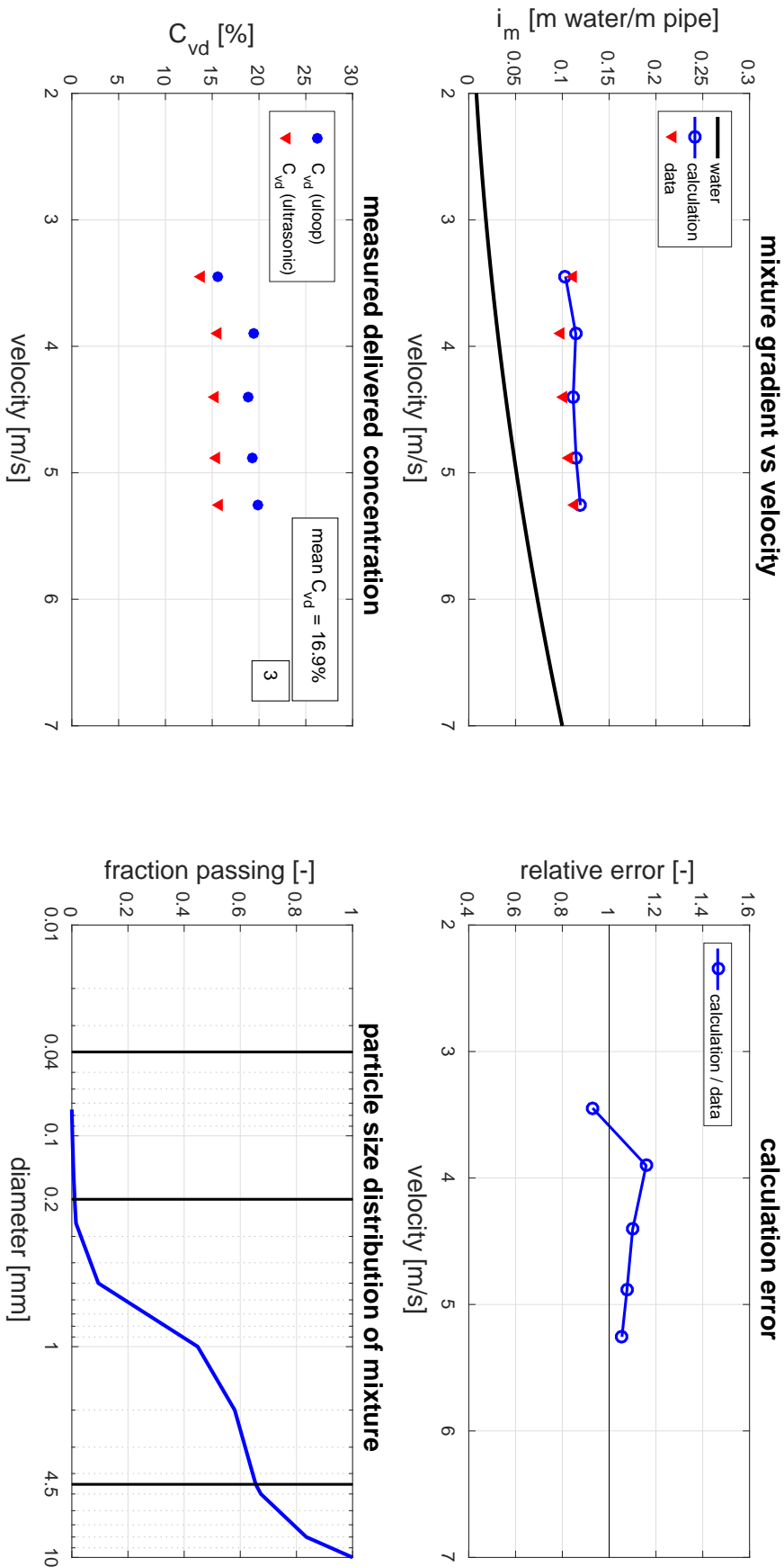
FIGURE F.10: Results of test 4b run 2 when calculating the stratified fraction with V_{50} model.